LMDZ5: A documentation

L'équipe de modélisation du Laboratoire de Météorologie Dynamique (LMD)

December 16, 2014

Contents

error Value needed explanation needed doubt

This document has been created from the existent old documentation disseminated in different documents and web pages, mostly in French. The list of the authors, without being exhaustive would be (in alphabetical order): S. Baek, O. Boucher, K. Dassas, J. Escribano, L. Fita, F. Forget, A. Gainusa-Bogdan, L. Guez, C. Hourdin, F. Hourdin, A. Idelkadi, M. P. Lefebvre, L. Li, F. Lott, J.-B. Madeleine, E. Millour, C. Risi, R. Sadourny, L. Van Phu.

Coordination and translation of this version of the documentation has been done by L. Fita.[1]

[1]on current contract with REMEMBER project funded by the SOC&ENV program of the French National Research Agency (ANR) (contract ANR-12-SENV-001)

Chapter 1

Introduction

This document attempts to be a complet description of the Global Circulation Model of the *Laboratoire de Météorologie Dynamique Zoomed* (LMDZ, http://lmdz.lmd.jussieu.fr/). Developed and maintained by the *Laboratoire de Météorologie Dynamique* (LMD, http://www.ipsl.fr/en/Organisation/IPSL-Labs/LMD), part of the *Institute Pierre Simone Laplace* (IPSL, http://www.ipsl.fr/en) of the *Centre national de la recherche scientifique* (CNRS, http://www.cnrs.fr/).

This document describes the LMDZ up to the 5th version of the GCM, which corresponds to the version number r2251 from November 2014. A reference citation for the model in its old LMDZ4 version is by Hourdin et al. (2006).

1.1 LMDZ: a General Circulation Model

LMDZ corresponds to the second generation of a climate model developed 30 years ago in the LMD initially described by Sadourny and Laval (1984). This version is more modular and flexible than the previous version. The character "Z" in the name makes reference to the capacity of refinement of the grid (Zoom, see section 4.7) in a selected area. Higher resolution is it possible due to a generalization of the codification of the numerical formulation with a grid where the distance factors along both distances can be arbitrarily selected.

Like the majority of climate models, LMDZ integrates on a sphere and in time the "primitive equations of the meteorology". These equations are a simplified version of the Navier-Stokes equations assuming that the atmosphere is always in hydrostatic equilibrium along the vertical and neglecting the vertical geometrical variations (thin layer hypothesis, see chapter 2). The kinetic moment related to the axis of the poles is for example computed using as distance to the axis: $a\cos\phi$. With, a is the planetary radius and ϕ the latitude, meanwhile $(a+z)\cos\phi$, would account on the altitude z of an air-parcel above surface.

LMD follows a discretization of the equations based on finite differences. It is preserves mass and momentum for the axis-symmetric component of the flow and the barotopic vorticity.

These equations can not be integrated at the viscous scale. Nowadays, on the global models, grid resolutions are comprised from tens to hundreds of kilometers depending on the applications. Thus, impact of the sub-grid processes on the large-scales, should be represented by parameterizations. It is also necessary to take into account fundamental processes like the visible and infrared transfer of radiation in the atmosphere, cloud processes or the interactions with the surface. In terms of modelers' vocabulary, parameterizations are grouped on the "physics" of the model, in opposition to the code which represents the "dynamics" of the large-scale. In case of application of the model on other planets, is the physic section which has to be changed the most, and more importantly the computation of the radiation transfer.

1.2 LMDZ: atmospheric component of the climate model of the IPSL

The climate system is a complex system, in which different components interact. The IPSL climate model (see figure 1.1) is constructed as the coupling of different models indepenently developed by te different partners of the Institute. These are:

- atmoshpere: LMDZ

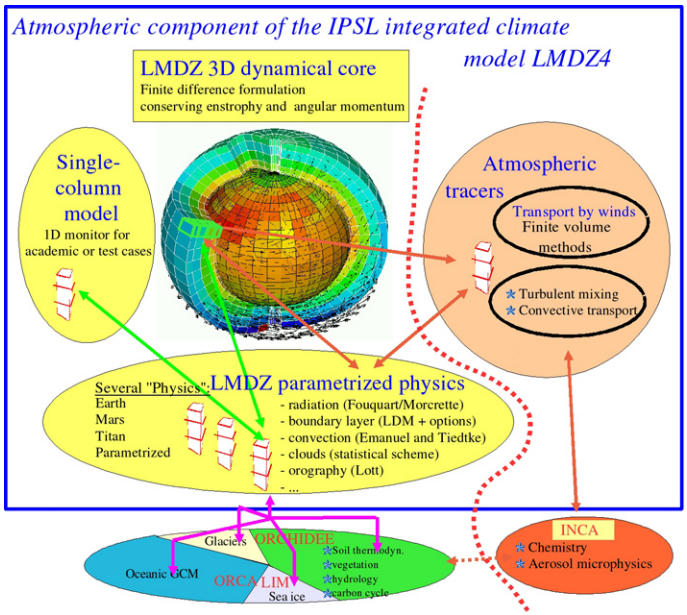

Figure 1.1: Schematic representation of the IPSL climate model

- ocean: NEMO
- land: ORCHIDEE
- aerosols: INCA

1.3 LMDZ et other planets

LMDZ is also used in the study of atmospheres of other planets. In this application, one mostly indtroduce significant modifications on the physcal part of the model due to the different composition and characteristics of such atmospheres. Whereas dynamics is the same for all the planets. Currently there are operative versions of the model for: Venus, Mars, Jupiter, Saturn, Titan and Pluto.

In order to keep this documentation with a 'manegable' size, a description of the different planetary uses is here not included.

1.4 Model main characteristics

LMDZ offer a series of main characteristics some of them are unique or different in comparison to other state-of-the-art GCMs. These main characterisitcs are:

- Hydrostatic dynamical core
- 4 different sub-grid surface types: land, ice over land, ocean and ice over ocean. Ice covered surfaces have dynamic characteristics
- Simulation of the full atmosphere ($p_{top} = 0\ hPa$)
- Yearly variations of the GHG global concentrations
- Tracer dynamics
- Zoom capabilities in a given region

- No full micro-physics: only evolution of vapour, rain and ice water spieces
- coupled to a series of excternal models: ORCHIDEE, NEMO, Chimère, INCA, REPROBUS and COSP
- use of the `SAVE` Fortran capability for memory efficiency
- Parallelized in both shared and distributed memory (see in appendix E list of variables related to the discretization of the grids)

1.4.1 Basic principles

The General Circulation Model (GCM) calculates the temporal evolution of the different `variables` that control or describe the meteorology and climate at different points of a `3D` *grid* that covers the entire atmosphere.

From an initial state, the model calculates the evolution of these variables, timestep by timestep:

- At instant t, we know variable X_t (temperature for example) at one point in the atmosphere.
- We calculate the evolution (the `tendencies`) $(\frac{\partial X}{\partial t})_1$, $(\frac{\partial X}{\partial t})_2$, etc. arising from each physical phenomenon, calculated by a `parameterization` of each of these phenomenon (for example, heating due to absorption of solar radiation).
- At the next time step $t + \delta t$, we can calculate $X_{t+\delta t}$ from X_t and $(\frac{\partial X}{\partial t})$. This is the *integration* of the variables in time. (For example, $X_{t+\delta t} = X_t + \delta t(\frac{\partial X}{\partial t})_1 + \delta t(\frac{\partial X}{\partial t})_2 + ...)$

The main task of the model is to calculate these tendencies $(\frac{\partial X}{\partial t})$ arising from the different parameterized phenomenon.

1.4.2 Dynamical-Physical separation

Organization of the LMDZ model is highly related to the split between "dynamic" (where the horizontal exchanges are taken into account) and "physic" (which can be seen as a juxtaposition of individual atmospheric columns).

This characteristic of the physic section is used in the sense that the coding of all the parameterizations is coded by an index which represents the horizontal grid (see a representation in figure 1.2).

This type of writing allows also to vectorize and parallelize the code. This approach also allows to have a one-dimensional version of the model of circulation (see section 4.3). In order to have this capability, one only need to write a program with which one can initialize the meteorological profiles on a given specific point of the globe where one call in a loop the physical package.

Another important aspect of the modular conception is that it allows to generate in parallel, of different "physics" interfaced with the same code dynamic. This point is essential for the studies at the LMD on Mars and Titan for example.

In practice, the 3D model operates in two parts:

- **dynamical part:** containing the numerical solution of the general equations for atmospheric circulation. This part (including the programming) is common to all versions of the model, and in general for all atmospheres of the terrestrial type.
- **physical part:** that is specific to the planet in question and which calculates the forced circulation and the climate details at each point.

The calculations for the dynamical part are made on a 3D grid with horizontal exchanges between the grid boxes, whereas the physical part can be seen as a juxtaposition of atmosphere *columns* that do not interact with each other (see diagram 2.1, and 1.2).

Generic description of the strucutre and subroutines called inside the physical package is given in figure 1.4.

The dynamical and physical parts deal with variables of different natures, and operate on grids that are differently constructed. The temporal integration of the variables is based on different numerical schemes (simple, such as the one above for the physical part, and more complicated, the *Matsuno-Leapfrog* scheme for the dynamical part, see section 2.4). The timesteps are also different.

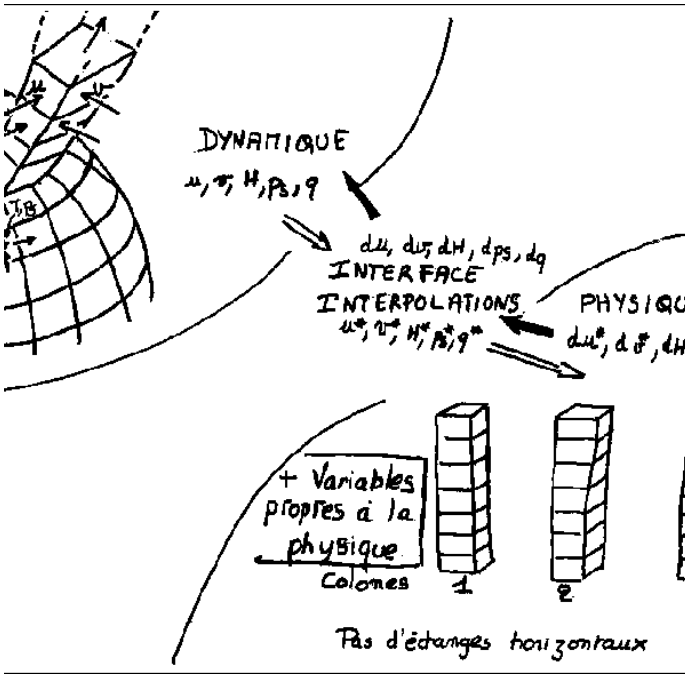

Figure 1.2: Split between the 3D dynamic and the 1D physic sections of the LMDZ code

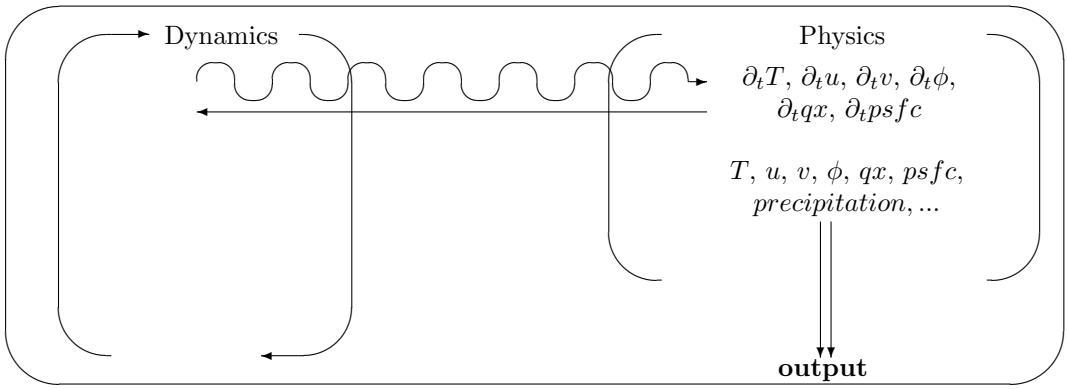

Figure 1.3: Schematic representation of the LMDZ interaction between dynamical and physical cores of the model. Tendency terms $\partial_t \chi$ are given by the dynamical corem modified by the physical processes and given back to the dynamics. Static and diagnostic fields are written in file inside the physical package

Figure 1.4: Schematic flux diagram of the LMDZ. Calls to `qcheck` (checking of conservation of water), `diagetpq` (conservation of energy and mass), `diagphy` (thermal and water mass fluxes and enthalpy and mass changes) are not included. On certain calls appears ':' which stands for different options according to an 'IF'. Information from `lmdzphys`. "/", stands for consecutive calls

```
.
|-- modipsl                    IPSL models folder
|   |-- bin
|   |-- config
|   |-- doc
|   |-- lib
|   |-- modeles                models
|   |   |-- IOIPSL             I/O tools from IPSL
|   |   |-- LMDZ5              LMDZ version 5
|   |   |-- ORCHIDEE           land/vegetation/CO2 cycle/... model
|   |-- tmp
|   `-- util
|-- modipsl.testing.tar.gz.1   compressed file with the testing simulation
`-- netcdf-4.0.1               netcdf libraries version 4.0.1
```

Figure 1.5: Main folder structure and main files of the LMDZtesting

The physical timestep is `iphysiq` times longer than the dynamical timestep, as the solution of the dynamic equations requires a shorter timestep than the forced calculation for the physical part.

In practice, the main program that handles the whole model (`gcm.F`) is located in the dynamical part. When the temporal evolution is being calculated, at each timestep the program calls the following:

1. Call to the subroutine that handles the total tendency calculation ($\frac{\partial X}{\partial t}$) arising from the dynamical part (`caldyn.F`)
2. Integration of these dynamical tendencies to calculate the evolution of the variables at the following timesteps (subroutine `integrd.F`)
3. Every `iphysiq` dynamical timestep, a call to the interface subroutine (`calfis.F`) with the physical model (`physiq.F`), that calculates the evolution of some of the purely physical variables (e.g: surface temperature `tsurf`) and returns the tendencies ($\frac{\partial X}{\partial t}$) arising from the physical part.
4. Integration of the physical variables (subroutine `addfi.F`)
5. Similarly, calculation and integration of tendencies due to the horizontal dissipation and the *sponge layer* is done every `idissip` dynamical time step.

The physical part can be run separately for a 1-D calculation for a single column using program `testphys1d.F` (see section 4.3).

1.5 Technical structure

A short introduction to the tecnical aspects is given here. For a more detailed explanation please see section 4.1).

1.5.1 Folders structure

LMDZ is organized in a series of folders (see figures 1.5 and 1.6). It has folders for different purposes. At the same time, LMDZ model has been succesfully coupled (see section 4.9) to complex land models like ORCHIDEE (http://orchidee.ipsl.jussieu.fr/), thus in the folder structure of the model also appeared other models as a result of the model coupling.

After a checkout from the repository, one obtains the following list of files and folders:

```
arch/       create_make_gcm*  libf/          offline.def   physiq.def
bld.cfg     gcm.def           makegcm*       orchidee.def  run.def
build_gcm*  guide.def         makelmdz_fcm*  output.def    traceur.def
```

.	
|-- IOIPSL	I/O tools from IPSL
		-- example	examples
		-- src	code source
	`-- tools	tools
|-- LMDZ5	LMDZ version 5 folder
		-- 000-README	general information
		-- BENCH48x36x19	benchmark simulation folder
		-- DefLists	
		-- arch	available compilation architectures
		-- arch.fcm -> arch/arch-local.fcm	file with architecure used during the compilation for fcm
		-- arch.opt -> .void_file	
		-- arch.path -> arch/arch-local.path	file with architecure used during the compilation
		-- bench_lmdz_48x36x19.tar	compressed file with benchmark run files
		-- beta_crf.data	
		-- bin	
		-- config	configuration for the benchmark run
		-- config.fcm	configuration file for the FCM[a] compilation tool
		-- create_make_gcm	utility for the generation of the Makefile
		-- libf	source code
		|-- bibio	seme I/O routines
		|-- cosp	folder with the COSP source
		|-- dyn3d	routines of the dynamical core (serial version)
		|-- dyn3dmem	routines of the dynamical core (shared memory version)
		|-- dyn3dpar	routines of the dynamical core (distributed memory version)
		|-- filtrez	longitudinal filter for polar regions
		|-- grid	dimensions (iim, jjm, llm) in (x, y, z)
		|-- phy1d	1D version of the physical package
		|-- phydev	development version of the physical package
		`-- phylmd	routines of the physical package
		-- libo	
		`-- local_48x36x19_phylmd_seq	
		-- makegcm	Makefile of the model
		-- makelmdz	
		-- makelmdz_fcm	
		-- tmp_src	
	`-- tools	tools folder
		-- fcm	compilation Perl utility
	`-- install_1d_src.sh	shell script to install 1D version of the model
`-- ORCHIDEE	source of the ORCHIDEE[b] model
|-- CVS	subversion folder
|-- patch_orchidee.tar	
|-- src_parameters	paramters
|-- src_sechiba	SECHIBA[c] model
`-- src_stomate	STOMATE model

[a] http://www.metoffice.gov.uk/research/collaboration/fcm/
[b] http://orchidee.ipsl.jussieu.fr/, (Krinner et al., 2005)
[c] (Ducoudré et al., 1993; de Rosnay and Polcher, 1998)

Figure 1.6: Folder structure and main files of the LMDZtesting/modipsl/modeles. Configuration for the test simulation LMDZ5 - BENCH48x36x19 (serial)

(* indicates executables). The eight `.def` are used for the execution of the programs `create_etat0_limit` and `gcm`. The folder `libf` contents the source code in Fortran. The other files:

`arch/  bld.cfg  build_gcm*  create_make_gcm*  makegcm*  makelmdz_fcm*`

are used for the compilation (see section 4.1.5). The folder `arch` has the specific information for the different compilations and machines. Compilation can be done in two different ways. One throughout the scripts `create_make_gcm` and `makegcm` and the other one using the files `makelmdz_fcm`, `bld.cfg` and `build_gcm`.

Usually except for `dyn3d` and `dyn3dpar`, files are the same for the serial and parallel configurations (in particular the physical section is the same)

All the program is written in Fortran. Actually all the physical section is written in the Fortran95 standard. Source files have different terminations according to the compilation processes: `.F` (fix format, with instructions for the pre-process), `.f90` (free format, without instructions for the pre-process), `.F90` (free format, with instructions for the pre-process) or `.h` (include files, usually conformal to the fix and the free format).

The main subroutine that takes into account physical aspects of the simulations is contained in the file called `physiq.F` (see section 1.5.2 and in appendix A).

An schematic representation of the main work-flow of the full model (in `phylmd` version) is given in figure 1.4. In the physics one will found that (see an scheme in figure 1.7):

- There is not an specific separation of schemes. Schemes of the clouds, boundary layer, convection are seen by the model as a whole uniq one.
- I/O processes occur inside the physical subroutine
- Physical subroutine only brings the tendencies of the state-variables to the dynamical core of the model for further integration

1.5.2 LMDZ physiq (phylmd)

All the physics schemes are called from the subroutine `physiq` which is located in the `libf/phylmd/physiq.F` file. A detailed decription of the sections and subroutines called inside the subroutine (in its full fisics version `phylmd`) is provided in figures A.2 and A.3. It is noticed how the subroutine generates the initial and boundary conditions at the first time-step. How it computes the different processes: surface, convection, clouds, radiation, sub-scale orographic effects. And finally if it is the right time-step, it writes the standard output files computing also the required statistics of the fields. Finally, if it is the last time step, it also downwrites the continuation or re-start file for continuous runs.

1.6 LMDZ in the web

Main web page of the model: http://lmdz.lmd.jussieu.fr/

To obtain on-line help (direct connection with the model developers), use the e-mail address: lmdz-svp@lmd.jussieu.fr

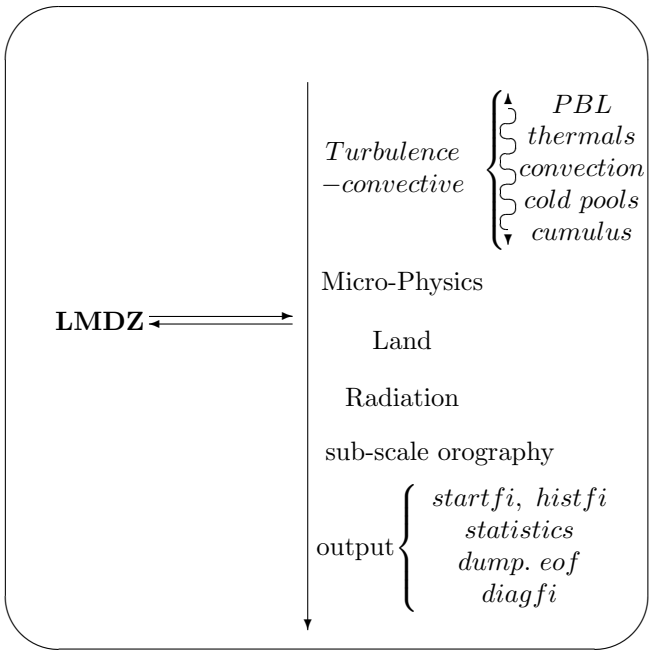

Figure 1.7: Schematic representation of the physics schemes used by LMDZ

Chapter 2

Dynamical core

2.1 Horizontal grid

Dynamics and physics use different grids. Figure 2.2 shows the correspondance and indexing of the physical and dynamical grids as well as the different locations of variables on these grids. To identify the coordinates of a variable (at one grid point up, down, right or left) we use coordinates `rlonu`, `rlatu`, `rlonv`, `rlatv` (longitudes and latitudes, in `radians`).

On the dynamical grid, values at `i=1` are the same as at `i=IM1` as the latter node is a redundant point (due to the periodicity in longitude, these two nodes are actualy located at the same place). Similarly, the extreme `j=1` and `j=JM1` nodes on the dynamical grid (respectively corresponding to North and South poles) are duplicated IM+1 times.

In contrast, the physical grid does not contain redundant points (only one value for each pole and no extra point along longitudes), as shown in figure 2.2. In practice, computations relative to the physics are made for a series of `ngrid` atmospheric columns, where `NGRID`=`IM`x(`JM`-1)+2.

As in other climatic models, variables are distributed along different grids (see figure 2.5).

- In the horizontal:
  - `Mass points`: center of the grid cell; temperature, humidity, geopotential, z-wind
  - `Wind points`: borders of the grid cell (staggered); x-borders for u-wind, y-borders for v-wind
- In the vertical:
  - `Mass points`: middle of the layer; temperature, winds and humidity
  - `z-staggered points`: base/top of the layer; geopotential, vertical velocity

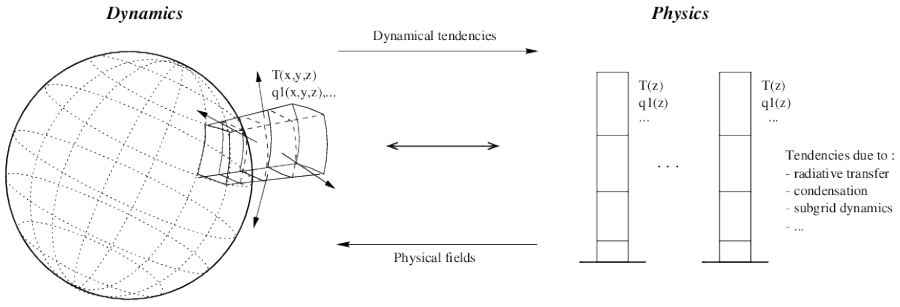

Figure 2.1: Physical/dynamical interface

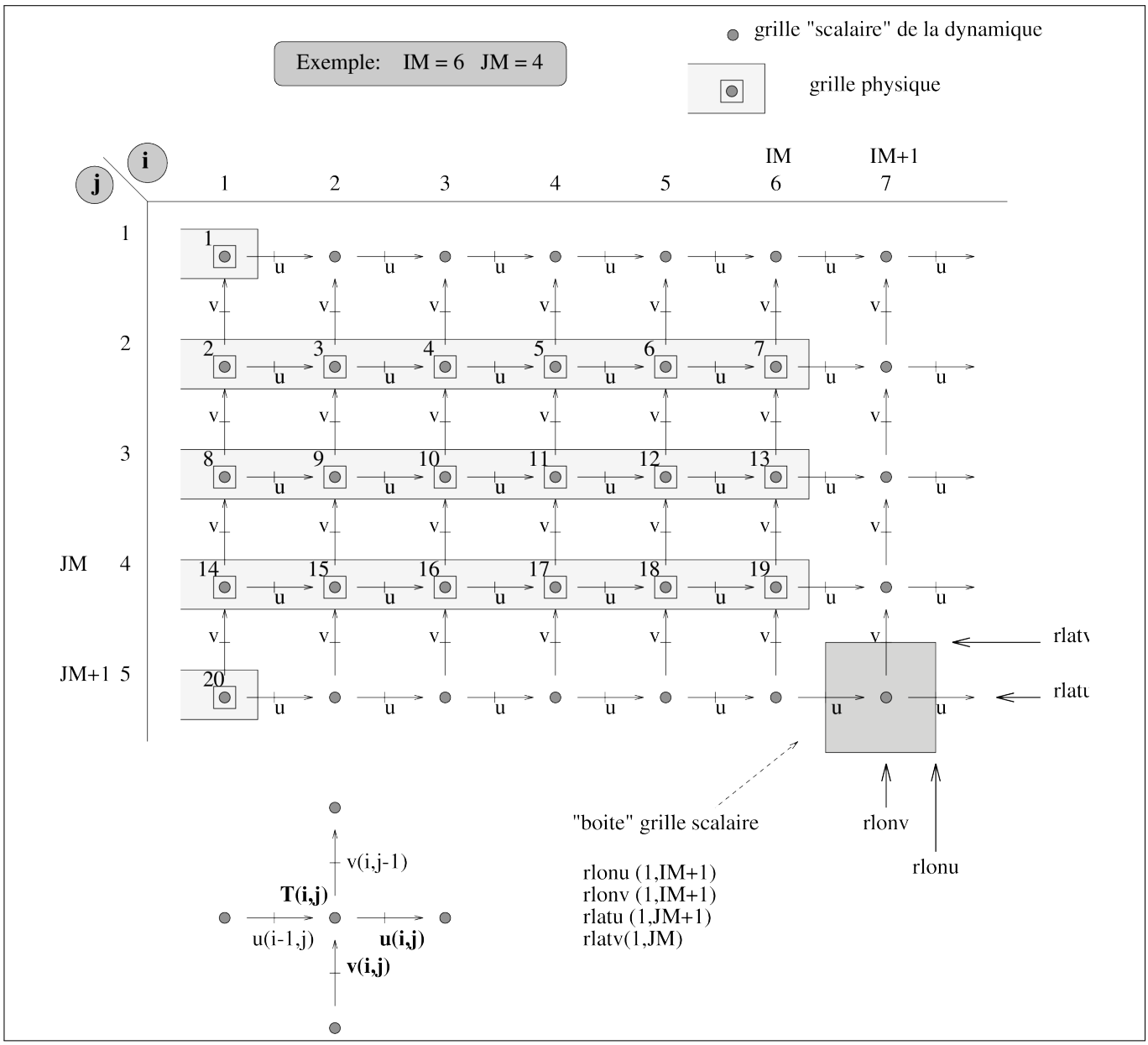

Figure 2.2: Dynamical and physical grids for a 6 × 7 horizontal resolution. In the dynamics (but not in the physics) winds u and v are on specific staggered grids. Other dynamical variables are on the dynamical "scalar" grid. The physics uses the same *scalar* grid for all the variables, except that nodes are indexed in a single vector containing NGRID=2+(JM-1)×IM points when counting from the north pole. N.B.: In the Fortran program, the following variables are used: `iim=IM`, `iip1=IM+1`, `jjm=JM`, `jjp1=JM+1`

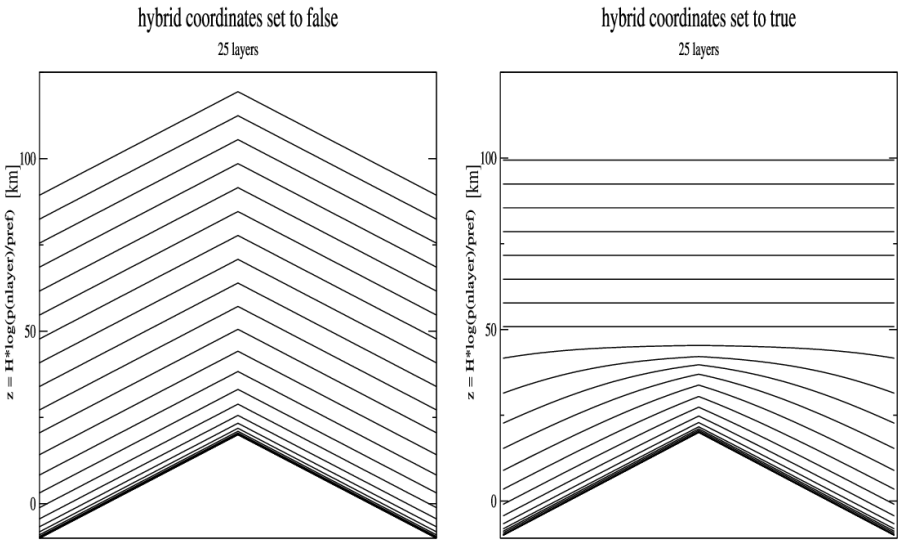

Figure 2.3: Sketch illustrating the difference between hybrid and non-hybrid coordinates

2.2 Vertical grid

The GCM was initially programmed using sigma coordinates $\sigma = p/ps$ (atmospheric pressure over surface pressure ratio) which had the advantage of using a constant domain ($\sigma = 1$ at the surface and $\sigma = 0$ at the top of the atmosphere) whatever the underlying topography.

However, it is obvious that these coordinates significantly disturb the stratospheric dynamical representation as the topography is propagated to the top of the model by the coordinate system. This problem can elegantly be solved by using a hybrid sigma-P (sima-pressure) hybrid coordinate which is equivalent to using σ coordinates near the surface and gradualy shifting to purely pressure p coordinates with increasing altitude.

Figure 2.3 illustrates the importance of using these hybrid coordinates compared to simple σ coordinates. The distribution of the vertical layers is irregular, to enable greater precision at ground level. In general we use 25 levels to describe the atmosphere to a height of 80 km, 32 levels for simulations up to 120 km, or 50 levels to rise up to thermosphere. This has been recently changed and current version of the LMDZ uses 79 levels (version to be used for the CMIP6 exercise).

The first layer describes the first few meters above the ground, whereas the upper layers span several kilometers. Figure 2.4 describes the vertical grid representation and associated variables.

2.2.1 Hybrid coordinate

Vertical coordinate is implicitly defined giving the pressure in the layer l of the model according to:

$$p_l = A_l + B_l p_s \tag{2.1}$$

By this way, vertical coordinate is not directly defined, it is given as the index of the layer starting at 1 at the surface to N a certain altitude of the model.

Close to the surface $A \sim 0$ and $B \sim 1$, while close to the top of the model $A \sim 0$ and $B \sim 0$ with $A >> Bp_s$

2.2.2 Mass of the cells

Pressure levels of the model defined by the relation given in equation 2.1, are defined at the interfaces between layers of the model with $p_1 = p_s$, and $p_{N+1} = 0$ where N is the number of vertical levels in the model. The air mass content

```
DYNAMICS                                              PHYSICS
--------                                              -------
[coordinates ap(),bp()]                               [pressures]

ap(llm+1)=0,bp(llm+1)=0  ****************************  plev(nlayer+1)=0
aps(llm),bps(llm)        .. llm .......... nlayer ...  play(nlayer)
ap(llm),bp(llm)          ****************************  plev(nlayer)
aps(llm-1),bps(llm-1)    .. llm-1 ........ nlayer-1 .  play(nlayer-1)
ap(llm-1),bp(llm-1)      ****************************  plev(nlayer-1)
                             :                 :
                             :                 :
                             :                 :
aps(2),bps(2)            ... 2  ............. 2  ....  play(2)
ap(2),bp(2)              ****************************  plev(2)
aps(1),bps(1)            ... 1  ............. 1  ....  play(1)
ap(1)=1,bp(1)=0          **********surface***********  plev(1)=Ps
```

Figure 2.4: Vertical grid description of the `llm` (or `nlayer`) atmospheric layers in the programming code (`llm` is the variable used in the dynamical part, and `nlayer` is used in the physical part). Variables `+ap`, `bp` and `aps`, `bps` indicate the hybrid levels at the interlayer levels and at middle of the layers respectively. Pressure at the interlayer is $Plev(l) = ap(l) + bp(l) \times Ps$ and pressure in the middle of the layer is defined by $Play(l) = aps(l) + bps(l) \times Ps$, (where Ps is surface pressure). Sigma coordinates are merely a specific case of hybrid coordinates such that $aps = 0$ and $bps = P/Ps$. Note that for the hybrid coordinates, $bps = 0$ above ~ 50 km, leading to purely pressure levels. The user can choose whether to run the model using hybrid coordinates or not by setting variable `hybrid` in `run.def` to `True` or `False`

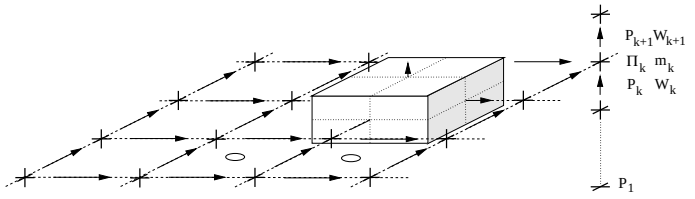

Figure 2.5: Variable distribution in the LMD grid

in a grid of the model comprise between the levels p_k and p_{k+1} is:

$$m_k = a\frac{p_k - p_{k+1}}{g} \tag{2.2}$$

where $a = c_u c_v$ is the air of the grid where the mass:

$$m_k = \frac{a}{g}\left[A_k - A_{k+1} + (B_k - B_{k+1})\, p_s\right] \tag{2.3}$$

2.2.3 Exner function

The calculation of the Exner function $\Pi = C_p p^\kappa$ is here presented. Instead for example of computing Π at the middle of the layer from an extrapolated pressure at the middle of the layer from the level pressures at the interfaces p_k (which is computational expensive), one purpose to use a supplementary relationship between levels p_k and the Exner function which is directly obtained from considerations along different forms of energy inside the atmospheric column (the same considerations which were chosen at the origin of the selection of the relative distribution of the σ and the s levels in the old formulation).

In fact, one important property of the hydrostatic approximation is the proportionality of the content of total, internal and potential energy on a grid cell, for example:

$$\int_0^\infty \Phi \rho dz = \int_0^\infty RT\rho dz \tag{2.4}$$

This relation is not evident in the numerical formulation. But if one selects an appropriate definition for Π, one can ensure the following identity:

$$\sum_{l=1}^{N} \Phi_l m_l - \Phi_s = \sum_{l=1}^{N} RT_l m_l = \sum_{l=1}^{N} \kappa\theta_l \Pi_l m_l \tag{2.5}$$

From the hydrostatic equation 2.30, one can write:

$$\Phi_l = \Phi_s + \sum_{k=1}^{l} \left[\overline{\theta}^z \delta_z \Pi\right]_k \tag{2.6}$$

with the convention (used in the model):

$$\left[\overline{\theta}^z\right]_1 = \theta_1 \tag{2.7}$$

The total gravity potential energy of the column can be therefore written as:

$$\begin{aligned}
\sum_{l=1}^{N} \Phi_l m - \Phi_s &= \sum_{l=1}^{N} m_l \sum_{1\le k\le l} \left[\overline{\theta}^z \delta_z \Pi\right]_k && (2.8)\\
&= \sum_{k=1}^{N} \sum_{k\le l\le N} \left[\overline{\theta}^z \delta_z \Pi\right]_k m_l && (2.9)\\
&= \sum_{k=1}^{N} \left[\overline{\theta}^z \delta_z \Pi\right]_k \times \frac{a}{g} p_k && (2.10)\\
&= \frac{a}{g} \sum_{k=1}^{N} \theta_k \left[\overline{p\delta_z \Pi}^z\right]_k && (2.11)
\end{aligned}$$

with the conventions:

$$\left[\overline{p\delta_z\Pi}^z\right]_1 = \frac{p_2\left(\delta_z\Pi\right)_2}{2} + p_s\left(\delta_z\Pi\right)_1 \tag{2.12}$$

and

$$\left[\overline{p\delta_z\Pi}^z\right]_N = \frac{p_{N-1}\left(\delta_z\Pi\right)_{N-1}}{2} \tag{2.13}$$

Then one can see that the equation 2.5 can be simply satisfied if one selects the levels Π following the relation $\overline{p\delta_z\Pi}^z = \kappa\Pi\delta_z p$ or even:

$$\frac{a}{g}\overline{p\delta_z\Pi}^z = \kappa\Pi m \tag{2.14}$$

Remark: In the old formulation, where the pressure levels were defined by $p = \sigma p_s$ and where one introduced $s = \sigma^\kappa$ at the middle of the layers, the previous relation was simply written as:

$$\left[\overline{\sigma\delta_z s}^z\right]_N = \frac{\sigma_{N-1}\delta_z s_{N-1}}{2} \tag{2.15}$$

and it was precisely used to define the s levels. According to this, the new formulation is exactly equivalent to the old one in the particular case where one choose $B = \sigma$ and $A = 0$ or the definition of the pressure levels.

2.3 Discretization of the Primitive equations

Using the previous discretizations of the space, now we can discretize the equations.

2.3.1 Mass flux

One can then introduce the three components of the mass flux as:

$$U = \overline{m}^X\tilde{u},\ V = \overline{m}^Y\tilde{v} \text{ and } W \tag{2.16}$$

where the vertical mass flux W is defined from:

continuity equation [1]

$$\frac{\partial m}{\partial t} + \delta_x U + \delta_y V + \delta_z W = 0 \tag{2.17}$$

Like in the old version, in order to solve this equation, one starts by the calculation of the accumulated mass convergence from the top of the atmosphere down to the considered level:

$$\Omega_k = \sum_{l=k}^{N}\left(\delta_x U + \delta_y V\right) \tag{2.18}$$

(which can be written in a more synthetic way as $\delta_z\omega = -\delta_x U - \delta_y V$). Convergence at the surface Ω_1 gives access to the evolution of the surface pressure:

$$\frac{a}{g}\frac{\partial p_s}{\partial t} = \Omega_1 \tag{2.19}$$

[1] δ_X notation is used to indicate that the difference is done between two consecutive points following the X direction $\overline{a}^X$ is for the arithmetic mean of the quantity a along the X direction

and finally, knowing that:

$$\frac{\partial m}{\partial t} = -\frac{a}{g}\delta_z B \frac{\partial p_s}{\partial t} = -\delta_z B \Omega_1 \tag{2.20}$$

one obtains integration the continuity equation:

$$-\delta_z B \Omega_1 - \delta_z \Omega + \delta_z W = 0 \tag{2.21}$$

from the top of the atmosphere, just to the k level:

$$1 \tag{2.22}$$

In order to obtain the temporal evolution of the surface pressure from the convergence of the horizontal wind in the column of air. One introduce the temporal derivative of the surface pressure also computed in the equation 2.17:

$$\frac{\partial p_s}{\partial t}\delta_z B + \delta_x U + \delta_y V + \delta_z W = 0 \tag{2.23}$$

then the equation 2.17 is vertically integrated from the top of the model in order to obtain the vertical mass flux at all the levels.

2.3.2 The other equations

Introducing:

Coriolis factor by air at the grid:

$$f = 2\Omega \sin\phi c_u c_v \tag{2.24}$$

where Ω is the planet rotational speed.

absolute potential vorticity:

$$Z = \frac{\delta_x \tilde{v} - \delta_y \tilde{u} + f}{\overline{m}^{X,Y}} \tag{2.25}$$

kinetic energy

$$K = \frac{1}{2}\left(\overline{\tilde{u}\tilde{u}}^{X} + \overline{\tilde{v}\tilde{v}}^{Y}\right) \tag{2.26}$$

movement equations take the following expression:

$$\frac{\partial \tilde{u}}{\partial t} - \overline{Z}^{Y}\overline{V}^{X,Y} + \delta_x\left(\Phi + K\right) + \overline{\theta}^{X}\delta_x \Pi + \frac{\overline{\overline{W}^{X}\delta_z \tilde{u}}^{Z}}{\overline{m}^{X}} = S_{\tilde{u}} \tag{2.27}$$

$$\frac{\partial \tilde{v}}{\partial t} + \overline{Z}^{X}\overline{U}^{X,Y} + \delta_y\left(\Phi + K\right) + \overline{\theta}^{Y}\delta_y \Pi + \frac{\overline{\overline{W}^{Y}\delta_z \tilde{v}}^{Z}}{\overline{m}^{Y}} = S_{\tilde{v}} \tag{2.28}$$

where $\Pi = C_p p^{\kappa}$ is the Exner function at the middle of the grid.

Thermodynamic equation is simply written (like continuity equation):

$$\frac{\partial\left(m\theta\right)}{\partial t} + \delta_x\left(\overline{\theta}^{X}U\right) + \delta_y\left(\overline{\theta}^{Y}V\right) + \delta_z\left(\overline{\theta}^{Z}W\right) = S_\theta \tag{2.29}$$

And finally,

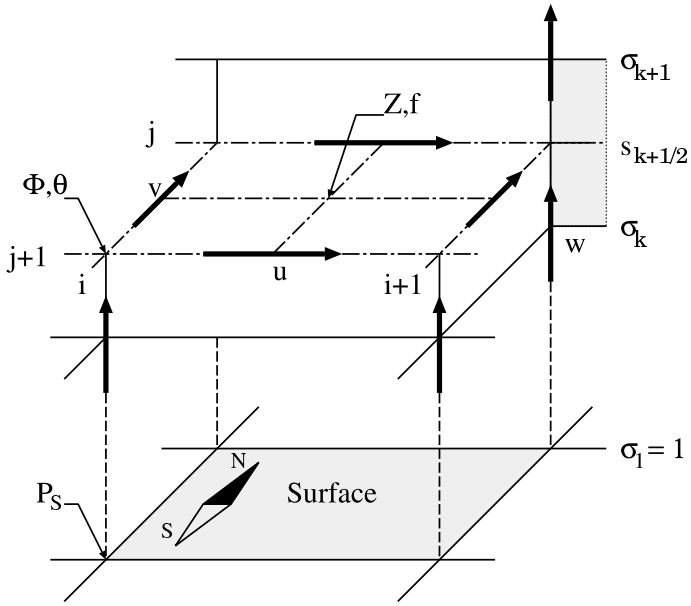

Figure 2.6: Variable distribution in the LMD grid

the hydrostatic equation:

$$\delta_z \Phi = -\overline{\theta}^z \delta_z \Pi \tag{2.30}$$

with $\overline{\theta}^z_1 = \theta_1$ and $\delta_z \Pi_1 = p_s^\kappa - \Pi_1$.

2.4 Temporal integration

Temporal intergration follows a predictor/predictan methodology complemented with a 5-steps (can be changed), Leapfrog scheme in order to ensure enough stability of the model. A schematic representation is given in the figure 2.7

2.5 Advection of tracers

2.6 High latitude filtering

In order to minimize projection problems at the poles, a smoothing filter based on fourier transforms is applied. It can be tunned by the `use_filtre_fft` flag in the `run.def` (see in appendix B.1).

2.7 Dissipation

2.7.1 Horizontal dissipation

In the module `inidissip`, with `ok_strato` the table `zvert` is computed from the function:

$$f(z) = 1 + \frac{\texttt{dissip\_factz} - 1}{2}\left(1 + \tanh\frac{z - \texttt{dissip\_zref}}{\texttt{dissip\_deltaz}}\right)$$

with the default values:

$$\texttt{dissip\_factz} = 4 \quad \text{(without dimension)} \tag{2.31}$$

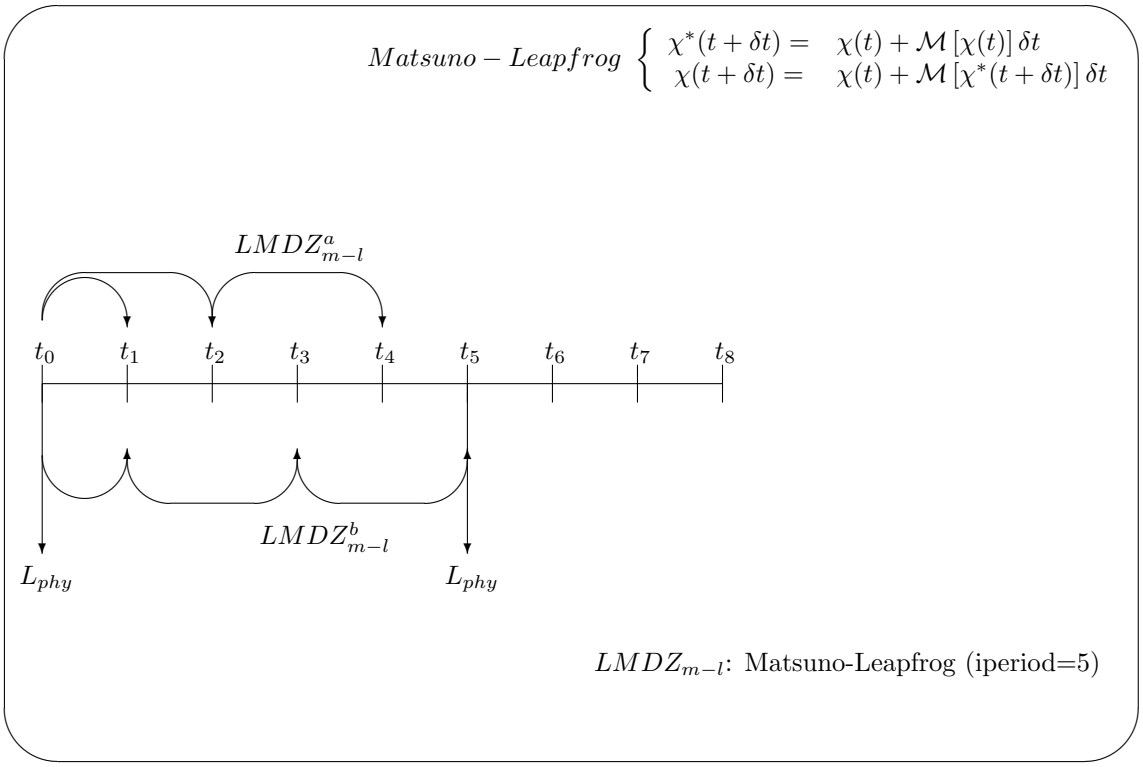

Figure 2.7: Schematic representation of the 'Matsuno-Leapfrog' temporal integration in LMDZ model

$$\texttt{dissip\_deltaz} = 10\ km$$
$$\texttt{dissip\_zref} = 30\ km$$

and $z = (8\ km) \times \ln(p_{\text{ref}}/p)$. The f function is strictly growing on $\mathbb{R}$ from 1 to `dissip_factz`. Its value is $\frac{\texttt{dissip\_factz}+1}{2}$ when the pseudo-high z is `dissip_zref` (see figure 2.8)

2.7.2 Vertical dissipation

2.8 Nudging

Nudging is a technique used to force the model to follow a given known evolution. It is basically controled by a 'relaxation' time (τ) that gives the speed at which the model state (u) should tend to the desired known condition (u_g). In order to avoid strong discontinuities, this technique is usually applied on the tendency terms of the equations. This methodologie is controled by `ffline.def` and `guide.def` files. In order to generate the necessary files for this technique, one should follow:

1. NOT KNOWN, not known, NOT KNOWN

   Exact resolution of:

$$\frac{\mathrm{d}u}{\mathrm{d}t} = -\frac{u - u_g}{\tau} \tag{2.32}$$

with

$$u_g(t) = \gamma t + u_{g0} \tag{2.33}$$

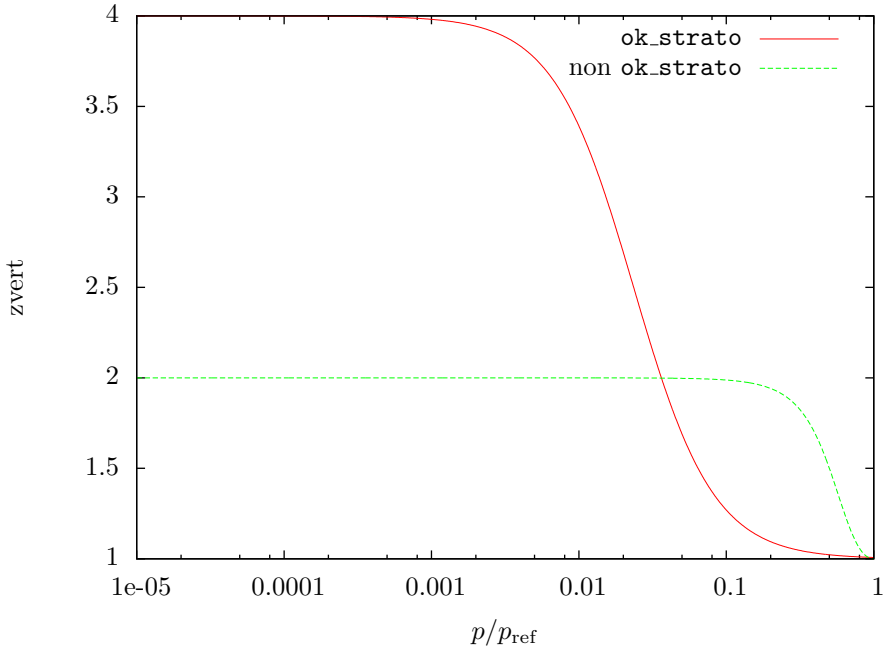

Figure 2.8: Vertical variation of the dissipative coefficient in `inidissip`

where γ, u_{g0} and τ are the known constants. The solution is:

$$u = u_g - \gamma\tau + (u_0 - u_{g0} + \gamma\tau)\exp(-t/\tau) \tag{2.34}$$

Assuming that u_g is linear between $t = 0$ and t_f. Is obtained:

$$\gamma = \frac{u_{gf} - u_{g0}}{t_f} \tag{2.35}$$

If we consider two dates, t and $t + \delta t$, took between $t = 0$ and t_f. We want to write $u(t + \delta t)$ as function of $u(t)$. Tacking the equation 2.34:

$$u(t + \delta t) = u_g(t + \delta t) - \gamma\tau + [u(t) - u_g(t) + \gamma\tau]\exp\left(-\frac{\delta t}{\tau}\right) \tag{2.36}$$

remplacing $u_g(t + \delta t)$ instead of $u_g(t)$:

$$u(t + \delta t) = u_g(t + \delta t)\left[1 - \exp\left(-\frac{\delta t}{\tau}\right)\right] + u(t)\exp\left(-\frac{\delta t}{\tau}\right) - \beta\gamma\delta t \tag{2.37}$$

with:

$$\beta := \frac{\tau}{\delta t} - \left(1 + \frac{\tau}{\delta t}\right)\exp\left(-\frac{\delta t}{\tau}\right) \tag{2.38}$$

β is a function of $\frac{\delta t}{\tau}$, and it can be shown that β is limited between 0 and .3 (see table 2.1). The term γ, inside the equation 2.32, which takes into account the variation of u_g, is not taken in the LMDZ.

2.8.1 Nudging of zonal mean

Assume that u_g has not a temporal dependence. u_g and τ are the known functions of λ. Note the zonal mean as one bar. One has to solve:

$\frac{\delta t}{\tau}$	0	$x_1 \approx 1.8$	$+\infty$
β	0	≈ 0.3	0

Table 2.1: Nuding, variation of β coefficient showing when one have into account the temporal variation of the field towards one wants to nudge (equation 2.38). x_1 is the solution of $e^x = x^2 + x + 1$.

$$(\partial_t u)(\lambda, t) = -\frac{\bar{u}(t) - \bar{u}_g}{\tau(\lambda)} \tag{2.39}$$

Having:

$$\tau' := \frac{1}{\overline{1/\tau}} \tag{2.40}$$

And tacking the zonal mean of 2.39, it is obtained:

$$\frac{\mathrm{d}\bar{u}}{\mathrm{d}t}(t) = -\frac{\bar{u}(t) - \bar{u}_g}{\tau'} \tag{2.41}$$

Where:

$$\bar{u}(t) - \bar{u}_g = (\bar{u}_0 - \bar{u}_g)e^{-t/\tau'} \tag{2.42}$$

Replacing in 2.39, and integrating on time:

$$u(\lambda, t) = u_0(\lambda) + \frac{\tau'}{\tau(\lambda)}(\bar{u}_g - \bar{u}_0)(1 - e^{-t/\tau'}) \tag{2.43}$$

One can re-write this equation between t and $t + \delta t$:

$$u(\lambda, t + \delta t) = u(\lambda, t) + \frac{\tau'}{\tau(\lambda)}[\bar{u}_g - \bar{u}(t)]\left[1 - \exp\left(-\frac{\delta t}{\tau'}\right)\right] \tag{2.44}$$

It is interesting to use the zonal mean nudging with a call depending on the longitude (let's say with a zoom?). If one brings t towards infinity in the equation 2.43, it is obtained:

$$u_\infty(\lambda) = u_0(\lambda) + \frac{\tau'}{\tau(\lambda)}(\bar{u}_g - \bar{u}_0) \tag{2.45}$$

If τ is a constant, then:

$$u_\infty(\lambda) = u_0(\lambda) + \bar{u}_g - \bar{u}_0 \tag{2.46}$$

Meaning that in comparison to u_0, u_∞ is simply uniformly shifted by the zonal mean which should be $\bar{u}_g$. But, if τ is not constant, then the shift at the infinity is not uniform, it can arbitrarily be big at certain longitudes. If we want to illustrate this effect with an example; with a periodic $\tau = 2\pi$, is defined along $[-\pi, \pi]$ by:

$$\tau(\lambda) = \tau_1[1 + 100\exp(-\lambda^2)] \tag{2.47}$$

where τ_1 is any constant, and if:

$$u_0(\lambda) = U\sin(\lambda) + \bar{u}_0 \tag{2.48}$$

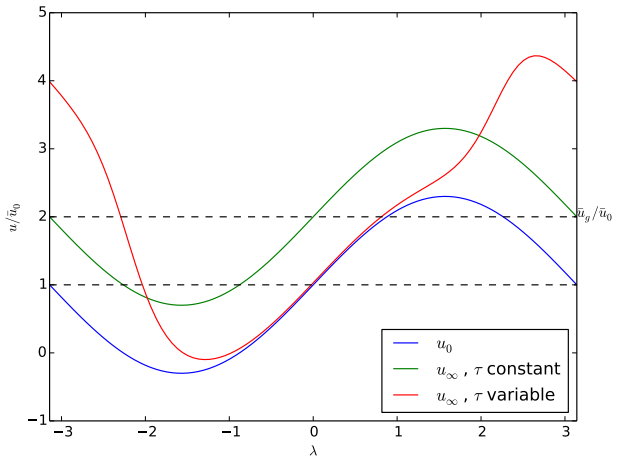

Figure 2.9: Example of zonal nudging. $U/\bar{u}_0 = 1.3$, $\bar{u}_g/\bar{u}_0 = 2$.

then it can be obtained the graphic shown in the figure 2.9, for certain values of U, $\bar{u}_0$ and $\bar{u}_g$.

The zonal nudging with an call depending on the longitude seems to do not have sens. Thus, we restrict in the LMDZ the use of zonal nudging to a grid with a regular distribution of latitudes.

For the fix nudging (`guide_add = .true.`), the equation of evolution is:

$$\frac{\mathrm{d}u}{\mathrm{d}t} = u_g/\tau \tag{2.49}$$

Neglecting the variation of u_g within the nudging time, the solution becomes:

$$u(t+\delta t) = u(t) + u_g \frac{\delta t}{\tau} \tag{2.50}$$

in the module `tau2alpha`, the fixed nudging is taken into account:

$$\alpha = \frac{\delta t}{\tau} \tag{2.51}$$

where on the other cases:

$$\alpha = 1 - \exp\left(-\frac{\delta t}{\tau}\right) \tag{2.52}$$

2.9 Border conditions and control parameters

Pure Earth simulators should not have too many inputs as border conditions. LMDZ is the atmospheric component of the IPSL climate model. In this case it requires different boundary conditions when it is run in the AMIP (externally forced atmospheric model) exercises such as: sea surface temperature, Green Hause Gases concentrations evolution. All these values are provided by the file `limit.nc` (see appendix C.3 for more details).

2.10 Interface between dynamics and physics

2.11 Variables used in the model

2.11.1 Dynamical variables

The dynamical state variables are the atmospheric temperature, surface pressure, winds and tracer concentrations. In practice, the formulation selected to solve the equations in the dynamics (see section 2.3) is optimised using the following less *natural* variables:

`potential temperature`
: θ (`teta` in the code), linked to temperature `T` by $\theta = T(P/Pref)^{-\kappa}$ with $\kappa = R/C_p$ (note that κ is called `kappa` in the dynamical code, and `rcp` in the physical code).

`surface pressure`
: `ps` in the code

`mass`
: the atmosphere mass in each grid box (`masse` in the code).

`the covariant meridional and zonal winds` `ucov` and `vcov`.
: These variables are linked to the *natural* winds by `ucov = cu * u` and `vcov = cv * v`, where `cu` and `cv` are constants that only depend on the latitude.

`mixing ratio of tracers`
: in the atmosphere, typically expressed in kg/kg (array `q` in the code).

`ucov` and `vcov`, *vectorial* variables, are stored on `scalari` grids u and v respectively (staggered points), in the dynamics (see section 2.2).

`teta`, `q`, `ps`, `masse`, *scalar variables*, are stored on the `scalar` grid of the dynamics.

2.11.2 Physical variables

In the physics, the state variables of the dynamics are transmitted via an interface that interpolates the winds on the scalar grid (that corresponds to the physical grid) and transforms the dynamical variables into more *natural* variables. Thus we have winds `u` and `v` (m.s^{-1}), temperature `T` (K), pressure at the middle of the layers `play` (Pa) and at interlayers `plev` (Pa), tracers `q`, etc. (kg/kg) on the same grid.

Furthermore, the physics also handle the evolution of the purely physical state variables:

`co2ice` CO_2 ice on the surface (kg.m^{-2})

`tsurf` surface temperature (K),

`tsoil` temperature at different layers under the surface (K),

`emis` surface emissivity,

`q2` wind variance, or more precisely the square root of the turbulent kinetic energy.

`qsurf` tracer on the surface (kg.m^{-2}).

2.11.3 Tracers

The model may include different types of tracers:

`dust particles`, which may have several modes

`chemical species`, which depict the chemical composition of the atmosphere

`water`, in vapor and ice particles

In the code, all tracers are stored in one three-dimensional array `q`, the third index of which corresponds to each individual tracer.

In input and output files (`startphy.nc`, see details in appendix C.2) tracers are stored seperately using their individual names. Loading specific tracers requires that the approriate tracer names are set in the `traceur.def` file (see in appendix B.5).

Chapter 3

Physics of the terrestrial model

In this section a short explanation of the physics contained in the model is given. Focuse is given on the physical core with which one solves the equations of the atmosphere and the physical packages used to parameterize the sub-scale processes.

Text of this document is partially taken directly (as it is) from the cited articles. Due to the large amount of this kind of text, no distinction with respect author's original one is done.

There is a simplified version of the physics which only computes "Newtoninan radiative equilibrium". Its content is on the folder `phydev`

3.1 PBL, convection and cumulus schemes

In LMDZ a big effort in the turbulent and convection physics of the model has been done. Previous version of the model (known as LMDZ-A Hourdin et al., 2013a) used the Mellor-Yamada pbl scheme (Mellor and Yamada, 1974) in combination with Emanuel's convective one (Emanuel, 1993). In a new set of physics schemes (LMDZ-B Hourdin et al., 2013b) huge modifications have been introduced and in this version (LMDZ v5): on the PBL scheme *'Thermals'* are tacking into account (Hourdin et al., 2002), a new scheme representing cold pools due to precipitating water evaporation (wakes) have been included (Grandpeix and Lafore, 2009) which at the same time a new closure methodology has been introduced in Emanuel's convection (based on sub-clouds processes Grandpeix et al., 2004). All these schemes interact among each other. By this reason, in LMDZ-B there is not such split of three specific schemes (pbl, deep convection and cumulus) such in other models.

All these changes have been reported with a huge positive impact. For example, a better representation of the low level clouds is attained, the daily cycle of precipitation over continents presents a maximum closer to the afternoon fixing a well known bias of the models (see Hourdin et al., 2013b).

Semi-detailed explanation of the schemes will be done following the same scheme as in (Hourdin et al., 2013a).

The new set of parameterizations relies on the separation of three distinct scales for the turbulent and convective subgrid-scale vertical motions:

1. The small scale (10100 m), associated with random turbulence, dominant in particular in the surface layer.
2. The boundary layer height (500 m-3 km) that corresponds to the vertical scale of organized structures of the convective boundary layer.
3. The deep convection depth (1020 km) of cumulonimbus, meso-scale convective systems or squall lines.

The first two scales dominate the vertical subgrid-scale transport in the boundary layer. In the *'B physics'*, the parameterization of this vertical transport relies on the combination of a diffusion scheme for small scale turbulence and a mass-flux model of the organized structures of the convective boundary layer, the so-called (*'thermal plume model' Hourdin et al., 2002; Rio and Hourdin, 2008)*.

3.2 Monitor of the physics

3.3 Planetary Boundary Layer scheme

Main characteristics combination of a:

- eddy diffusion
- *'thermal plume model'*: mass-flux representation of the organized thermal structures of the convective boundary layer

The boundary layer parameterization now relies on the combination of a classical eddy diffusion (Yamada, 1983) with a mass-flux representation of the organized thermal structures of the convective boundary layer, the so-called (*'thermal plume model' Hourdin et al., 2002; Rio and Hourdin, 2008)*. It enables one to represent the upward convective transport in the mixed layer although this layer is generally marginally stable (Hourdin et al., 2002), solving a long recognized limitation of eddy diffusion (Deardorff, 1966). Mass-flux schemes account reasonably well for the organized structures (thermal plumes, or rolls) of the convective boundary layer. Their properties are used in the new model version for coupling with deep convection and also to better parameterize the boundary layer clouds (Rio and Hourdin, 2008; Jam et al., 2013).

The computation of the eddy diffusivity $\mathcal{K}_z$ is based on a prognostic equation for the turbulent kinetic energy, according to (Yamada, 1983). It is mainly active in practice in the surface boundary layer, typically in the first few hundred meters above surface.

The mass flux scheme represents an ensemble of coherent ascending thermal plumes in the grid cell as a mean plume. A model column is separated in two parts: the thermal plume and its environment. The vertical mass flux in the plume $f_{th} = \rho \alpha_{th} w_{th}$ (where ρ is the air density, w_{th} the vertical velocity in the plume and α_{th} its fractional coverage) varies vertically as a function of lateral entrainment e_{th} (from environment to the plume) and detrainment d_{th} (from the plume to the environment):

$$\frac{\partial f_{th}}{\partial z} = e_{th} - d_{th} \tag{3.1}$$

For a scalar quantity q (total water, potential temperature, chemical species, aerosols), the vertical transport by the thermal plume (assuming stationarity) reads:

$$\frac{\partial f_{th} q_{th}}{\partial z} = e_{th} q - d_{th} q_{th} \tag{3.2}$$

q_{th} being the concentration of q inside the plume (air is assumed to enter the plume with the concentration of the large scale, which is equivalent to neglect the plume fraction α_{th} in this part of the computation). The time evolution of q finally reads:

$$\frac{\partial q}{\partial t} = -\frac{1}{\rho} \frac{\partial \overline{\rho w' q'}}{\partial z} \tag{3.3}$$

with

$$\overline{\rho w' q'} = f_{th} \left(q_{th} - q \right) - \rho \mathcal{K}_z \frac{\partial q}{\partial z} \tag{3.4}$$

The vertical velocity w_{th} in the plume is driven by the plume buoyancy $g(\theta_{th} - \theta)/\theta$. The thermal plume fraction is also an internal variable of the model. The computation of w_{th}, α_{th}, e_{th} and d_{th} is a critical part of the code. Detailed tests on two different versions of the e_{th} and d_{th} computation are presented in detail by Rio and Hourdin (2008) and Rio et al. (2010) respectively.

3.4 The model of thermals

Let us consider a vertical profile of potential temperature typical of the Convective Boundary Layer (CBL), with an unstable surface layer (SL) of height z_s, a neutral mixed layer (ML) topped by a stable atmosphere (entrainment zone

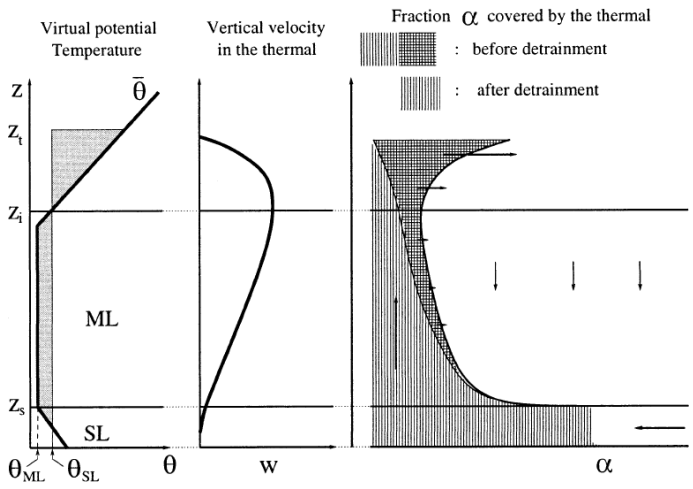

Figure 3.1: Schematic representation of a thermal from (Hourdin et al., 2002)

plus free atmosphere) as shown in Fig. 3.1. Although the entrainment layer may or may not be an inversion layer, we will use the classical notation z_i for the height of the top of the mixed layer (following chapter 1 Stull, 1988).

In this idealized environment, the thermal is introduced as a simple plume of buoyant air coming from the SL. Buoyancy is expressed as the gravity times the relative difference between virtual potential temperature inside and around the thermal plume. The virtual potential temperature is

$$\theta_v = T\left(\frac{p_0}{p}\right)^{\kappa}(1+0.61q) \tag{3.5}$$

where T is the air temperature, $p_0 = 10^5\ Pa$, $\kappa = 0.287$, and q is the specific humidity in $kgkg^{-1}$. In this section, in order to avoid the use of multiple indices, the virtual potential temperature is notified θ.

If the plume does not mix with its environment, its virtual potential temperature is that of the SL, θ_{SL}. If, in addition, the thermal is assumed to be stationary and frictionless, the vertical velocity inside the plume, in absence of phase change of water, is given by

$$\frac{dw}{dt} = w\frac{\partial w}{\partial z} = g\frac{\theta_{SL}-\theta_{ML}}{\theta_{ML}} \tag{3.6}$$

(horizontal pressure differences between the plume and its environment are neglected). The air is uniformly accelerated in the ML until the level where the mean potential temperature $\overline{\theta}(z)$ exceeds θ_{SL}. This level will be retained for definition of z_i. At this level, the square of the vertical velocity w_{max} obtained by vertically integrating Eq. 3.6 over the depth of the CBL is twice the convective available potential energy (CAPE) defined as

$$CAPE = \int_0^{z_i} dz\ g\frac{\theta_{SL}-\theta_{ML}}{\theta_{ML}} \tag{3.7}$$

Above z_i, w is still positive (overshooting) but decreases to finally vanish at the height z_t (top), where

$$\int_0^{z_t} dz\ g\frac{\theta_{SL}-\overline{\theta}}{\overline{\theta}} = 0. \tag{3.8}$$

The integral corresponds to the shaded area on the left-hand side of Fig. 3.1 and the CAPE to that part of the integral below z_i. After reaching z_t, air parcels coming from the plume are heavier than the environment and should sink again. This will not be considered here.

What is required for transport computations is not the vertical velocity but rather the mass flux per unit area, $f = \alpha\rho w$, where α is the fraction of the horizontal surface covered by ascending plumes and ρ is the air density. As a first step, we assume that f is constant within the ML (no detrainment). In order to determine this constant value, it is necessary to invoke the geometry of the thermal cell. Results will depend on geometry of the plume (for further details see Hourdin et al., 2002).

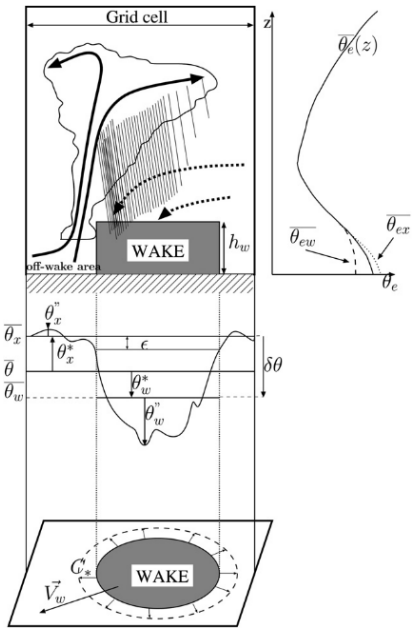

Figure 3.2: Schematic representation of a wake from (Grandpeix and Lafore, 2009)

3.5 Cold pools

The wake model is fully described in Grandpeix and Lafore (2009); Grandpeix et al. (2009). Only a short descriptive view of the scheme is presented here.

The model represents a population of identical circular cold pools (the wakes) with vertical frontiers over an infinite plane containing the grid cell. The wakes are cooled by the convective precipitating downdrafts, while the air outside the wakes feeds the convective saturated drafts (see figure 3.2).

The wake centers are assumed statistically distributed with a uniform spatial density $\mathcal{D}_{wk}$. The wake state variables are their fractional coverage $\sigma_w(\sigma_w = \mathcal{D}_{wk}\pi r^2$, where r is the wake radius), the potential temperature difference $\delta\theta(p)$ and the specific humidity difference $\delta q_v(p)$ between the wake region (w) and the off-wake region (x). $\delta\theta(p)$ and $\delta q_v(p)$ are non zero up to the homogeneity level $p_h = 0.6p_s$ (where p_s is the surface pressure). Above p_h the sole difference between (w) and (x) regions lies in the convective drafts (saturated drafts in (x) and unsaturated ones in (w)).

Wake air being denser than off-wake air, wakes spread as density currents, inducing a vertical velocity difference $\delta w(p)$ between regions (w) and (x) $(\delta w(p) > 0)$. The vertical profile $\delta w(p)$ is imposed piecewise linear. Especially, between surface and wake top (the altitude h_w where $\delta\theta$ crosses zero) the slope corresponds to wake spreading without lateral entrainment nor detrainment.

The wake geometrical changes with time are due to the spread, split, decay and coalescence of the wakes. Split, decay and coalescence are merely represented by imposing a constant density $\mathcal{D}_{wk}$ and by assuming that when σ_w reaches a maximum allowed value $(= 0.5)$ some wakes vanish (i.e. mix with the environment) while others split so that the fractional cover σ_w stays constant. The spreading rate of the wake fractional area σ_w reads:

$$\partial_t \sigma_w = 2\mathcal{C}_* \sqrt{\pi \mathcal{D}_{wk} \sigma_w} \tag{3.9}$$

where $\mathcal{C}_*$, the mean spread speed of the wake leading edges, is proportional to the square root of the *WAke Potential Energy WAPE*: $\mathcal{C}_* = \kappa_* \sqrt{2WAPE}$ and $WAPE = -g \int_0^{h_w} \frac{\delta\theta_v}{\overline{\theta_v}} dz$, where, κ_*, the spread efficiency, is a tunable parameter in the range $1/3 - 2/3$ and θ_v is the virtual potential temperature.

The energy and water vapor equations are expressed at each level yielding prognostic equations for $\delta\theta(p)$ and $\delta q_v(p)$ as well as contributions to the average temperature $\overline{\theta}$ and average humidity $\overline{q_v}$ equations.

The convective scheme is supposed to provide separately the apparent heat sources due to saturated drafts and to unsaturated drafts, which makes it possible to compute the differential heating and moistening feeding the wakes.

At this stage there is not interaction or dynamics among weaks from neighbourg gris points.

3.6 Deep cloud convection

Main characteristics as combination of:

- Emanuel's scheme
- New closure: sub-cloud processes: ALE, CIN, ALP from *'thermal plume model'* and *cold pool* parameterizations

Emanuel (1991) convection scheme is the base for the deep convection in LMDZ, but with a modification in its closure methodology based on the sub-cloud processes. The coupling of the convective parameterization with those of sub-cloud processes is done through the notions of *Available Lifting Energy* (ALE, which must overcome the *Convective INhibition*, or CIN, for triggering) and *Available Lifting Power* (ALP) that controls the convective closure. Both quantities are computed from internal variables of the *'thermal plume model'* and of a new parameterization of the cold pools created by re-evaporation of convective rainfall in the sub-cloud layer (Grandpeix and Lafore, 2009; Grandpeix et al., 2009).

This version uses the buoyancy sorting mass-flux scheme of (Emanuel, 1993), with modified mixing (Grandpeix et al., 2004) and splitting of the tendencies due to saturated and unsaturated drafts. The precipitation efficiency is computed as a function of the in-cloud condensed water and temperature following (Emanuel and Živković Rothman, 1999). It is bounded by a maximum value ep_{max} which is slightly less than unity to allow some cloud water to remain in suspension in the atmosphere instead of being entirely rained out (Bony and Emanuel, 2001).

The ALE allows to overcome the *Convective INhibition* (CIN) so that convection is triggered when $ALE > |CIN|$. The closure consists in prescribing the mass flux M at the top of the inhibition zone as:

$$M = \frac{ALP}{2w_B^2 + |CIN|} \tag{3.10}$$

where w_B is the updraft speed at the level of free convection. The original constant value $w_B = 1m/s$ was replaced by a function of the level of free convection as explained below.

In this version, two processes are taken into account for both ALE and ALP: (1) the ascending motions of the convective boundary layer, as predicted by the thermal plume model and (2) the air lifted downstream of gust fronts. ALE is the largest of the lifting energies provided by the two processes: $ALE = max(ALE_{th}, ALE_{wk})$ where ALE_{th} scales with w_{th}^2 and $ALE_{wk} = WAPE$ (see eq. 3.9). ALP is the sum of the lifting powers provided by the two processes: $ALP = ALP_{th} + ALP_{wk}$ where ALP_{th} scales with w_{th}^3 and ALP_{wk} scales with $\mathcal{C}_*^3$ (see eq. 3.9).

This coupling between cold pools (generated by convection) and convection (triggered in turn and fed by cold pools) allows for the first time to get an autonomous life cycle of convection, not directly driven by the large scale conditions.

There is currently under-development a stochastic convective triggering methode which is being attached to the convection.

3.7 Cumulus scheme

The initial cumulus scheme used in LMDZ is based on the Tiedkte scheme (Tiedtke, 1989). Nowadays is based in Emanuels' scheme (Emanuel, 1993), with a bi-gaussian statistical cloud scheme (Jam et al., 2013).

The fractional cloudiness α_c and condensed water q_c are predicted by introducing a subrid-scale distribution $P(q)$ of total water q so that:

$$\alpha_c = \int_{q_{sat}}^{\infty} dq\ P(q) \tag{3.11}$$

$$q_c = \int_{q_{sat}}^{\infty} (dq\ q - q_{sat}) P(q) \tag{3.12}$$

where $q_{sat}(T)$ is the grid averaged saturation specific humidity in the mesh.

For deep convection (see scheme in figure 3.3), we assume that the subgrid-scale condensation and rainfall can be handled by the Emanuel scheme, so that this statistical cloud scheme is used only to predict the fractional cloudiness for the radiative transfer. Following Bony and Emanuel (2001), the in-cloud water ($q_{inc} = q_c/\alpha_c$) predicted by the convective scheme is used, through an inverse procedure, to determine the variance σ of a generalized log-normal

function bounded at 0. With this particular function, the skewness of $P(q)$ increases with increasing values of the unique width parameter $\xi = \sigma/q$.

For other types of clouds, the statistical cloud scheme is used to compute not only the cloud properties for radiation but also *'large scale'* condensation.

If the thermal plume is not active in the grid box (in practice if $f_{th} = 0$ see equation 3.1), the width parameter ξ of the generalized log-normal function is specified as a function of pressure: $\xi(p)$ increases linearly from 0 at surface to $\xi_{600} = 0.002$ at 600 hPa, then to $\xi_{300} = 0.25$ at 300 Pa. It is kept constant above.

When $f_{th} > 0$ in the grid box, two options are available. Either we use the Bony and Emanuel (2001) procedure to invert the width parameter ξ from the knowledge of the condensed water computed in the thermal plumes (like what is done for deep convection) or we use a new statistical cloud scheme proposed by Jam et al. (2013) in which the sub-grid scale distribution of the water saturation deficit (rather than total water) is parameterized as the sum of two Gaussian functions, representing the variability within and outside the thermal plume respectively. The width of each Gaussian varies as a function of the thermal plume fractional cover α_{th} and of the contrast in saturation deficit between the plume and its environment.

A fraction f_{iw} of the condensed water q_c is assumed to be frozen. This fraction varies as a function of temperature from $f_{iw} = 0$ at 273.15 K to $f_{iw} = 1$ at 258.15 K. The condensed water is partially precipitated. Derived from Zender and Kiehl (1997) formula for an anvil model, the associated sink is

$$\frac{dq_{iw}}{dt} = \frac{1}{\rho}\frac{\partial}{\partial z}\left(\rho w_{iw} q_{iw}\right) \tag{3.13}$$

where $w_{iw} = \gamma_{iw} \times w_0$, $w_0 = 3.29(\rho q_{iw})^{0.16}$ being a characteristic free fall velocity (in m/s) of ice crystals given by Heymsfield and Donner (1990) and γ_{iw} a parameter introduced for the purposes of model tuning (ρ in kg/m^3).

For liquid water, following Sundqvist (1978), rainfall starts to precipitate above a critical value clw (0.6 g/kg in the reference version) for condensed water, with a time constant for auto-conversion $\tau_{convers}$ ($= 1,800$ s) so that

$$\frac{dq_{lw}}{dt} = -\frac{q_{lw}}{\tau_{convers}}\left[1 - e^{-(q_{lw}/clw)^2}\right] \tag{3.14}$$

A fraction of the precipitation is re-evaporated in the layer below and added to the total water of this layer before the statistical cloud scheme is applied. For ice particles, we assume that all the precipitation re-evaporates. For liquid water, following Sundqvist (1988), we assume that

$$\frac{\partial P}{\partial z} = \beta\left[1 - q/q_{sat}\right]\sqrt{P} \tag{3.15}$$

where P is the precipitation flux, and β a tunable parameter.

The effective radius of cloud droplets depends on the aerosol concentration which is specified as a function of space and season as explained by Dufresne et al. (2013) this issue. The effective radius of ice crystals varies linearly as a function of temperature between $er_{iw,max}$ at 0 $°C$ and $er_{iw,min}$ at -84.1 $°C$.

The second point concerns the treatment of stratocumulus. Although some encouraging work is done currently on the thermal plume model in that direction, the current version does not represent properly strato-cumulus clouds. Strato-cumulus are known to be especially prominent at the eastern side of tropical oceans. On the other hand, the Yamada (1983) scheme alone performs quite well for those particular conditions. A kludge is thus introduced in the model, which consists in identifying the atmospheric columns with a sharp temperature inversion at the boundary layer top, and turning off the thermal plume model in those particular cases. In practice, if

$$\frac{T\partial\theta}{\theta\partial p} < -0.08 K/Pa \tag{3.16}$$

then the thermal plume parametrization is arbitrarily switched off. This test is in fact inherited from the standard LMDZ5 model where it was used to switch between two different computations of the Kz coefficient with the same goal of contrasting the regions of strato-cumulus and trade wind cumulus on tropical oceans.

3.8 Large-scale condensation

This section describes `fisrtilp.F90` which computes clouds and precipitation at the large scales.

$$
Cumulus \begin{cases} \begin{matrix} Deep \\ convection \end{matrix} : & Emanuel \ + sub-cloud\ closure \\ other: & statistical,\ \xi \begin{cases} \begin{cases} Emanuel \\ (PDF_{inside} \ + \ PDF_{outside})\,|_{H_2O\ sat.\ deficit} \end{cases} & plume\ active \\ \begin{cases} lin.\ up\ to\ 0.002 & p \geq 600\ hPa \\ lin.\ up\ to\ 0.25 & 600\ hPa\ > p \geq 300\ hPa \\ ct.\ 0.25 & p < 300\ hPa \end{cases} & plume\ inactive \end{cases} \\ \begin{matrix} Strato \\ -cumulus \end{matrix} : & huge\ \frac{T\partial\theta}{\theta\partial p}\ Switch\ off\ plume \end{cases}
$$

Figure 3.3: Schematic representation of the diagram flow for the cumulus parameterization

3.8.1 Variables

The adjustment is done in 4 principal parameteres: on the low level clouds `cld_lc_lsc`, maximum evaporation efficency of the convective precipitation ($\epsilon_{p,max}$), humidty profile $\sigma/\bar{q}$ above 300 hPa `ratqshau` and a correction factor on the downfall speed of the ice of cristal in the stratiform clouds `fallv_lsc`. When the variable `ratqs` is lowered that promotes saturation. The paramter $\epsilon_{p,max}$ is related to ϵ_p which concerns about the efficency of the precipitation. It corresponds to the fraction of condensed water which precipitates in the clouds related to deep convection. Vertical profile $epsilon_p$ it depends either of te pressure or the temperature. $\epsilon_{p,max}$ is used to adjust the model, since it imposes a maximum value on the fraction of precipitated water. An increase on $\epsilon_{p,max}$ lowered the entraintment, thus it diminishes humidity at the top of the toposphere and that of the high clouds.

Explanation of the `fisrtilp.F90` is given following subversion revision 1909.

LMDZ is a model of prediction (Le Treut and Li, 1991) of total water (vapour + cloud water) and of diagnostic for the cloud water and the cloud fraction.

3.8.2 Large-scale saturated water dynamics

A first guess of the saturated humidity q_{sat} is computed. Vertical speeds are computing as function of the mass flux throughout the calculation of `omega` which is based on Tiedtke (1993) convective scheme. Emannuel's convective scheme is continuosly called. Emanuel's scheme has a ice cloud fraction a_{ice} (Bony and Emanuel, 2001), which varies from 0 to 1 and it evolves linearly between only two temperatures. After tat, quantites of mixing between liquid and solid water are computed according to[1]:

$$q_{liq}^{in} = q_c^{in}(1 - a_{ice}) \tag{3.17}$$

$$q_{ice}^{in} = q_c^{in}\ a_{ice} \tag{3.18}$$

After this, the sub-grid cloud fraction and saturated water is computed (see equation 7 from Hourdin et al., 2013b). There are two different ways to compute the width of the distribution: physically (as it is done in Bony and Emanuel, 2001) or statistically (see Jam et al., 2013). A little bit of diffusion is adjusted in order to represet the shallow convection when a strong inversion is present.

Then thermals are called followed by a dry adjustment. Finally width of the sub-grid disribution `ratqs` is computed. Clouds settle in the latest stages of `fisrtilp`.

Other considerations are:

- **Mixed phase:** it is represented in the model by a ice fraction which varies only between two temperatures: [−15°C,0°C] pour LMDz 5 and [−33°C,0°C] for LMDz 6 (based on Doutriaux-Boucher and Quaas, 2004) (see figure 3.4)
- **cristal-ice size:** For the radiation, model uses a relation from (Iacobellis and Somerville, 2000, equation 6) with radius in the 20-60 μm range. Liquid droplets sizes lay between 10 and 15 μm.

[1] Careful, there are other ice fractions: on the deep convection (from Emanuel scheme), large scale (fisrtilp), radiation (newmicro) and saturated downfalls

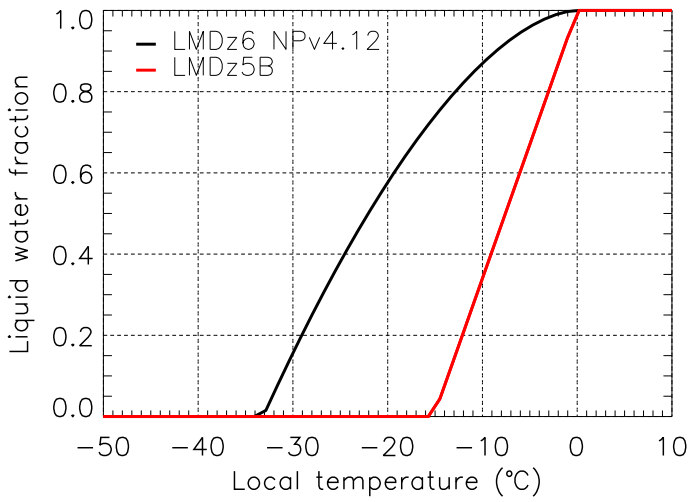

Figure 3.4: Curves of liquid/ice water mixing ratios for different versions of LMDZ

- **cristal-ice speed fall:** Terminal speed of precipitating ice cristals $w_0 = 3.29(\rho q_{iw})^{0.16}$ is taken from airplane measuremnts of ice clouds (see Heymsfield, 1977; Heymsfield and Donner, 1990). It depends on the mass without radius considerations. A distinction is made as function to the tpe of clouds: convective (`fallvc`) or large-scale (`fallvs`). `fallvc` is only used in that grid points within a deep convection region.
- **Mixing saturation ratio:** It is computed following (eq. 2 in Li, 1998).
- **Evaporation of precipitation:** There are two different methods if one takes into account the ice thermodynamics:
  - Without: evaporation amount is computed after Klemp and Wilhelmson (1978) and (section 3.3.1 in Jam, 1998). Ice is completely re-evaporated, and above temperature `t_coup`, mass flux from droplets is set to zero. After this, water vapour (`zq`) is updated and latent heat release is finally computed. Mas flux from ice cristals is set to zero.
    - `zrfl`: mass flux of loquid droplets
    - `zifl`: mass flux of ice cristals
  - With:
- **Precipitation/settlement:** These aspects are kept in `zfroi` given by equation 8 from Hourdin et al. (2013b), by the following equation:

$$\frac{dq_{iw}}{dt} = \frac{1}{\rho}\frac{\partial}{\partial z}(\rho w_{iw} q_{iw});\ where,\ w_{iw} = \gamma_{iw} w_0 \tag{3.19}$$

- **Ice cloud radiative properties:** These properties are computing following Boucher et al. (1995) and for example equation D of Boucher and Lohmann (1995).

3.9 Dry convective adjustment

3.10 Surface interface

3.10.1 f_cdrag_oce

Is a unitless coefficient used in the bulk formula of air-sea turbulent heat fluxes, to account for differences in the neutral exchange coefficients for heat and momentum. Since LMDZ uses the same neutral drag coefficient for momentum and heat fluxes, this `f_cdrag_oce` is multiplied with that neutral drag coefficient to obtain the neutral heat exchange coefficients used in the calculation of the air-sea sensible and latent heat fluxes.

`f_cdrag_oce` was set to 0.8 in IPSL-CM5A and previous versions, in agreement with the empirically-determined C_{DN}/C_{EN} ratio reported in Smith (1988). However, in IPSL-CM5B this was used as a tuning parameter, set to 0.7 to compensate for a tendency for exaggerated evaporation at the sea surface.

Other `f_cdrag`'s of the model are set to 1.

3.11 Tracers in the physics of the model

3.12 Radiation transfer

Two different radiative schemes are available in the model. Basically the old ECMWF radiative scheme (Morcrette, 1991), which is currently being substituted by the new ECMWF radiative scheme labelled RRTM.

3.12.1 Morcrette 1991

Radative scheme in LMDZ is an adapted version from (Morcrette, 1991). At the time of this document is being written, LMD team is working to implement the rrtm scheme (version? rrtm, rrtmg?)

Are there in LMDZ independent vertical layers used for the radiation scheme, or does it use the same ones of the model vertical discretization?

How does LMDZ incorporate the time-evolution of GHG gases? How does it deal with different scenarios?

Is the outputted cloud fraction the same one 'used' by the radiative scheme?

Radiation scheme has suffered different evolutions from a first one (of 1979, EC1) with the interaction between line absorption and scattering using a photon path distribution method to the last version (1989, C3, the implemented one) summarized in table 3.1

The transmission functions τ are computed with the help of an empirical function (Geleyn, 1977) for the reduced (u_r) and unreduced (u) amounts of absorbers (CO_2, CH_4, N_2O, CO and CO_2):

$$-\ln \tau = \frac{au}{\sqrt{1+bu^2/u_r)}} + cu_r \tag{3.20}$$

where cu_r, continuum absorption, coefficients a, b and c incorporate the temperature dependence of the absorption (linearly dependent on 1/T) fitted to the experimental data from (McClatchey et al., 1972; Vigroux, 1953).

Last version of the scheme has evolved from narrow-band models to high spectral resolution (225 spectral intervals in the longwave, 208 in the shortwave) ones. Which have been compared to line-by-line calculations (Scott and Chédin, 1981) and in situ measurements. These detailed models were then degraded by introducing simplifying assumptions, making them more computationally efficient. In that process, the sensitivity of the outputs (fluxes and heating/cooling rates) to the various assumptions have been monitored (Morcrette and Fouquart, 1985, 1986). In the longwave, those studies showed that one of the causes for major systematic errors is the use of wide spectral intervals which tend to overestimate the effects of the strong lines, thus giving a poor representation of the temperature and pressure dependence of the absorption.

Clear-sky longwave fluxes are evaluated with an emissivity method incorporating a parameterization giving a correct representation of the temperature and pressure dependence of the absorption (Morcrette et al., 1986). Clouds are introduced as gray bodies with a longwave emissivity depending on the cloud liquid water path, following (Stephens, 1978).

Table 3.1: Summary of ECMWF radiative scheme characteristics for clear/covered sky and short/longwave spectrum

Sky	wave	characteristic	method
Clear sky		Rayleigh scattering	Parametric expression of the Rayleigh optical thickness
		Aerosol scattering and absorption	Mie parameters for five types of aerosols based on climatological models (WMO, 1984)
	shortwave [a]	Gas absorption	From AFGL 1982 compilation of line parameters
		H_2O	One interval
		Uniformly mixed gases[b]	One interval
		O_3	Two intervals
		H_2O	Six spectral intervals, e- and p-type continuum absorption included between 350 and 1250 cm^{-1}
	longwave [c]	CO_2	Overlap between 500 and 1250 cm^{-1} in three intervals by multiplication of transmission
		O_3	Overlap between 970 and 1110 cm^{-1}
		Aerosols	Absorption effects using an emissivity formulation
Cloudy sky		Droplet absorption and scattering	Employs a delta-Eddington method with τ and w determined from LWP, and preset g and r_e
	shortwave	Gas absorption	Included separately throughout the photon path distribution method
		scattering	Neglected
	longwave	Droplet absorption	from LWP using an emissivity formulation
		Gas absorption	As for clear sky, longwave above

[a] two-stream formulation is employed together with photon path distribution method (Fouquart and Bonnel, 1980) in two spectral intervals (0.25-0.68 & 0.68-4.0 μm)

[b] CO_2, CH_4, N_2O, CO and O_2

[c] Broad-band flux emissivity method with six intervals covering the spectrum between zero and 2620 cm^{-1}. Temperature and pressure dependence of absorption following (Morcrette et al., 1986). Absorption coefficients fitted from AFGL 1982.

Shortwave fluxes are computed using a photon path distribution method to separate the contributions of scattering and absorption processes to the radiative transfer. Scattering is treated with a delta-Eddington approximation. Transmission functions are developed as Padé approximates. Coefficients for the molecular absorption are calculated from the 1982 version of the Air Force Geophysics Laboratory (AFGL) line parameters compilation. Cloud shortwave radiative parameters are the optical thickness and single-scattering albedo linked to the cloud liquid water path, and a prescribed asymmetry factor (Fouquart, 1988). In EC3 a distinction is made between various cloud types by defining the optical thickness as a function not only of the liquid water path in the cloud, but also of the effective radius are r_e of the cloud particles, with r_e varying with height from 5 μm in the planetary boundary layer to 40 μm at 100 hPa. This last feature is an empirical attempt at dealing with the variation of cloud type with height, as smaller water droplets are observed in low-level stratiform clouds, whereas larger particles are found in cumuliform and cirriform clouds. This radiation scheme has already been extensively tested in the ECMWF model (Morcrette, 1990) and was introduced in the operational forecast model on May 2, 1989.

3.12.2 RRTM

New radiative scheme in LMDZ adopts the RRTM version originated from Cycle `CY25R1` of ECMWF.

Table 3.2: Spectral distribution of the absorption by Atmospheric Gases in RRTM. CCl_4 and CFC22 are presented not accounted for in the ECMWF model

Spectral intervals (cm^{-1})	**g-points**	**Gases included**	
		Troposphere	**Stratosphere**
10-250	8	H_2O	H_2O
250-500	14	H_2O	H_2O
500-630	16	H_2O, CO_2	H_2O, CO_2
630-700	14	H_2O, CO_2	O_3, CO_2
700-820	16	H_2O, CO_2, CCl_4	O_3, CO_2, CCl_4
820-980	8	H_2O, CFC11, CFC12	CFC11, CFC12
980-1080	12	H_2O, O_3	O_3
1080-1180	8	H_2O, CFC12, CFC22	O_3, CFC12, CFC22
1180-1390	12	H_2O, CH_4	CH_4
1390-1480	6	H_2O	H_2O
1480-1800	8	H_2O	H_2O
1800-2080	8	H_2O	
2080-2250	4	H_2O, N_2O	
2250-2380	2	CO_2	CO_2
2380-2600	2	N_2O, CO_2	
2600-3000	2	H_2O, CH_4	

Longwave radiation

Since cycle 22R3 of the version ECMWF, two longwave radiation schemes are available, the pre-cycle `22R3` by Morcrette (1991), and the Radiative Radiation Transfer Model (RRTM). LMDZ uses RRTM for longwave radiation by default but we can choose the pre-cycle `22R3` scheme by Morcrette (1991) by setting `LRRTM=.FALSE.` in `suecrad.F90`.

Next text commes from `http://nwmstest.ecmwf.int/research/ifsdocs/CY25r1/pdf_files/Physics.pdf`, (ECMWF, 2002).

As stated in (Mlawer et al., 1997), the objective in the development of RRTM has been to obtain an accuracy in the calculation of fluxes and heating rates consistent with the best line-by-line models. It utilizes the correlated-k methode and shows its filiation to the *Atmospheric and Environmental Research, Inc. (AER)* line-by-line model (LBLRTM Clough et al., 1989, 1992; Clough and Iacono, 1995) through its use of absorption coefficients for the relevant k-distributions derived from LBLRTM. Therefore the k-coefficients in RRTM include the effect of the CKD2.2 water vapour continuum (Clough et al., 1989).

The main point in the correlated-k method (Lacis and Oinas, 1991; Fu and Liou, 1992) is the mapping of the ab- sorption coefficient $k(\nu)$ from the spectral space (where it varies irregularly with wavenumber ν) to the g-space (where $g(k)$ is the probability distribution function, i.e. the fraction of the absorption coefficients in the set smaller than k). The effect of this reordering is a rearrangement of the sequence of terms in the integral over wavenumber in the radiative transfer equation (RTE), which makes it equivalent to what would be done for monochromatic radiation.

In the ECMWF model, no provision is presently taken for scattering in the longwave. Therefore, in order to get the downward radiance, the integration over the vertical dimension is simply done starting from the top of the atmosphere, going downward layer by layer. At the surface, the boundary condition (in terms of spectral emissivity, and potential reflection of downward radiance) is computed, then, in order to get the upward radiance, the integration over the vertical dimension is repeated, this from the surface upward.

The accuracy of absorption coefficients has been established by numerous and continuing high-resolution validations of LBLRTM with spectroscopic measurements, in particular those from the Atmospheric Radiation Measurement program (ARM). Compared to the original RRTM (Mlawer et al., 1997), the version used at ECMWF has been slightly modified to account for cloud optical properties and surface emissivity defined for each of the 16 bands over which spectral fluxes are computed. For efficiency reason, the original number of g-points ($256 = 16 \times 16$) has been reduced to 140 (see table 3.2). Other changes are the use of a diffusivity approximation (instead of the three-angle integration over the zenith angle used in the original scheme) to derive upward and downward fluxes from the radiances, and the modification of the original cloud random overlapping assumption to include (to the same degree of approximation

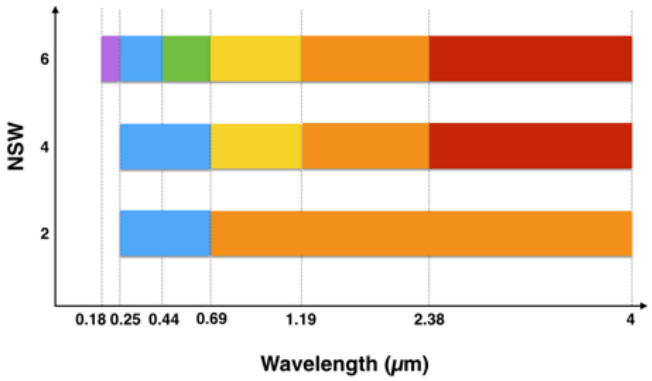

Figure 3.5: Schematic representation of the band-width included in the LMDZ from the RRTM scheme

as used in the operational SW scheme) a maximum-random overlap- ping of cloud layers. Given the monochromatic form of the RTE, the vertical integration is simply carried out one layer at a time from the top-of-the-atmosphere to the surface to get the downward fluxes. The downward fluxes at the surface are then used with the spectral surface emissivities and the surface temperature to get the upward long- wave fluxes in each of the 140 subintervals. Then the upward fluxes are obtained in a similar fashion from the surface to the ToA.

For the relevant spectral intervals of the RRTM schemes, ice cloud optical properties are derived from Ebert and Curry (1993), and water cloud optical properties from Fouquart (1987). Whereas in the operational scheme the cloud emissivity used to compute the effective cloud cover is defined over the whole LW spectrum from spectrally averaged mass absorption coefficients and the relevant cloud water and/or ice paths (following Smith and Lei, 1992), in RRTM, the cloud optical thickness is defined as a function of spectrally varying mass absorption coefficients and relevant cloud water and ice paths, and is used within the true cloudy fraction of the layer. Alternate sets of cloud optical properties are also available for RRTM, based on Savijarvi and Raisanen (1997) for liquid water clouds, and Fu et al. (1998) for ice clouds.

Shortwave radiation

Two shortwave radiation scheme is available like longwave radiation, (Morcrette, 1991) and RRTM. LMDZ uses (Morcrette, 1991) method by default and we can switch on RRTM by choosing `LSRTM=.TRUE.` in `suecrad.F90`. Compared to the previous radiative version of LMDZ, new version can compute up to 6 shortwave bands. The available number of shortwave band is 2,4, and 6 and this can be modified with NSW variable in definition files of LMDZ. The range of shortwave bands are shown in figure 3.5.

3.13 Land scheme

On a full climate simulation, one usually activates the full ORCHIDEE land model, but for some other purposes there is a simple bucket scheme.

3.13.1 Bucket scheme

It is a two layer (2m deep) land model for temperature and precipitation. Moisture content follows a saturation scheme based on a β parameter.

3.14 Ocean scheme

On a full climate simulation, one usually couple LMDZ with the full NEMO ocean model, but for some other purposes there is a simple ocean surface scheme and a shallow water one.

3.14.1 Surface ocean

3.14.2 Shallow water ocean

3.15 Aerosols

The LMDZ model can take into account both aerosol–radiation and aerosol–cloud interactions, the latter in a very simplified way. Aerosol effects are managed in the LMDZ configuration files (i.e. physiq.def) through a number of flags: `aerosol_couple`, `flag_aerosol`, `flag_aerosol_strato`, `aer_type`, `new_aod`, `ok_ade` and `ok_aie`. When one runs LMDZ without the aerosol-chemistry INCA module, the flag `aerosol_couple` must take the value `.false.` (in practice `aerosol_couple = n`). In such case, the model uses pre-calculated monthly tropospheric aerosol climatologies and the flag `flag_aerosol` takes control over which aerosols are used. It can take the following values:

0: Without aerosols

1: Only sulphate

2: Only black carbon (BC)

3: Only organic material (POM)

4: Only sea salts

5: Only dust

6: All aerosols

With `flag_aerosol > 0`, the model needs input files with aerosol monthly concentrations. In any of the previous given cases the file `aerosols.nat.nc` is needed and corresponds to natural (i.e. pre-industrial) aerosols. Another flag labelled `aer_type` is needed in order to determine which aerosol period is taken into account. If `aer_type` has the value '`preind`', then the pre-industrial aerosol concentrations are used and only the file `aerosols.nat.nc` is needed (see its content un appendix C.6). If the flag takes the value '`actuel`', the model uses a typical modern (e.g. representative of years 1980) aerosol climatology with the file `aerosols1980.nc`. If the flag takes the value '`scenario`', then the aerosols become scenario dependent with a filename like `aerosolsXXXX.nc` and a resolution of 10 years. And finally if the flag takes the value '`annuel`', then the aerosols are for a given particular year and the input file has a name of `aerosols[YYYY].nc` where `[YYYY]` is the running year. This will be referred to as the total aerosol in contrast to the natural aerosol of the `aerosols.nat.nc` file.

One can additionally impose a monthly climatology of stratospheric aerosol with the flag `flag_aerosol_strato`. In that case the model expects a file named aerosol.strat.nc. The previous flag `aer_type` does not apply to stratospheric aerosol and the user needs to be careful with the management of the input files.

Monthly aerosol climatologies are available at a few horizontal and vertical resolutions for both tropospheric and stratospheric aerosols. However they need to be interpolated to non-standard grids. Note that in LMDZ5, an L39 model can digest L19 aerosol climatologies. In that case the interpolation is done online.

With the flag `new_aod` one selects the "new" parameterization of the optical depth of the aerosols. This option is activated by default and it is no longer needed in the `config.def`. One should be aware that the old optical depth of the aerosols (`new_aod=n`) is not compatible with the flag `flag_aerosol=1` (only sulphates). This is an old option which is not recommended and not further described here.

In the case where `flag_aerosol > 0`, the two flags `ok_ade` and `ok_aie`, with possible values `y` and `n`, control the aerosol-radiation interactions (i.e. the direct effect) and aerosol–cloud interactions (i.e. the indirect effect), respectively. Switching on or off one of these two effects control whether natural or total aerosols are used for that effect. The flags `ok_ade` and `ok_aie` are actually independent from each other. Importantly `flag_aerosol` should be `>0` in case one or both of the two flags `ok_ade` or `ok_aie` is activated, which at the same time activates the diagnostics of the radiative forcing (e.g. variables `topswad` and `topswai`).

In the case where `ok_aie` is activated, one needs to choose the explicit calculation of the cloud droplets concentration (CDNC) with the flag `ok_cdnc=y`. On the contrary, if `ok_aie` is not activated, one can choose either `ok_cdnc=y` (where CDNC is then explicitly computed from an empirical relation which is aerosol dependent) or `ok_cdnc=n` (in which case an effective radius is directly computed). `bl95_b0=1.7` and `bl95_b1=0.2` correspond to the parameters of the

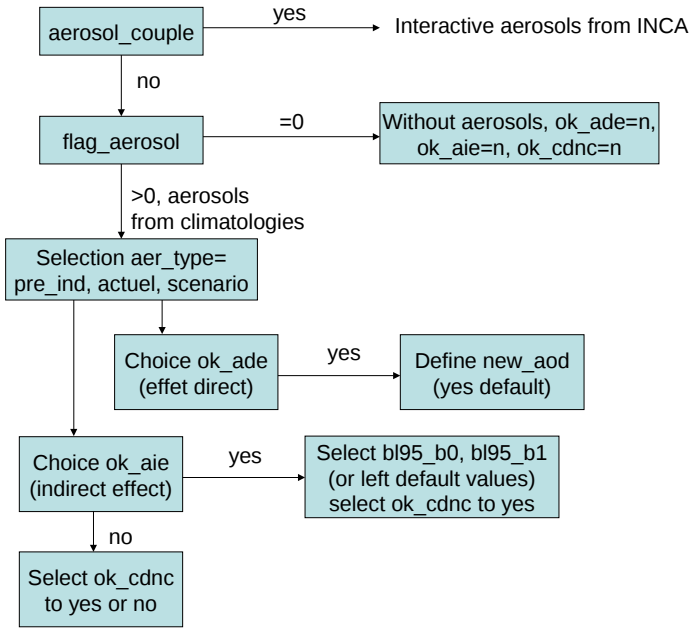

Figure 3.6: Flow diagram of the flags used in LMDZ to manage the aerosol effects in LMDz

relationship between aerosol mass concentration and CDNC, following the original parameterisation of Boucher and Lohmann (1995).

Experts users might want to compute the direct and indirect effects of the aerosols but nevertheless remove the aerosol effects when advancing the model from one time step to the next. In that case the aerosols are purely diagnostic and do not influence the model's meteorology. In order to make it possible, it is necessary to activate `flag_aerosol > 0` and define `ok_ade`/`ok_aie` as one desires, and set the variable `AEROSOLFEEDBACK_ACTIVE` to `.false.` inside the subroutine `sw_aeroAR4.F90`. This requires of course to recompile the model.

The flag `aerosol_couple` should be set to '`y`' in order to take into account the interactive aerosols from the INCA model. For historical reasons, there are several sets of aerosol optical properties used to compute aerosol–radiation interactions (i.e. the direct effect). If the old radiation scheme is used (`rrtm=0`), aerosol optical properties are computed in the INCA module for interactive aerosols (`aerosol_couple=y`) but in phylmd for climatological aerosols (`aerosol_couple=n`). However the parametrisations are similar.

For aerosol–radiation interactions (i.e., the aerosol direct and semi-direct effects), aerosol optical properties are prescribed for each aerosol species. These properties vary spectrally and are available for the old radiation scheme (non RRTM) on two bands and have been revised for the new radiation scheme (`rrtm=1`). In this case there is now a single routine for both `aerosol_couple=y` and `aerosol_couple=n`. The effects in the longwave are not accounted for for tropospheric aerosols and are only accounted for for stratospheric aerosols in the case `rrtm=1`. The calculations of aerosol optical properties use the methodology of Reddy et al. (2005) but the values have been updated. They vary as a function of waveband and relative humidity.

Figure 3.6 shows the diagram flow of the different flags used in LMDZ to manage the effects of aerosols.

3.16 Subgrid-scale orography

Effects of subgrid-scale orography (SSO) are accounted for both through drag and lifting effects on the obstacles and through generation and propagation in the atmosphere of gravity waves (Lott and Miller, 1997).

The assumption is that the mesoscale flow dynamics can be described by two conceptual models, whose relevance depends on the non-dimensional height of the mountain, viz.

$$H_n = \frac{NH}{|U|} \tag{3.21}$$

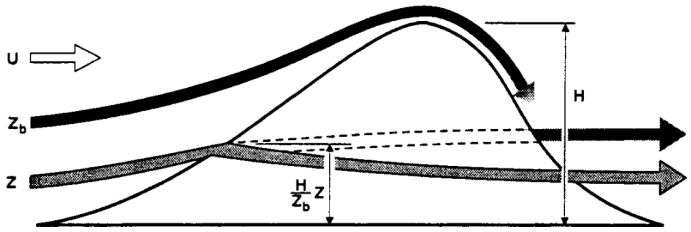

Figure 3.7: Schematic representation of the drag introduced by a mountain from (Lott and Miller, 1997)

where H is the maximum height of the obstacle, U is the wind speed and N is the Brunt-Väisälä frequency of the incident flow (see figure 3.7).

At small H_n, all the flow goes over the mountain and gravity waves are forced by the vertical motion of the fluid. Suppose that the mountain has an elliptical shape and a height variation determined by a parameter b in the along-ridge direction and by a parameter a in the cross-ridge direction, such that

$$\gamma = a/b \leq 1 \tag{3.22}$$

then the geometry of the mountain can be written in the form

$$h(x,y) = \frac{H}{1 + x^2/a^2 + y^2/b^2} \tag{3.23}$$

In the simple case when the incident flow is at right angles to the ridge the surface stress due to the gravity wave has the magnitude

$$\tau_w = \rho_0 b \mathcal{G} \mathcal{B}(\gamma) N U H^2 \tag{3.24}$$

provided that the Boussinesq and hydrostatic approximations apply. In Eq. 3.24 $\mathcal{G}$ is a function of the mountain sharpness (Phillips, 1984), and for the mountain given by Eq. 3.23, $\mathcal{G} \approx 1.23$. The term $\mathcal{B}(\gamma)$ is a function of the mountain anisotropy, γ, and can vary from $\mathcal{B}(0) = 1$ for a two-dimensional ridge to $\mathcal{B}(1) = \pi/4$ for a circular mountain.

At large H_n the vertical motion of the fluid is limited and part of the low-level flow goes around the mountain. The depth, Z_b, of this blocked layer, when U and N are independent of height, can be expressed as

$$Z_b = H max\left(0, \frac{H_n - H_{nc}}{H_n}\right) \tag{3.25}$$

where H_{nc} is a critical non-dimensional mountain height of order unity. The depth Z_b can be viewed as the upstream elevation of the isentropic surface that is raised exactly to the mountain top (Fig. 3.7). In each layer below Z_b the flow streamlines divide around the obstacle, and it is supposed that flow separation occurs on the obstacle's flanks. Then, the drag, $\mathcal{D}_b(z)$, exerted by the obstacle on the flow at these levels can be written as

$$\mathcal{D}_b(z) = -\rho_0 C_d l(z) \frac{U|U|}{2} \tag{3.26}$$

Here $l(z)$ represents the horizontal width of the obstacle as seen by the flow at an upstream height z, and C_d, according to the free streamline theory of jets in ideal fluids, is a constant having a value close to unity (Kirchoff, 1877; Gurevich, 1965). According to observations, C_d can be nearer 2 in value when suction effects occur in the rear of the obstacle (Batchelor, 1967). In the proposed parametrization scheme this drag is applied to the flow, level by level, and will be referred to as the drag of the 'blocked' flow, $\mathcal{D}_d$. Unlike the gravity-wave-drag scheme, the total stress exerted by the mountain on the 'blocked' flow does not need to be known *a priori*. For an elliptical mountain, the width of the obstacle, as seen by the flow at a given altitude $z < Z_b$, is given by

$$l(z) = 2b\sqrt{\frac{Z_b - z}{z}} \tag{3.27}$$

In Eq. 3.27, it is assumed that the level Z_b is raised up to the mountain top, with each layer below Z_b raised by a factor H/Z_b (Fig. 3.7).This will lead, effectively, to a reduction of the obstacle width, as seen by the flow when compared with the case in which the flow does not experience vertical motion as it approaches the mountain. Then applying Eq. 3.26 to the fluid layers belowZ_b, the stress due to the blocked-flow drag is obtained by integrating from $z = 0$ to $z = Z_b$, viz.

$$\tau_b \approx C_d \pi b \rho_0 Z_b \frac{U|U|}{2} \tag{3.28}$$

However, when the non-dimensional height is close to unity, the presence of a wake is generally associated with upstream blocking and with a downstream Foehn (e.g. Fig. 3.7). This means that the isentropic surfaces are raised on the windward side and become close to the ground on the leeward side. If we assume that the lowest isentropic surface passing *over* the mountain can be viewed as a lower rigid boundary for the flow passing over the mountain, then the distortion of this surface will be seen as a source of gravity waves, and since this distortion is of the same order of magnitude as the mountain height, it is reasonable to suppose that the wave stress will be given by Eq. 3.24, whatever the depth of the blocked flow, Z_b, although it is clearly an upper limit to use the total height, H. Then, the total stress is the sum of a wave stress, τ_w, a blocked-flow stress whenever the non-dimensional mountain height $H_n > H_{nc}$, i.e.

$$\tau \approx \tau_w \left\{ 1 + \frac{\pi C_d}{2\mathcal{G}\mathcal{B}(\gamma)} max\left(0, \frac{H_n - H_{nc}}{H_n^2}\right) \right\} \tag{3.29}$$

The addition of low-level drag below the depth of the blocked flow, Z_b, enhances the gravity-wave stress term in Eq. 3.29 substantially. Two pair of correct values when compared with two numerical experiments would be $C_d = 2$, $H_{nc} = 0.4$ and $C_d = 1$, $H_{nc} = 0.75$. In the later case, the smaller value of C_d is probably related to the reduction of upstream blocking in three-dimensional simulations. A larger H_{nc} corresponds to a reduction of the nonlinear effects due to the three-dimensional dispersion of the mountain waves. In the scheme, these effects are partly taken into account by allowing the value of C_d to vary with the aspect ratio of the obstacle, as in the case of separated flows around immersed bodies (Landweber, 1961), while at the same time setting the critical number H_{nc} equal to 0.5 as a constant intermediate value. Note also that for large H_n, Eq. 3.29 overestimates the drag in the three-dimensional case, because the flow dynamics become more and more horizontal, and the incidence of gravity waves is diminished accordingly. In the scheme a reduction of this kind in the mountain-wave stress could have been introduced by replacing the mountain height given in Eq. 3.24 with a lower 'cut-off' mountain height, $H(H_{nc}/H_n)$. Nevertheless, this has not been done in the parametrization scheme partly because a large non-dimensional mountain height often corresponds to slow flows for which the drag given by Eq. 3.29 is then, in any case, very small.

3.17 Stratosphere physics

Chapter 4

LMDZ: Use

A more detailed infomation about the real use of the model is here provided

4.1 Input/Output

In order to run the model a set of different files are needed while others will be created:

- input files:
  - configuration files: `config.def`, `gcm.def`, `run.def`, `traceur.def`, `physiq.def`
  - initial conditions: `startphy.nc`, or `restartphy.nc` if is a *restart* simulation
  - boundary conditions: `limit.nc`
  - aerosols: `aerosols[YYYY].nc`, `aerosols.XXXXXX.nc`
- output files:
  - full configuration files: `used_config.def`, `used_gcm.def`, `used_run.def`, `used_traceur.def`, `used_physiq.def`
  - output files: `histins.nc`, `histday.nc`, `histmonth.nc`
  - restart file: `restartphy.nc`
  - parameters: `paramLMDZ_phy.nc`
  - tracers: `histrac.nc`

4.1.1 State variables and input/output from the physics

Like all the NetCDF files of the GCM, are constructed on the same model. They contain:

- a header with a `controle` variable followed by a series of variables defining the (physical and dynamical) grids
- a series of non temporal variables that give information about surface conditions on the planet.
- a `time` variable giving the values of the different instants at which the temporal variables are stored (a single time value (t=0) for start, as it describes the dynamical initial states, and no time values for `startphy.nc`, as it describes only a physical state).

headers The headers of the input files always begin with a `control` variable (see in appendix C.3), that is allocated differently in the physical and dynamical parts. The other variables in the header concern the (physical and dynamical) grids. They are the following:

- the horizontal coordinates
  - `rlonu`, `rlatu`, `rlonv`, `rlatv` for the dynamical part,

  - `lati`, `long` for the physical part,

- the coefficients for passing from the physical grid to the dynamical grid
  - `cu`,`cv` only in the dynamical header
- and finally, the grid box areas
  - `aire` for the dynamical part,
  - `area` for the physical part.

Surface conditions The surface conditions are mostly given in the physical NetCDF files by variables:

- `phisfi` for the initial state of surface geopotential,
- `albedodat` for the bare ground albedo,
- `inertiedat` for the surface thermal inertia,
- `zmea`, `zstd`, `zsig`, `zgam` and `zthe` for the subgrid scale topography.

For the dynamics:

- `physinit` for the initial state of surface geopotential

Remark: variables `phisfi` and `physinit` contain the same information (surface geopotential), but `phisfi` gives the geopotential values on the physical grid, while `physinit` give the values on the dynamical grid.

Physical and dynamical state variables To save disk space, the initialization files store the variables used by the model, rather than the *natural* variables.

- For the dynamics:

  `ucov` and `vcov` the covariant winds
  These variables are linked to the *natural* winds by
  `ucov = cu * u` and `vcov = cv * v`

  `teta` the potential temperature,

  or more precisely, the potential enthalpy linked to temperature `T` by $\theta = T\left(\frac{P}{Pref}\right)^{-K}$

  the tracers,

  `ps` surface pressure.

  `masse` the atmosphere mass in each grid box.

- *Vectorial* variables `ucov` and `vcov` are stored on *staggered* grids u and v respectively (in the dynamics) (see section 2.2).
- Scalar variables `h`, `q` (tracers), `ps`, `masse` are stored on the *scalar* grid of the dynamical part.
- For the physics:

  `co2ice` surface dry ice,

  `tsurf` surface temperature,

  `tsoil` temperatures at different layers under the surface,

  `emis` surface emissivity,

  `q2` wind variance,
  or more precisely, the square root of the turbulent kinetic energy.

  - the surface *tracer* budget (kg m^{-2}),

- All these variables are stored on the *physical* grid (see section 2.2).

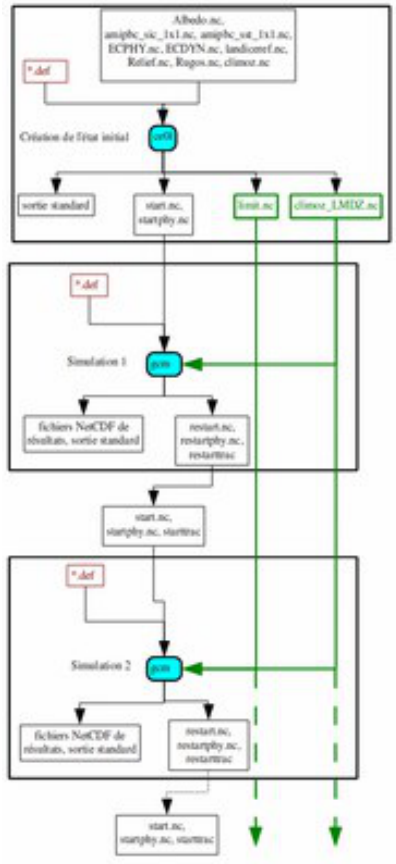

Figure 4.1: Schematic representation of the generation of the initial and control conditions

4.1.2 Real case initialization: ce0l

The executable file `ce0l` creates the files for the initial and the limit conditions at the desired resolution. It uses a given general files from which it interpolates the required data to run the model (see and scheme on figure 4.1). All this files can be found in `http://www.lmd.jussieu.fr/~lmdz/LMDZ_Init/`. These files are:

- `amipbc_sic_1x1.nc`: sea-ice fraction (`sic` variable, from AMIP II project)
- `amipbc_sst_1x1.nc`: sea-surface temperature (from AMIP II project)
- `Rugos.nc`: seasonal climatologies of the roughness length (excluding the topographic contribution). Obtained from NASA
- `Relief.nc`: it contains the global topography data-set (usually U.S. Navy 10-Minute Global Elevation and Geographic Characteristics[1]). There is a version with a correction of the topography at the Antartide[2]
- `Albedo.nc`: albedo data-set from Y. Polcher
- `ECDYN.nc, ECPHY.nc`: Re-analysis files for a given period at 1° of resolution

[1] `http://rda.ucar.edu/datasets/ds754.0/`
[2] `http://lmdz.lmd.jussieu.fr/documentation/guides/short-guide/utilisation-comme-boite-noire-1/overview/Relief-nc.gz`

4.1.3 Ozone tracer

Independently from the type of ozone file used by the radiative transfer, it is possible to introduce a tracking algorithm for the ozone, with a given pre-scribed parameterization. Chemical parameterization has been updated by D. Cariolle and H. Teyssèdre (Cariolle and Teyssèdre, 2007).

Required parameters are given in a netCDF file called `coefoz_v2_8.nc`. It corresponds to the 2.8 version of the Cariolle & Teyssèdre parameterization. This file contains the fields at pressure levels, latitude and month of the year. `ce0l` will re-grid the fields at the given resolution and for each day. In order to do that, one should rename `coefoz_v2_8.nc` to `coefoz.nc`, which should be in the `ce0l` execution folder. `traceur.def` should include a line for the ozone in the following form (remember to increase the total number of tracers, first line in the file):

```
10 10 O3
```

`ce0l` wil produce a file called `coefoz_LMDZ.nc`. This file should be included in the folder where the simulation will be run. `ce0l` will also provide an initial ozone state for the tracking of the ozone (in the `start.nc` file). This initial state will correspond with the reference distribution included in `coerfoz.nc`.

Evolution of the ozone will be keep in the file `histrac.nc` with the other tracers.

4.1.4 Ozone

Ozone field is contained in the variable `wo`. This variable is used in the procedure `physiq` and it is declared in the module `phys_state_var_mod`. At the first pass through into `physiq`, the procedure `phys_state_var_init` is used to initialize `wo`. If the model is not coupled to INCA (see reference 4.9.3, `wo` is: only modified by `ozonecm` or by reading of a file (see figure 4.2).

Reading of a file which contains the ozone field

The starting point is a NetCDF file with the ozone field distributed as function of the latitude, pressure and month of the year. Latitudinal and pressure grids can be anyone. Ozone field is interpolated by LMDZ in latitude and time in `ce0l` (see reference 4.1.2). Temporal re-griding is done by a linear interpolation generating the values for each 360 part of year from the monthly values. Vertical re-grding is done after in `gcm` (see section 1.1). It is seen so, that the effect of the temporal variation of the surface pressure at a given 360 part of the year is neglected (see figure 4.3).

File readed by `ce0l` should be called by `climoz.nc`. `ce0l` creates a new NetCDF file: `climoz_LMDZ.nc`.

Justification of one coding option

By the temporal interpolation done in `ce0l`, we allow to have an input file with 12 or 14 months[3]

An other option would be to allow 12 months in `climoz.nc` and to read three files `climoz.nc` in `ce0l`: a complete year, December only in another file and January only as the last file. This would simplify the coding of the files `climoz.nc` and complicate coding in `ce0l`: it would systematically require three files of climatologies as input, where two might eventually be symbolic links towards the third.

Program `gcm` reads `climoz_LMDZ.ncm`, which should contain the ozone molar fraction as function of the latitude, pressure and date. Grid in latitude should be already the same as the one in `gcm`. Date is given as an index taken between 1 and 360, independently of the calendar used in `gcm`. When a 360 days calendar is used, it corresponds to each day of the year, for another calendar, index corresponds to a 360th of the year.

At each pass through the procedure `physiq`, as function of the current date, we will decide which state of the ozone do we require, that means, which index from the 360th. This value of the index is kept in `ro3i` from `physiq`. The name `ro3i` means 'required ozone index'. Thus, `ro3i` is copmuted at each pass in `physiq` (this variable is not kept). Another ozone variable inside `physiq`, `co3i` keeps the temporal index of the ozone field which is already in the variable `wo`. The name `co3i` stands for 'current ozone index'. `co3i` is initialized at 0 during the compilation and this value is recognized as meaning that `wo` has still not been defined.

In order to compute `ro3i`, we consider L as the length of the actual year and t the passed time after the start of the year. (t is the exact length, a priori not the exact number of days, see figure 4.4)

Then we have:

[3]See in the LMDZ site: Accueil → Documentation → Guides → LMDZ pas à pas → Utilisation comme boîte noire → http://lmdz.lmd.jussieu.fr/documentation/guides/short-guide/utilisation-comme-boite-noire-1/le-champ-dozone.

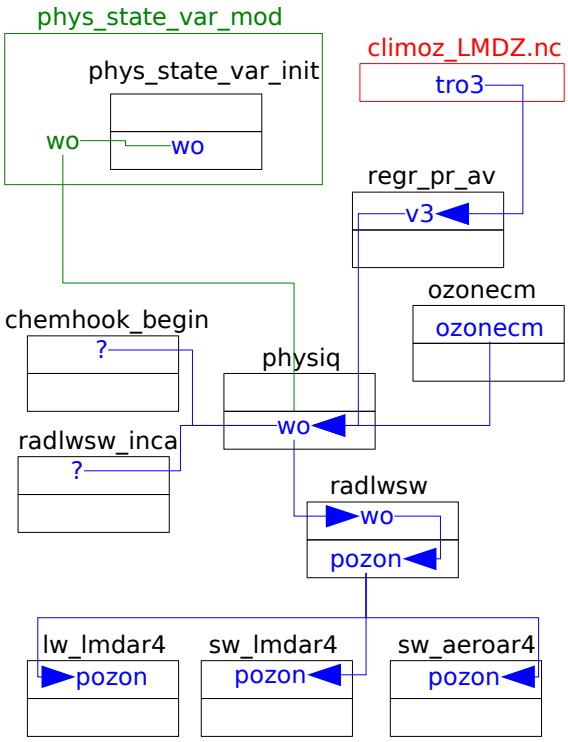

Figure 4.2: Flux of the variable `wo`, which contains the ozone field. A rectangle can correspond to a procedure, module or file. Green color is associated to the modules, black to procedures and red to the files. A procedure is represented by the piling up of two rectangles: the top one is the interface of the procedure, meanwhile bottom rectangle contains local data. A module's variable is green at module level. A module variable used or defined by a procedure, is the seen within the procedure by use (known as 'use association') or by descent ('host association') and re-written at the level of this procedure in blue. The other variables than the ones of the module are also in blue. If the procedure is a function, then in the interface, the name of the function is retaken to designate its result. A blue line marks a reading or writing in a file or affectation. A green line marks an association by use or descent. An arrow at one or other end of the line marks the sens of the data transfer (some transfers can be done in both sens)

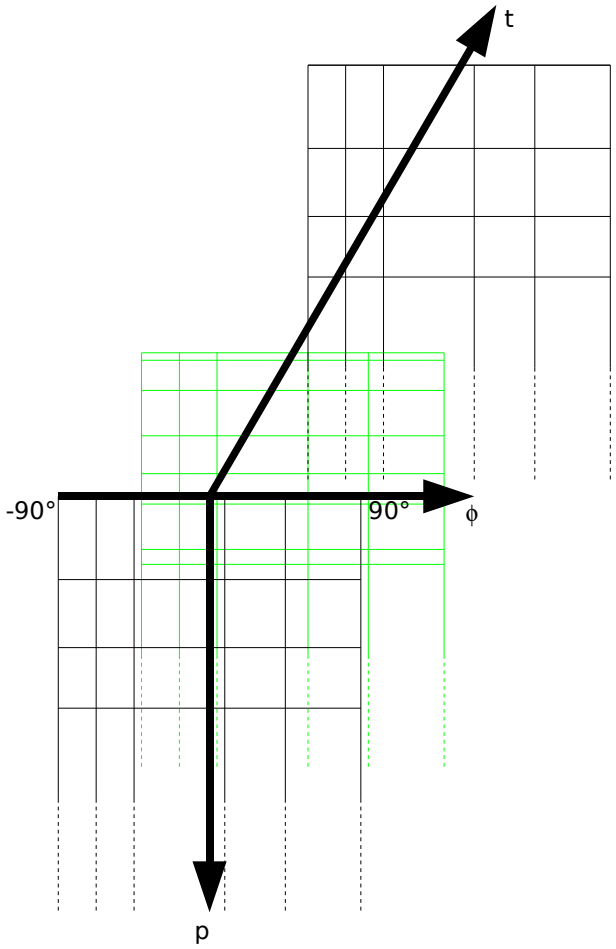

Figure 4.3: Re-griding of the ozone field by LMDZ. Re-griding by mean in latitude and pressure. Temporal linear interpolation. Monthly values (black) are taken as the values at the middle of the month. In green the re-grid latitude-pressure at a given intermediate day. Re-grid in latitude is the same at all dates. Pressure re-grid changes each day

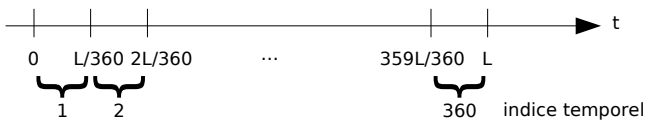

Figure 4.4: Temporal ozoe index as function of the time passed after the start of the year

$$\texttt{ro3i} = E\left(\frac{t}{L/360}\right) + 1 \tag{4.1}$$

where E is the entire part. In theory $t < L$ since $\texttt{ro3i} \leq 360$. In `physiq`, we add a test for the case where $t/L \times 360$ would give by rounding a value higher or equal to 360. In `physiq`, t is given by:

```
days_elapsed + jh_cur - jh_1jan
```

and L is given by `ioget_year_len(year_cur)`. These two expressions are the days.

The variable `jh_cur` in `physiq` has a status of private OpenMP variable, thus, we also privatize `co3i` (and `ro3i`).

Program `gcm` does not read one time all the 360 states of the ozone. It reads the state when it requires, which that happens at each 360th of the year.

4.1.5 Compilation

Some details about the compilation with `makelmdz_fcm`.

- pre-process macros are partially chosen inside the script `makelmdz_fcm`, and the rest in the configuration file `arch.fcm`
- Selected macros for the `makelmdz_fcm` are contained in the variable `CPP_KEY`
- Selected macros for the `arch.fcm` are contained in the variable `FPP_DEF`
- In the file `blg.cfg`, one read which two ensemble of macros are used for the pro-processor:

  ```
  bld::tool::fppkeys    %CPP_KEY %FPP_DEF
  ```

- `makelmdz_fcm` choose macros according to the configuration of the program independently of the compiler.
- For the default configuration (that means only with the option `arch` in the command line), `makelmdz_fcm` selects the following macros: `CPP_IOIPSL` and `CPP_PHYS` Spatial resolution of the model is specified in the file `grid/dimensions.h`. `makelmdz_fcm` creates the file `dimensions.h` using the script `grid/dimension/makdim`

Description of all the options of compilation for the `makelmdz_fcm` (not completed):

- `-arch`: which architecture file should be used (in `arch` folder)
- `-mem`:
- `-parallel`: which kind of parallel compilation: `mpi`, distributed memory; `omp` shared memory; `mpi_omp`, shared and distributed memory
- `-d`: dimensions of the domain `[dimx]x[dimy]x[dimz]`
- `-j`: copmilation style `8`, compilation is done using all the available cpus in the machine (it makes simulatenous compilation of the code, making the processes much more faster)

4.2 configuration files

LMDZ is configured throughout the use of different ASCII files `[ver].def` located at the same folder where the simulation is run. They attain different aspects of the configuration of the model, from period and domain of simulation to which values should be given to different constants inside the physical schemes.

A brief detail of the values inside these files is given with an attempt to keep track the meaning of certain values according to the equations described from the schemes.

See appendix B.3, B.1

4.3 one-column

"In the last decades, single-column models have become a central tool for the development and evaluation of physical parameterizations. In this approach, the coupling between the local atmospheric column and large scale dynamics is replaced by an imposed forcing: surface fluxes or temperature, large-scale advection of heat and moisture plus radiative heating if not computed interactively. A number of case studies have been developed addressing in particular convection and clouds. The case studies are often derived from field campaign experiments for which a lot of in-situ or remote sensing observations are available." (Hourdin et al., 2013b).

In this configuration, the physical parameterizations are the same in 3D and 1D model. 1D model is very quick and easy to run. We used this framework to develop new parameterizations (see for example Bechtold et al., 2000) used in some of CMIP5 runs (IPSL-CM5B).

Installation and use of the 1D model that is associated with LMDz and its concurrent use with the 3D model. There are two main differences between the 1D and 3D models: firstly, the 1D model is more 'homemade' than the 3D one (it has been designed just for that and it's an ideal tool to fiddle with). Switching from 1D to 3D can then be done with few changes so that the 1D install script can run with several 3D versions. Installing the model itself is done in a similar way than for the 3D model except that you have to install the 3D model before installing the 1D one.

4.3.1 Compilation and execution

Installation is done throughout the run of the `instal1d.sh` script which is available from `http://www.lmd.jussieu.fr/~lmdz/DistribG95/instal1d.sh`. First step is to get the script and to run it blindly (don't forget to change rights and allow execution) in the same directory you ran `install.sh`.

The script should run smoothly without errors. While running the script, which may take a few minutes, you'll see messages corresponding to the download of various elements via `wget` or informational messages from the compiler. The script ends with the execution of 6 test simulations: arm_cu, rico, sandufast, fire, twpice, amma, with 2 different options of the physics: NPv3.2 and NPv5.0. At the end and if everything goes well, a pdf file appears with the results (`rneb` & `precip`) of all cases.

4.3.2 Available cases

In directory `LMDZtesting`, one should find at the same level than modipsl, a directory 1D/CAS in which are different directories with 1D test cases (see table 4.1):

In directory `LMDZtesting/modipsl/modeles/LMDZ5/libf/phylmd`: it's the same directory than for 3D. It contains files necessary to run the 1D model (main program `lmdz1d.F`, various routines concerning forcing for each case and some modifications allowing to 'force' some part of the model).

In the following diagram (figure 4.5), you can visualize where are stored the files characteristic of each case (latitude, longitude, type of surface, albedo, ...), the control files of different physics (`*def` files) and the results.

In order to run a case, one has to execute `LMDZtesting/1D/run.sh` changing:

- `listecas`: you choose the list of cases you are interested in
- `listedef`: you choose one or several physics

There is not yet a clear standard format for the files used as input data for the 1D simulations. It is currently being on an exercise to standardize current ASCII files to NetCDF files. A good example of an ASCII file, would be the one from the `amma` case. An almost finished NetCDF would be the one provided for the `cindynamo` case.

4.4 Aqua-planets

For academic studies one can run the model in an aqua-planet model (Earth only with sea sruface). Main boundary coindition of this kind of simualtions is the sea surface temperature which follows standard distributions (Held and Suarez, 1994). This configuration is usefull to anlayse the dynamics of the model under a highly controlled and simplified 3D conditions.

Initial conditions are internally generated throught a series of subroutines araound the `iniaqua` procdure. It is activated when one selects `iflag_phys` (above 100).

Table 4.1: Input data for the 1D LMDZ cases

case	description	references
amma	diurnal cycle of convection over land in semi-arid conditions	(Lothon et al., 2011; Couvreux et al., 2012)
arm_cons		
arm_cu	1 day continental cumulus	http://www.knmi.nl/samenw/eurocs/
ayotte	dry convection	(Ayotte et al., 1996; Hourdin et al., 2002)
case_e	7 days squall line during Toga_Coare	(Bechtold et al., 2000)
cindynamo	Dynamics of Madden Julian Oscillation	
dice	Diurnal land/atmosphere coupling case	http://appconv.metoffice.com/dice/dice.html
eq_rd_cv	radiative-convective equilibrium	
fire	diurnal cycle of stratocumulus	(Chlond et al., 2004; Duynkerke and Teixeira, 2001)
gabls4	boundary layer with strong stability with a snow surface in the Antarctica	http://www.cnrm.meteo.fr/aladin/meshtml/GABLS4/GABLS4.html
hapex92_init	10 days squall line over ouest Africa	(Grandpeix et al., 2009)
ihop	distribution of water vapor and improving the prediction of convection	
rico	2 days oceanic cumulus	http://www.knmi.nl/samenw/rico/
sandufast	transition case from stratocumulus to cumulus, fast option	http://www.mpimet.mpg.de/en/mitarbeiter/irina-sandu/transition-cases.html
sanduref	reference option	
sanduslow	slow option	
toga	4 monthes of Toga_Coare campaign	(Bechtold et al., 2000)
twpice	3 weeks during TWP-Ice campaign	http://acrf-campaign.arm.gov/twpice/

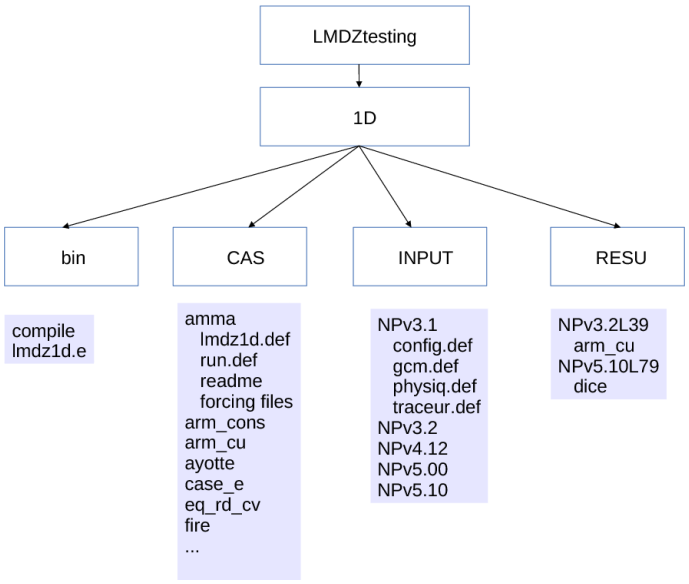

Figure 4.5: Diagram of the simulation of 1D case with the LMDZ model

Table 4.2: EXample of scheme card of the LMDZ5 physics B (NPv3.1)

scheme	**LMDZ-B**
radiation	ECMWF rad
pbl	Mellor and Yamada + Thermal plume model
convection	Emanuel + modified mixing and modified closure (ALP, ALE, CIN) + cold pool (wake)
clouds	Bonny and Emanuel statistical + prediction from subgrid-scale distribution of cloudiness and condensed water + statistical water saturation deficit model
micro-physics	$\emptyset$
land	SECHIBA/ORCHIDEE
others	Subgrid-scale orography (SSO)

4.5 Terra-planets

Recently a terra-planet version of the the model has also been developed. In this configuration, there is not water bodies in the surface of the planet.

4.6 Physics versions

From the appendix tables D.1 to D.17, the changes on the configuration `.def` files from one LMDZ version to the following one are provided. This is presented in an consecutive way. These means, that only that changes occurred from one version to the following one are provided. These different versions have been use to develop the model and 10-years runs with each version have been carried out. Doing it in this climatological way, one ensures that the model does not have strong biases or deficiencies.

The series of versions are the following ones

1. `AR4.0:` repository version r1818, June 2013
2. `NPv3.1:` r1818, June 2013
3. `NPv4.12:` r2009
4. `NPv412bis:`
5. `NPv412OR11:`
6. `NPv412qsat:`
7. `NPv412tglaceOff:`
8. `NPv416:`
9. `NPv417:`
10. `NPv418:`
11. `NPv5.01:` r2251, November 2014

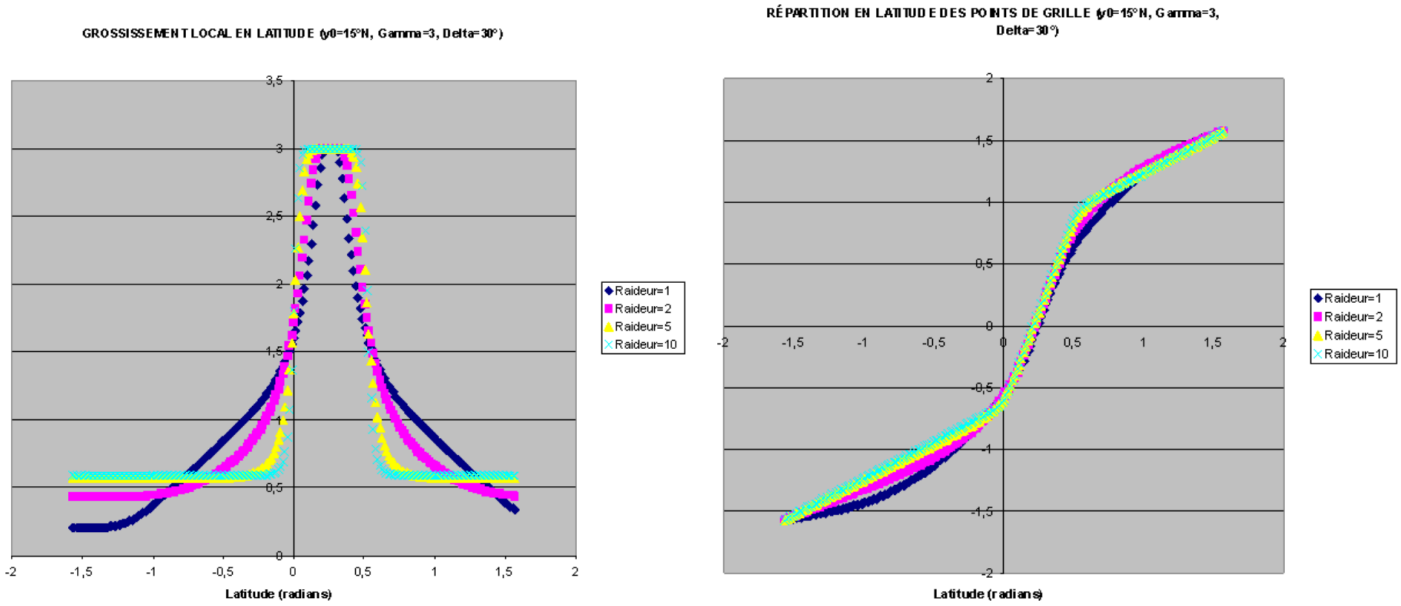

Figure 4.6: Re-finning distribution (left) and pseudo-latitude (Y, right) as function of latitude, for a zoom in latitude centered at 15° N, re-finning $\gamma = 3$, and window $\delta = 30°$ as function of different rigidity factors $\tau = 1, 2, 5, 10$

4.7 Zoom

In order to allow the re-refinement of the LMDZ simulations without increasing the computational cost of the simulations, a zoom capability has been added in the LMDZ GCM model (in fact the 'Z' stands for Zoom). Basically the idea is to increase grid resolution over a given area without increasing the number of grid points. This will produce a redistribution of the longitudes and latitudes.

Zoom (or coordinate stretching) of the LMDZ model is defined independently for each direction, longitude by x and latitude by y, according to 4 parameters:

1. x_0, and/or y_0: Abscissa of the center of the zoom (in radians)
2. γ: Scale factor at the center of the zoom (in relation to the sam, by regular grid)
3. δ: width of the zoom window (in radians)
4. τ: rigidity of the transition from the center to the outside of the zoom

Stretching functions are based on connexions among hyperbolic tangents, from which one can obtain relatively uniform resolutions inside and outside of the zoom.

One should notice that γ and δ are not independent, since one should not deform too much the grid outside the zoomed region: this degradation (in comparison to the original grid) is at the order of $(2\pi - \gamma\delta)/(2\pi - \delta)$ in longitude, or $(\pi - \gamma\delta)/(\pi - \delta)$ in latitude. One reasonable limit would be to have more than the half of the number of the points within the zoom. This condition limits the following thresholds at each direction:

$$\left.\begin{array}{ll} \gamma\delta < \pi & longitude \\ \gamma\delta < \pi/2 & latitude \end{array}\right\} \tag{4.2}$$

which provides a maximum degradation around $\pi/(2\pi - \delta)$ outside the zoom. Condition 4.2 is only enough for an infinity rigidity of the transition. One will see (see figures 4.6 and 4.7), that we need to be more strict if we are using strong refinements with small rigidities.

One will notice also that transition between inner and outside regions will be much faster than τ when it is large. The standard rigidity of the transition is around 1. Deformation effects due to variations into the resolution along the borders of the zoomed window will be more marked for larger rigidities.

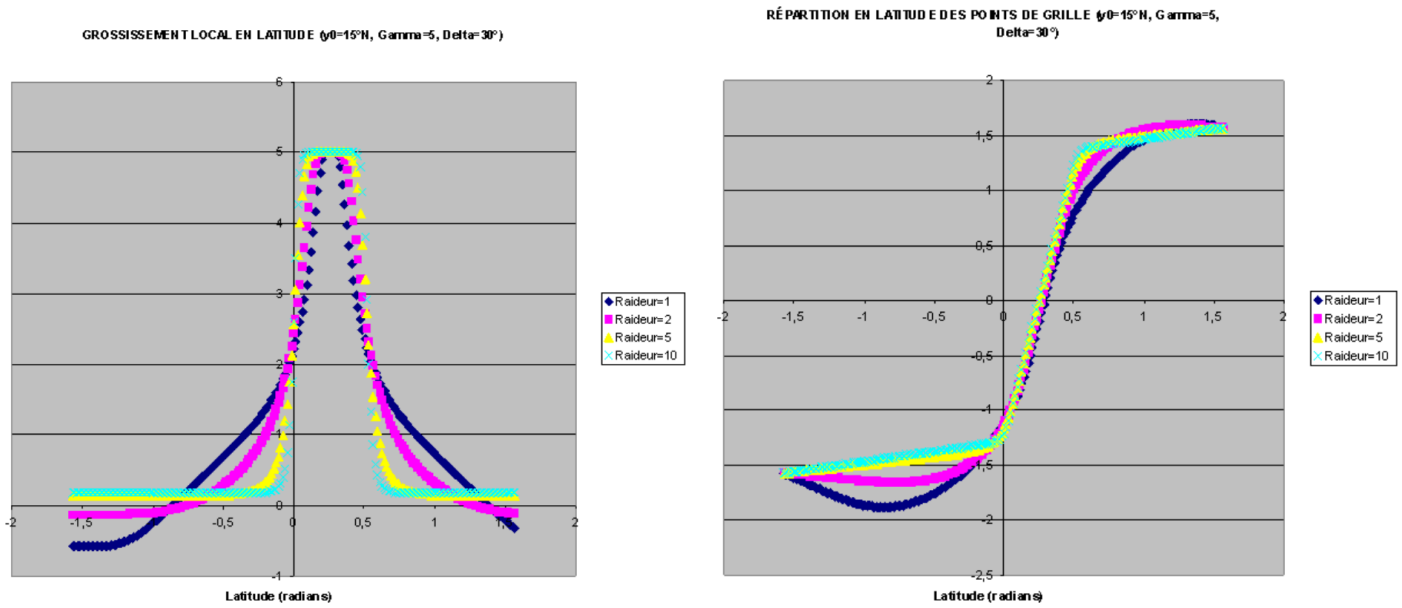

Figure 4.7: As in figure 4.6, but with a re-finning $\gamma = 5$. One can not accept $\tau = 1, 2$ since we obtain negative refinements outside the zoom window

In order to avoid the introduction of large degradations to the approximations, the structure of the zoom will be defined throughout analytical applications. In order to obtain quasi-uniform resolutions inside and outside the zoom window (and consequently at the transition zones), refinement will be based on series of hyperbolic tangents (tanh). Inside and outside the zoomed window correspond to the tangent to the asymptotes of tanh which varies littlely. We define:

$$\mathcal{T}(x) = \tanh(x);\ (-\infty < x < +\infty);\ \left\{ \begin{array}{c} \mathcal{T}(-\infty) = -1 \\ \mathcal{T}(+\infty) = 1 \end{array} \right. \tag{4.3}$$

In order to make easier the notation, we will also use the Heavisyde function ($\mathcal{H}$) in order to re-define the intervals or to re-sort the indices.

$$\mathcal{H}(x) = \left\{ \begin{array}{ll} 0 & x \leq 0 \\ 1 & x > 0 \end{array} \right. \tag{4.4}$$

Zoom on the longitude

Reference longitude will be taken within the range $(-\pi, +\pi)$, longitude origin is located at the center of the grid. We start by the definition of a new longitude $\tilde{x}$ centered at the center of the zoom: $\tilde{x}_0 = 0,\ -\pi < \tilde{x} < \pi$. It is related to the original longitude by:

$$x' = x_0 + \tilde{x} \tag{4.5}$$

$$x = x' - 2\pi\mathcal{H}(x' - \pi) + 2\pi\mathcal{H}(-x' - \pi) \tag{4.6}$$

one then takes the derivative (or local refinement) of the working coordinate $\tilde{X}$, which also covers the $(-\pi, +\pi)$ range centered at the center of the zoom:

$$\tilde{X}'(\tilde{x}) = \frac{d\tilde{X}}{d\tilde{x}} = g(\tilde{x}) = \beta + (\gamma - \beta)F(\tilde{x}; \delta, \tau) \tag{4.7}$$

where:

$$F(\tilde{x};\delta,\tau) = \mathcal{T}\left[\frac{\tau(\frac{1}{2}\delta - \tilde{x})}{\tilde{x}(\pi - \tilde{x})}\right] \tag{4.8}$$

for $0 \leq \tilde{x} \leq \pi$. In order to impose,. along the same range, a variation of $\tilde{X}$ between 0 and π, imposes:

$$\int_0^\pi d\tilde{x}\ g(\tilde{x}) = \pi \tag{4.9}$$

from which, the expression of β becomes:

$$\beta = \frac{\gamma \int_0^\pi d\tilde{x} F(\tilde{x};\delta,\tau) - \pi}{\int_0^\pi d\tilde{x} F(\tilde{x};\delta,\tau) - \pi} \tag{4.10}$$

from $\tilde{X}'(\tilde{x})$ one obtain $\tilde{X}(\tilde{x})$ within the range 0 to π along a regular grid $\tilde{x}_m$ fine enough (about 30,000 points) in order to reduce the errors on the following calculations. Then one anti-symmetrizing the function $\tilde{X}(\tilde{x})$ in order to obtain the other range $-\pi < \tilde{x} < 0$:

$$\tilde{X}'(-\tilde{x}) = \tilde{X}'(\tilde{x});\ or\ \tilde{X}(-\tilde{x}) = -\tilde{X}(\tilde{x}) \tag{4.11}$$

then $\tilde{X}$ covers also the range $-\pi, +\pi$ like $\tilde{x}$. The regular grid as function of the zoomed grid, centered at its center follows:

$$\tilde{X}_m = -\pi + \frac{2\pi\left(\tilde{m} - \frac{1}{2}\right)}{M};\ \tilde{m} = 1, M \tag{4.12}$$

we solve:

$$\tilde{X}(\tilde{x}_m) = \tilde{X}_m \tag{4.13}$$

in order to obtain the longitudes of the points at the zoomed grid:

$$x''_m = x_0 + \tilde{x}_m \tag{4.14}$$
$$x'_m = x''_m - 2\pi\mathcal{H}\left(x''_m - \pi\right) + 2\pi\mathcal{H}\left(-x''_m - \pi\right) \tag{4.15}$$

it only left to re-sort the grid points within the interval $(-\pi, +\pi)$ through the definition of m_0 which:

$$x'_{m_0} = min(x'_m) \tag{4.16}$$

which derive us to a re-sorted field:

$$m = (-1 + M\mathcal{H})(m_0 - \tilde{m}) + 1 \tag{4.17}$$
$$x_m = x'_m \tag{4.18}$$

scale factor associated to the grid becomes:

$$x'_m = x'(X_m) = \frac{1}{X'(x_m)} \tag{4.19}$$

Zoom on the latitude

In this case the problem is slightly different due to the fact that the zoomed grid might not be centered at the equator, and also due to the absence of multiple valuation for the latitude (see figures from 4.8 to 4.10). Taking y_0 as the latitude at the center of the zoom. Formulation of latitudinal zoom will depend on the position of the center with respect to the Equator. It will be defined as before, but on a domain $[2y_0\mathcal{H}(-y_0) - pi/2, 2y_0\mathcal{H}(y_0) + pi/2]$, symmetric

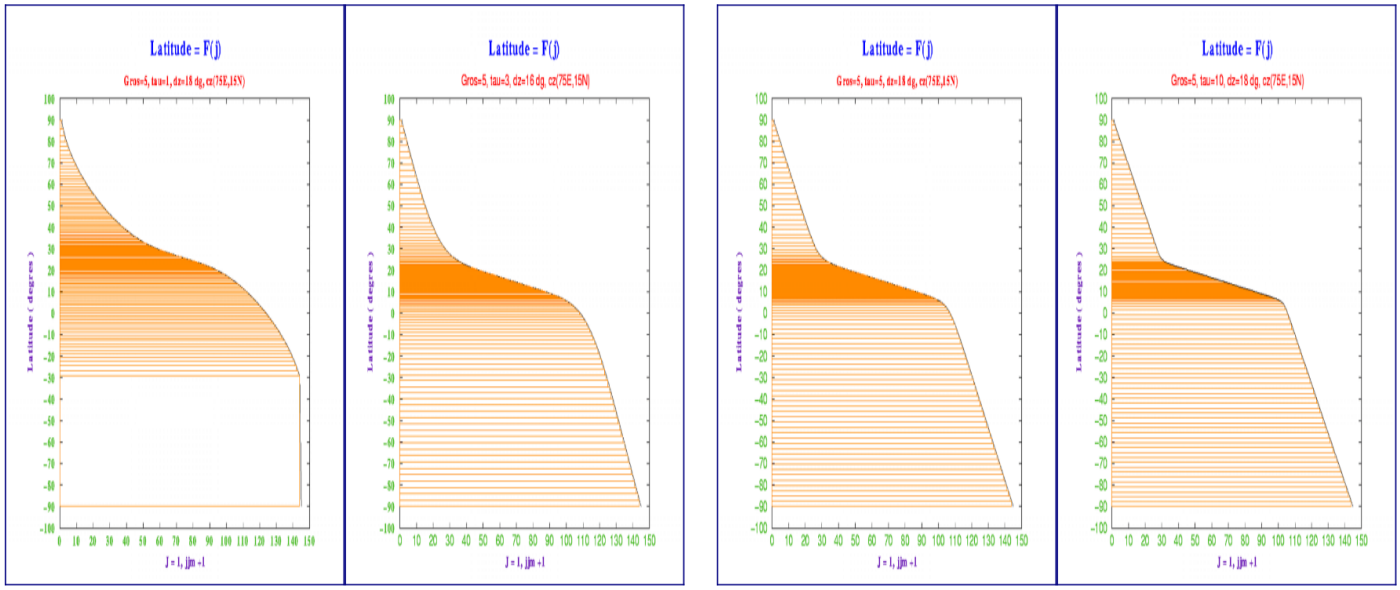

Figure 4.8: Latitudes of the grid points for a grid of 192x144 grid points with a zoom centered at N 15°, 75° E, refinement factor $\gamma = 5$, window $\delta = 0.1\ rad = 18°$, for different rigidity values $\tau = 1$ (left), $\tau = 3$ (2nd left), $\tau = 5$ (3rd left), $\tau = 10$ (right)

from the center of zoom, thus from here to now, it is understood as the pole of the Hemisphere, at the center of the zoom.

Following 4.7, it is defined also by analogue:

$$\tilde{Y}'(y) = \frac{dY}{dy} = g(y) = \beta + (\gamma - \beta)F(y;\delta,\tau) \tag{4.20}$$

where:

$$F(y;\delta,\tau) = \begin{cases} \mathcal{T}\left[\frac{\tau(y-y_0+\frac{\delta}{2})}{\left[y-2y_0\mathcal{H}(-y_0)+\frac{\pi}{2}\right](y_0-y)}\right] & \pi/2 \le y \le y_0 \\ \mathcal{T}\left[\frac{\tau(y_0+\frac{\delta}{2}-y)}{(y_0-y)\left[2y_0\mathcal{H}(y_0)+\frac{\pi}{2}-y\right]}\right] & y_0 \le y \le +\pi/2 \end{cases} \tag{4.21}$$

the condition to impose is that Y goes from $-\pi/2$ to $+\pi$, when y goes from $-\pi/2$ to $+\pi$:

$$\int_{-\pi/2}^{+\pi/2} dy\ g(y) = \pi \tag{4.22}$$

frmo which β becomes:

$$\beta = \frac{\gamma \int_{-\pi/2}^{+\pi/2} dy F(y;\delta,\tau) - \pi}{\int_{-\pi/2}^{+\pi/2} dy F(y;\delta,\tau) - \pi} \tag{4.23}$$

From $Y'(y)$ one obtains $Y(y)$ from a regular grid y_m fine enough (about 30,000 points) in order to minimize the source of errors for the following steps.

Then, one gives the regular grid on the 'm' space including pole South and pole North as:

$$Y_m = \frac{-\pi}{2} + \pi\frac{m-1}{M};\ m = 1, M+1 \tag{4.24}$$

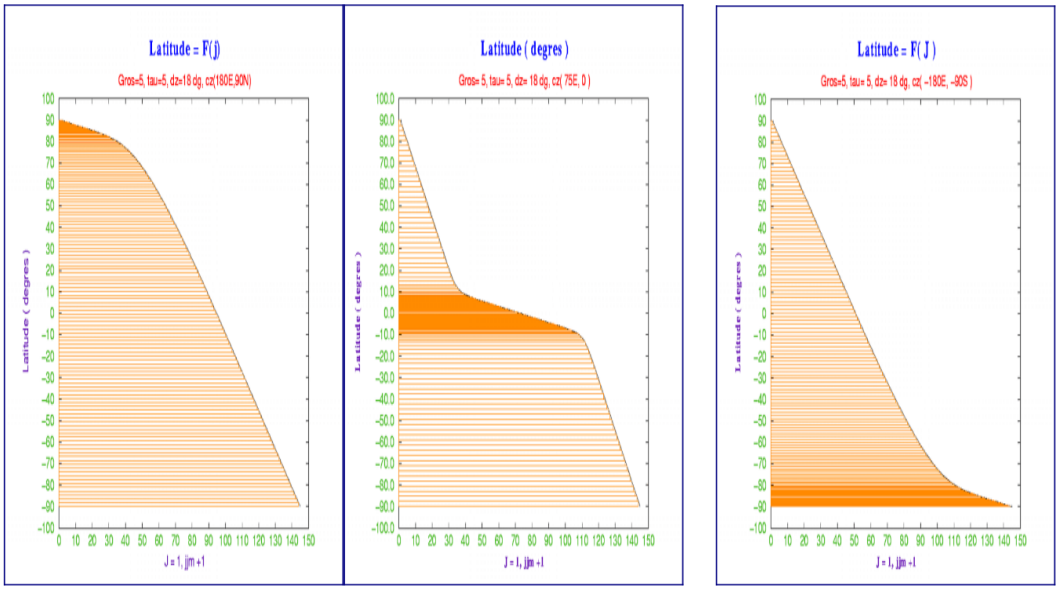

Figure 4.9: As in figure 4.8, but with a zoom centered at N 90°, 180° E (left), N 0°, 75° E (middle), S 90°, 180° E (right)

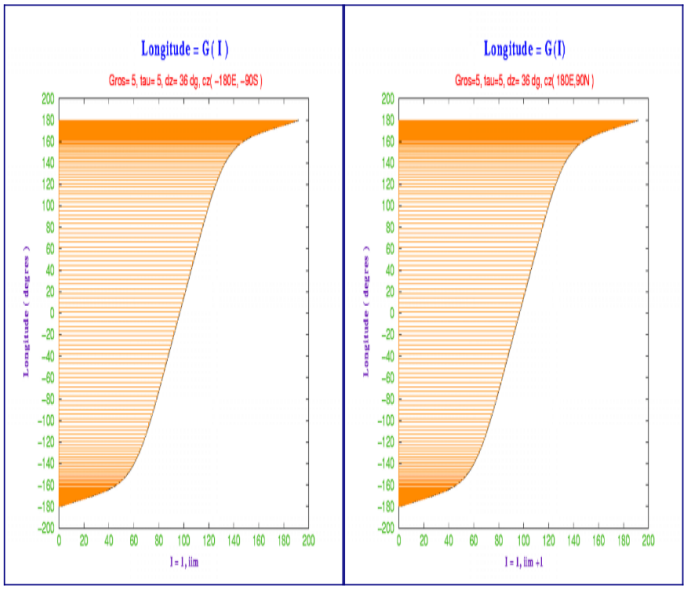

Figure 4.10: As in figure 4.8, but for the longitudes and a zoom centered at S 90°, 180° W (left), N 90°, 180° E (right)

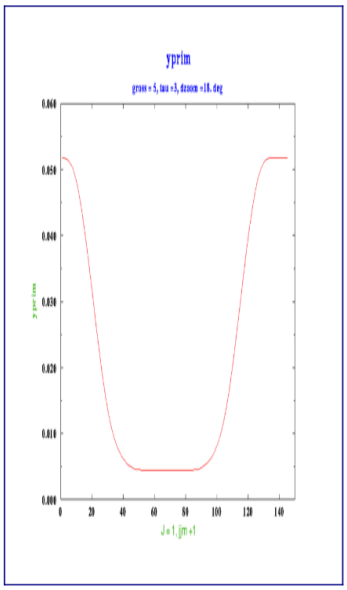

Figure 4.11: Representation of the derivative grid points y' (equation 4.26) at the U grid points

where M is the meridional resolution of the model in number of intervals, from which one solves:

$$Y(y_m) = Y_m \tag{4.25}$$

in order to obtain the latitudes y_m of the zoomed grid points.
Finally, the scale factor associated to the zoom would be (see figure 4.11 as an example):

$$y'_m = y'(Y_m) = \frac{1}{Y'(y_m)} \tag{4.26}$$

Control of the parameters

On practice one impose a limit, which is considered as acceptable outside the zoomed window: ε (re-finning on the range 0 and 1, typically of the order around 0.2 or 0.1). This is the fifth parameter of the zoom. This impose the condition:

$$2\beta - \gamma > \varepsilon \tag{4.27}$$

If this condition is not satisfied, an error message from the procedure on charge of the zoom will appear:

`Votre choix de paramtres n'est pas acceptable. Vous devez:`

`Ou modrer le grossissement,` (diminish γ)

`Ou restreindre la fentre du zoom,` (diminish δ)

`Ou accentuer la raideur,` (increase τ)

`Ou tolrer plus de dgradation hors du zoom,` (diminish ε)

Some final examples are provided in figures 4.12, 4.13 and 4.14

4.8 Surface stations

Model can provide time-series at given latitudes and longitudes from its internal integratrion time-steps values. This would mimic records from surface stations.

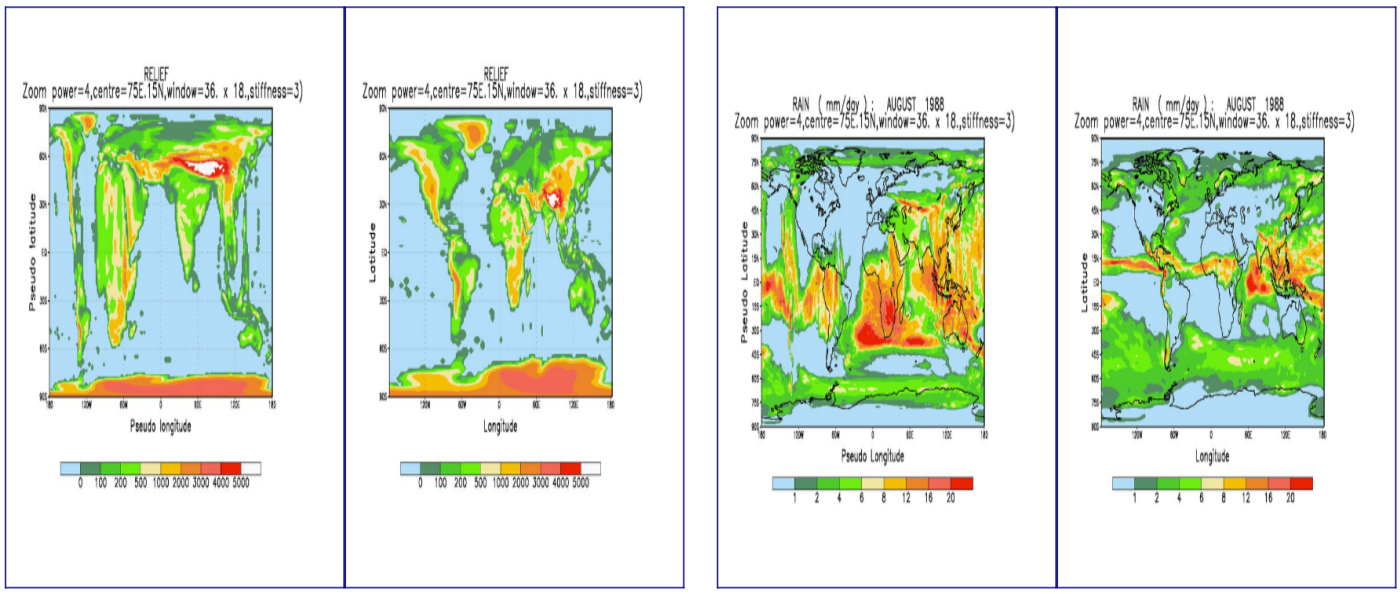

Figure 4.12: Example of the representation of the topography for the different sets of coordinates. **anamorphic**: topography using the pseudo-longitudes/latitudes from which one sees a bigger India due to the zoom (left), and the other one using the standard longitudes/latitudes (2nd left). Precipitation field in both systems of coordinates: anamorphic (3d left), normal (right)

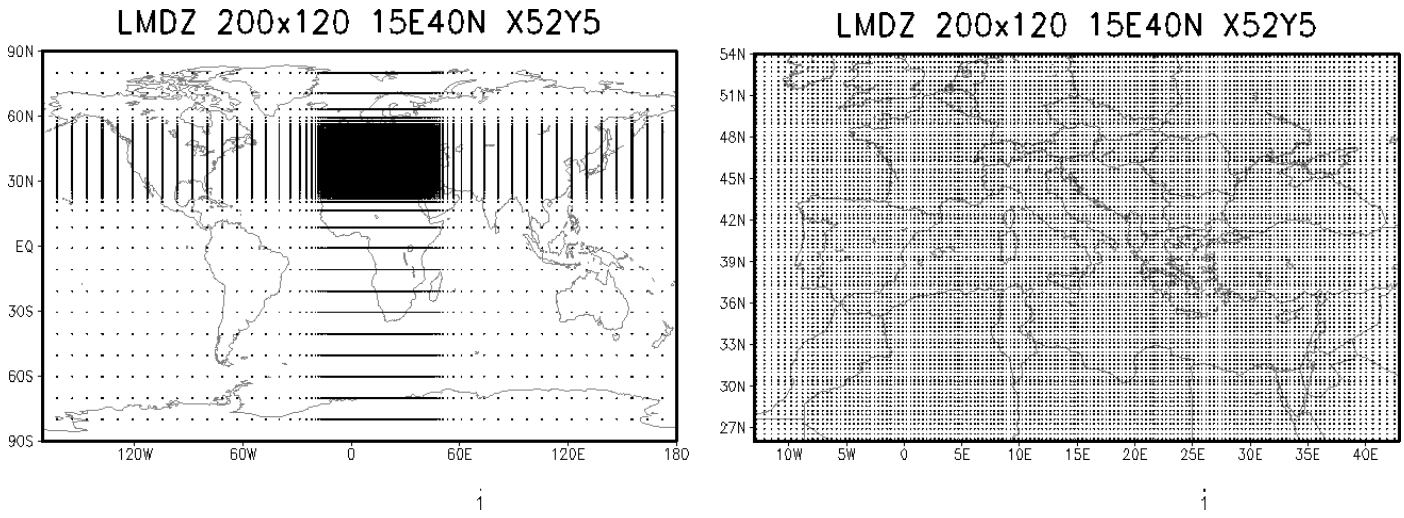

Figure 4.13: Example of LMDZ zoom over the Mediterranean basin. Global domain with a lon,lat stretching of the grid (left), detailed view of the distribution of the grid points in the zoomed area (right)

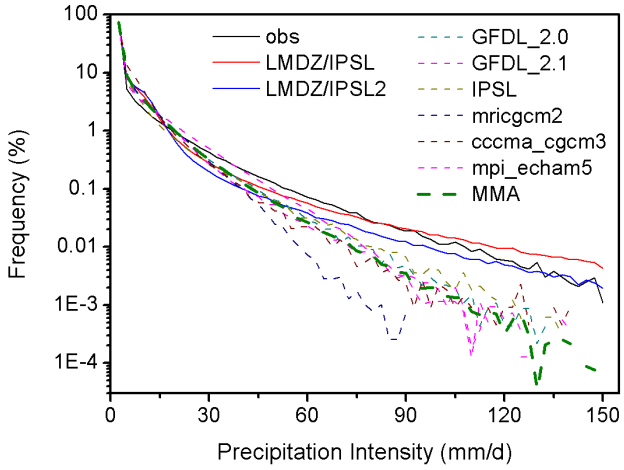

Figure 4.14: Spectral distribution of rainfall in southeast China, comparison between the observation, LMDZ/CTRL, LMDZ/CTRL2, and a few other coarse-resolution global models. Added values of high-resolution models can be clearly identified

4.9 Couplings

As it has been said, LMDZ has been coupled to different models to build the IPSL climate model. Some short explanations about these differents models is here provided.

4.9.1 Orchidee

Orchidee (`http://orchidee.ipsl.jussieu.fr/`) (Krinner et al., 2005) is a dynamic global vegetation model designed as an extension of an existing surface-vegetation-atmosphere transfer scheme which is included in a coupled ocean-atmosphere general circulation model. It is controlled by the `orchidee.def` file.

The dynamic global vegetation model simulates the principal processes of the continental biosphere influencing the global carbon cycle (photosynthesis, autotrophic and heterotrophic respiration of plants and in soils, fire, etc.) as well as latent, sensible, and kinetic energy exchanges at the surface of soils and plants. As a dynamic vegetation model, it explicitly represents competitive processes such as light competition, sampling establishment, etc. It can thus be used in simulations for the study of feedbacks between transient climate and vegetation cover changes, but it can also be used with a prescribed vegetation distribution. The whole seasonal phenological cycle is prognostically calculated without any prescribed dates or use of satellite data. Orchidee is based in three components:

- SVAT ESCHIBA Ducoudré et al. (1993); de Rosnay and Polcher (1998) for the basics interchanges between atmosphere and soil
- Dynamic Global Vegetation Model (DGVM LPJ) (Sitch et al., 2003) for the vegetation dynamics
- Saclay Toulouse Orsay Model for the Analysis of Terrestrial Ecosystems (STOMATE) based in *plant functional types (PFT)* for photosynthesis, carbon allocation, litter decomposition, soil carbon dynamics, maintenance and growth respiration and phenology

SVAT SECHIBA

Surface-vegetation-atmosphere transfer (SVAT) SECHIBA Ducoudré et al. (1993); de Rosnay and Polcher (1998) has been developed as a set of surface parameterizations for the LMDZ. SVAT simulate exchanges of sensible, latent and kinetic energy at the surface. SECHIBA describes exchanges of energy and water between the atmosphere and the biosphere, and the soil water budget. In its standard version, SECHIBA contains no parameterization of photosynthesis. Time step of the hydrological module is of the order of 30 min.

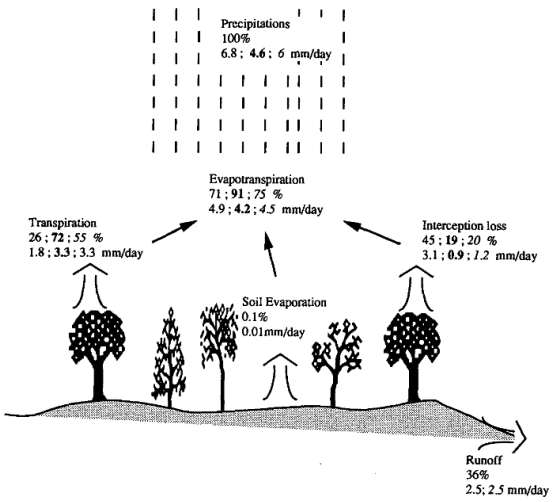

Figure 4.15: Example of water balance (Amazonian) for a given precipitation amount and the respective percentages from measured values (first, bold Shuttleworth, 1988) and simulated (second, italic Sato et al., 1989) from (Ducoudré et al., 1993)

For each grid point eight land surface types (bare soil plus seven vegetation classes) are defined, each of them covering a fractional area of the grid box and allowed to be found simultaneously. Over each of these covers the transfers are computed: evaporation from soil, transpiration from plants through a resistance defined by concepts of stomatal resistance and architectural resistance, and interception loss from the water reservoir over the canopy (see an schematic representation in figure 4.15). These fluxes are then averaged over the period box to derive the total amount of water vapor that is transferred to the first level of the atmospheric model. Parameterization of soil water allows for the moistening of an upper layer, of variable depth, during a rainfall event. The scheme requires prescription of a restricted number of parameters: seven for each class of vegetation not found and four for the soil not found.

SECHIBA represents:

- *latent heat flux:* exchanges of water vapor between the soil/vegetation system and the atmosphere
- *soil hydrological cycle*

Vegetation is treated as a single element in the equations. However, because different fractions of vegetation types can coexist in the grid box, certain vegetation contributions such as evapotranspiration will be the result of the combination of all the classes of vegetation within the grid box.

For sensible heat flux calculations vegetation and soil are considered as a single element.

Total latent heat flux (E_a) would be the weighted combination of snow sublimination (E_s), soil evaporation (E_g), canopy transpiration (E_{tr}) and evaporation of foliage water (E_i, intercepted precipitation and dew). Each of one is computed following:

$$E_{s,g,tr,i} = \alpha_{s,g,tr,i}\rho\frac{\Delta q_{s,g,tr,i}}{\sum_\ell r_\ell} \tag{4.28}$$

where $\Delta q_{s,g,tr,i}$ is the gradient of specific humidity between the evaporating surface and the overlying air, and limited by a sum of resistances (r_ℓ). $\alpha_{s,g,tr,i}$ is the fraction of grid box evaporating and ρ air density. This formulation was introduced by Monteith (1963) and is known by the 'big-leaf' or 'single-leaf' model.

There is an *aerodynamic resistence* (r_a) that opposes the transfer of water vapor which is inversely proportional to the product of the surface drag coefficient (C_d) and the wind speed (V_a).

$$r_a = \frac{1}{C_d V_a} \tag{4.29}$$

Table 4.3: Equations for each element of the latent heat flux decomposition from (Ducoudré et al., 1993)

	Δq	α	$\sum_\ell r_\ell$
Snow sublimation	$q_{sat}(T_g) - q_a$	$\frac{S_n}{S_{cr}}$	r_a
Soil evaporation	$h_g q_{sat}(T_g) - q_a$	$\left(1 - \frac{S_n}{S_{cr}}\right)(1 - \sigma_f)$	$r_a + r_g$
Canopy transpiration	$h_g q_{sat}(T_g) - q_a$	$\left(1 - \frac{S_n}{S_{cr}}\right)\sigma_f \left(1 - \left(\frac{W_{dew}}{W_{dmax}}\right)^{2/3}\right)$	$r_a + r_0 + r_c$
Evaporation of foliage water	$q_{sat}(T_g) - q_a$	$\left(1 - \frac{S_n}{S_{cr}}\right)\sigma_f \left(\frac{W_{dew}}{W_{dmax}}\right)^{2/3}$	$r_a + r_0$

Table 4.4: Canopy parameters prescribed in SECHIBA

Parameters	Tundra	Grassland	Grassland + shrub cover	Grassland + tree cover	Decidius forest	Evergreen forest	Rain forest
LAI Summer	1	2	2.5	3.5	5	4	8
LAI Winter	0	1.5	1	1.5	0	3	8
r_0 (sm^{-1})	10	2	2.5	3	40	50	25
k_0 $(kgm^{-2}s^{-1}\ 10^{-5})$	5.0	30.0	25.0	28.0	25.0	12.0	24.0

Soil evaporation is calculated following a *bulk aerodynamic method* (see section 4.9.1) as a combination of the surface relative humidity (h_g) and a soil resistance (r_g, see equation 4.30) which are function of the soil moisture. Soil resistance has a dependency on the soil type tacking its values from observations (Matthews, 1983b,a, 1984).

$$r_g = r_{soil} \frac{D_u}{D_t} \frac{W_{umax} - W_u}{W_{umax}} \tag{4.30}$$

The *architectural resistance* (r_0) would take into account the aerodynamic resistance between leaves and canopy top. In this scheme canopy is defined as a single layer, and a resistance is included following (Saugier and Katerji, 1991). Values are taken from a Perrier (personal communication) and are function of the vegetation type (see table 4.4)

The *canopy resistance* (r_c, see equation 4.31) summarizes the bulk stomatal and leaf aerodynamical resistances. It depends on the solar radiation (R_s) and the water vapor concentration deficit (δc) simulated above canopy being inversely proportional to the single-sided Leaf Area Index (LAI). Is empirically based (Lohammar et al., 1980; Jarvis, 1976), and in this scheme it does not depend on soil moisture.

$$r_c = \frac{1}{LAI} \frac{R_s + R_{s0}}{R_s} \frac{a + \lambda \delta c}{k_0} \tag{4.31}$$

For the gradients of specific humidity between evaporating surface and the air above requires the computation of the *surface relative humidity* (srh). In the scheme srh is given as function of the soil water content and a retention coefficient (h_g).

$$h_g = exp\left(-c \frac{D_u}{D_t} \frac{W_{umax} - W_u}{W_{umax}}\right) \tag{4.32}$$

Part of the precipitated water can be intercepted by the foliage. A result of this, when leaves get wet, they can not transpire. This effect is taken into account and it depends on the incident rainfall and a maximum water storage ($W_{dmax} = 0.5 LAI$) which depends on the LAI index

$$\begin{aligned} \frac{\partial W_{dew}}{\partial t} &= \sigma_f P_r - E_i \\ W_{dew} &\leq W_{dmax} \end{aligned} \tag{4.33}$$

The total soil depth is limited to the root zone. The maximum water that a soil grid point can hold is computed as the difference between the profiles of soil moisture at saturation and at wilting point. The soil has an upper dynamic layer with variable depth where all the dynamics occur (*'bulk method'*, see section 4.9.1), acting the rest as a *reservoir*. When it rains soil is filled from top to bottom. Soil is dried when evapotranspiration is larger than precipitation. Runoff occurs when soil is saturated. Canopy transpiration ceases when soil is completely dry (i.e. at the wilting point). In SECHIBA only two soil layers are considered.

The *stomatal aperture* which determines the transpiration is given as a function of r_c; LAI; $R_{s0} = 125\ Wm^{-2}$, half light saturation factor; $a = 23 \times 10^{-3}\ kgm^{-2}$; k_0 and δc and $\lambda = 1.5$. a. R_{s0} and λ are the same for all vegetation types due to the lack of measurements.

Bare soils are described by:

- $D_t = 1\ m$, total depth (root zone)
- $W_{tmax} = 150\ kgm^{-2}$, maximum amount of water it can hold (g.e.: 70-80 sand, 150 clay, 200 loam). A mean value was chosen.
- $r_{soil} = 33000\ sm^{-1}$, resistance exerted by 1 m of dry soil. Averaged values from different kind of soils
- $c = 0.8$, empirical constant used to compute srh from (Choisnel, 1977)

Bulk aerodynamic method

Total evapotranspiratoin (E_a) is proportional to the potential rate (E_p). The coefficient of proportionality (β) is a function of total soil moisture (W_t) and it is known as *'aridity coefficient'*:

$$E_a = \beta E_p,\ \beta = \begin{cases} 1, & if\ W_t > W_c \\ \frac{W_t}{W_c}, & if\ W_t \leq W_c \end{cases} \tag{4.34}$$

where, $W_c = 0.5 W_{tmax}$, critical amount of soil moisture, above which it is assumed that evapotranspiration takes place at the potential rate, and E_p is function of the gradient of specific humidity between the surface and the overlying air:

$$E_p = \rho \frac{q_{sat}(T_g) - q_a}{r_a} \tag{4.35}$$

where r_a, aerodynamic resistance (see equation 4.29). Water in the soil is held in only one reservoir, the root zone, which is filled from bottom to top by precipitation and emptied from top to bottom by evaporation. This is way it is called *'bucket'*. Runoff occurs only when the soil is saturated, that is, when $W_t = W_{tmax}$

4.9.2 Chimère

It is a full atmospheric chemistery model Menut et al. (2013). The CHIMERE (http://www.lmd.polytechnique.fr/chimere/) multi-scale model is primarily designed to produce daily forecasts of ozone, aerosols and other pollutants and make long-term simulations (entire seasons or years) for emission control scenarios. CHIMERE runs over a range of spatial scale from the regional scale (several thousand kilometers) to the urban scale (100-200 Km) with resolutions from 1-2 Km to 100 Km. CHIMERE proposes many different options for simulations which make it also a powerful research tool for testing parameterizations, hypotheses. CHIMERE is a parallel model that has been tested on machines ranging from desktop PCs running the GNU/Linux operating system, to massively parallel supercomputers (HPCD at ECMWF).

4.9.3 INCA

It is a full complex aerosol model with much more capabilities than the standard ones included in the model. http://www-lsceinca.cea.fr/

INCA (INteraction with Chemistry and Aerosols) is a chemistry and aerosol model coupled to the Laboratoire de Météorologi Dynamique (LMD) General Circulation Model, LMDz. INCA is developed at the Laboratoire des Sciences du Cimat et de l'Environnement (LSCE) in collaboration with other laboratories within IPSL.

LMDzINCA accounts for emissions, transport (resolved and sub-grid scale), photochemical transformations, and scavenging (dry deposition and washout) of chemical species and aerosols interactively in the GCM. Several versions of the INCA model are currently used depending on the envisaged applications with the chemistry-climate model. The standard model resolution is 96x95 (3.75°longitude x 1.9°latitude) and 144x142 (2.5°longitude x 1.3°latitude). The standard vertical resolution includes 39 sigma-p hybrid levels. The GCM also offers the possibility to zoom over specific regions, reaching horizontal resolutions of 50x50 km^2 over the region of interest. The model can be run in a nudged mode, relaxing to ECMWF winds and temperature. An off-line version of the GCM has also been developed in order to minimize the required computing time for transport simulations.

LMDz-INCA constitutes the atmospheric component of the IPSL coupled atmosphere-ocean-biosphere model and is often coupled to the ORCHIDEE biosphere model in order to determine interactively the exchange of chemical species (emissions, deposition) between the atmosphere and the surface.

LMDzINCA accounts for emissions, transport (resolved and sub-grid scale), photochemical transformations, and scavenging (dry deposition and washout) of chemical species and aerosols interactively in the GCM. Several versions of the INCA model are currently used depending on the envisaged applications with the chemistry-climate model. The standard model resolution is 96x72 (3.75 x 2.5 degrees in resp. longitude and latitude) with 19 sigma-p hybrid vertical levels. The GCM also offers the possibility to zoom over specific regions, reaching horizontal resolutions of 50x50 km2. The model can be run in a nudged mode, relaxing to ECMWF winds and temperature. An off-line version of the GCM has also been developed in order to minimize the required computing time for transport simulations. This model is still under development and constitutes the atmospheric component of the IPSL coupled atmosphere-ocean-biosphere model.

4.9.4 REPROBUS

REPROBUS (Reactive Procecesses Ruling the Ozone Budget in the Stratosphere, http://ether.ipsl.jussieu.fr/ether/pubipsl/reprobus_fr.jsp) is a 3D model which schematizes the chemistery of different 55 chemical species throughout 147 chemical reactions at the stratosphere (Lefèvre et al., 1994). Hetherogenous reactions are also taken into account. The liquid PSC are descrived using the model from Carslaw et al. (1995). Wind and temperature files are imposed every 6 hours from ECMWF analysis. A 15 minutes time step is used for the chemical calculations.

4.9.5 COSP

The CFMIP Observation Simulator Package (COSP, http://cfmip.metoffice.com/COSP.html). Is a numerical package, to facilitate the exploitation of A Train data in numerical models. The undergoing developingof the system that allows to simulate the signal that CloudSat/CALIPSO would see in a model-generated world. It is a flexible tool to simulate active instruments in models (climate, forecast, cloud-resolving). The ISCCP simulator is also included in the package.

There are several groups involved in the project:

- Met Office Hadley Centre
- LMD/IPSL (Laboratoire de Météorologie Dynamique/Institut Pierre Simon Laplace)
- LLNL (Lawrence Livermore National Laboratory)
- CSU (Colorado State University)
- UW (University of Washington)

The approach is to create a modular code in `FORTRAN90` that can be plugged in different types of models, from GCMs to cloud CRMs.

This satellite-airbone simulator is controlled via the `cosp.def` configuration file.

Chapter 5

Others

5.1 Water isotopes

Since 2008, water isotopes and tagging have been implemented in different versions of LMDZ (Risi et al., 2010b). They are presently in LMDZ5A and LMDZ5B. The isotopic version of LMDZ is sometimes called *LMDZ-iso*.

The implemented water isotopes are $H_2^{16}O$, HDO and the $H_2^{18}O$ (Risi et al., 2010b). They have been evaluated against isotopic observations from precipitation, terrestrial water and water vapor, as measured in-situ, by ground-based remote-sensing or by satellite (Risi et al., 2012, 2013b). $H_2^{17}O$ has also been implemented (Risi et al., 2013a), but results are unsatisfactory in the most recent versions of LMDZ-iso. The radioactive isotope HTO has been recently implemented (Cauquoin et al., 2014).

Water tagging allows to 'colour' water molecules and their isotopic counterparts depending on their origin or on the processes they undergo. For example, it is possible to color the water molecules evaporated over the Mediterranean Sea, the water molecules transpired by the vegetation, or water molecules that have been processed in the unsaturated downdrafts of convective systems. It is a very useful tool to analyze the water cycle (Risi et al., 2010a).

LMDZ-iso has been used in a wide range of configurations: AMIP, global nudged, nudged and zoomed over different regions (Tibet, South America, West Africa, Indonesia, North America... (e.g. Vimeux et al., 2011)), or forced by limit conditions from different climatic periods (last maximum glacial, last interglacial, Heinrich events, mid Holocene, future climate projections, ... (e.g. Eagle et al., 2013)). This reflects the wide range of applications of LMDZ-iso, from the interpretation of paleoclimatic archives to the understanding of the present-day water cycle.

LMDZ-iso can be coupled to an isotopic, non-parallel version of ORCHIDEE (Risi et al., 2010a), called *ORCHIDEE-iso*. The coupling with a more recent, parallel version of ORCHIDEE-iso is under work. It is planned to couple LMDZ-iso and ORCHIDEE-iso to an isotopic version of NEMO (ocean model), opening the possibility to have an isotopic version of the IPSL coupled model within the next few years.

5.2 WRF integration

An integration of the physics of the LMDZ model into the limited area model, 'Weather Research and Forecasting' (WRF,`http://www.wrf-model.org`) model (Skamarock et al., 2008). The goal is to create an hybrid model in which, one use WRF's dynamical core and LMDZ physics. With this new tool one expect:

- Open a new way to complement the development of LMDZ physic schemes
- Perform limited area runs with LMDZ physics
- Test LMDZ physics resolution limitations with an appropiated dynamical core

Fore more details, please visit tracking development page of the project: `http://web.lmd.jussieu.fr/trac-LMDZ_WRF`

5.3 Inversion of aerosols

A simplified aerosol model has been coupled to LMDZ model Huneeus et al. (2009), and it has been used to estimate sources of aerosol through a top-down approach (e.g. Huneeus et al., 2012) which combines information from a priori emission inventories, atmospheric modelling and satellite observations in order to have a better estimate of aerosol emissions. The aerosol model includes two bins of coarse dust aerosols, one of fine mode aerosols, one of coarse sea salt aerosol and one for gaseous precursors of aerosols.

Recently, the dust emission scheme from CHIMERE Menut et al. (2013) (see section 4.9.2) has been included in the LMDZ Hourdin et al. (2014) and also has been coupled in the simplified aerosol model. With this emission scheme and the zoom capability (see section 4.7) of the LMDZ model, it is possible to perform a more detailed regional inversion of aerosol sources. This will increase the accuracy of aerosols emissions estimates in the regional and global scales.

Bibliography

Ayotte, K. W., Sullivan, P. P., Andrén, A., Doney, S. C., Holtslag, A. A. M., Large, W. G., McWilliams, J. C., Moeng, C.-H., Otte, M. J., Tribbia, J. J., and Wyngaard, J. C. (1996). An evaluation of neutral and convective planetary boundary-layer parameterizations relative to large eddy simulations. Boundary-Layer Meteorology, 79(1-2):131–175.

Batchelor, G. K. (1967). An Introduction to Fluid Dynamics. Cambridge University Press.

Bechtold, P., Redelsperger, J.-L., Beau, I., Blackburn, M., Brinkop, S. ., Grandpeix, J.-Y., Grant, A., Gregory, D., Guichard, F., How, C., and Ioannidou, E. (2000). A gcss model intercomparison for a tropical squall line observed during toga-coare. 11: Intercomparison of single-column models and a cloud-resolving model. Q. J. R. Meteorol. Soc., 126:865888.

Bony, S. and Emanuel, K. A. (2001). A parameterization of the cloudiness associated with cumulus convection; evaluation using toga coare data. J. Atmos. Sci., 58:3158–3183.

Boucher, O. and Lohmann, U. (1995). The sulfate-ccn-cloud albedo effect. Tellus B, 47(3):281–300.

Boucher, O., Treut, H. L., and Baker, M. B. (1995). Precipitation and radiation modeling in a general circulation model: Introduction of cloud microphysical processes. J. Geophys. Res., 100:16395.

Cariolle, D. and Teyssèdre, H. (2007). A revised linear ozone photochemistry parameterization for use in transport and general circulation models: Multi-annual simulations. Atmospheric Chemistry and Physics, 7:2183–2196.

Carslaw, K. S., Luo, B., and Peter, T. (1995). An analytic expression for the composition of aqueous hno3-h2so4 stratospheric aerosols including gas phase removal of hno3. Geophys. Res. Let., 22(14):1877–1880.

Cauquoin, A., Landais, A., Jean-Baptiste, P., Fourré, E., and Risi, C. (2014). Implementation of tritium (HTO) in the LMDZ general circulation model. under preparation.

Chlond, A., Müller, F., and Sednev, I. (2004). Numerical simulation of the diurnal cycle of marine stratocumulus during firean les and scm modelling study. Q. J. R. Meteorol. Soc., 130(604):3297–3321.

Choisnel, E. (1977). Un modèle agrométéorologique opérationnel de bilan hydrique utilisant des données climatiques. Les besoins en eau des cultures. Proc. Conférence internationale CIID. Paris.

Clough, S. A. and Iacono, M. I. (1995). Line-by-line calculation of atmospheric fluxes and cooling rates, 2. application to carbon dioxide, ozone, methane, nitrous oxide and the halocarbons. J. Geophys. Res., 100D:16519–16536.

Clough, S. A., Iacono, M. J., and Moncet, J.-L. (1992). Line-by-line calculations of atmospheric fluxes and cooling rates: Application to water vapor. J. Geophys. Res., 97D:15761–15786.

Clough, S. A., Kneizys, F. X., and Davies, R. W. (1989). Line shape and the water vapor continuum. Atmos. Res., 23:229–241.

Couvreux, F., Rio, C., Guichard, F., Lothon, M., Canut, G., Bouniol, D., and Gounou, A. (2012). Initiation of daytime local convection in a semi-arid region analysed with high-resolution simulations and amma observations. Q. J. R. Meteorol. Soc., 138(662):56–71.

de Rosnay, P. and Polcher, J. J. (1998). Modelling root water uptake in a complex land surface scheme coupled to a gcm. Hydrol. Earth Syst. Sci., 2(2/3):239–255.

Deardorff, J. W. (1966). The counter-gradient heat flux in the lower atmosphere and in the laboratory. J. Atmos. Sci., 23:503–506.

Doutriaux-Boucher, M. and Quaas, J. (2004). Evaluation of cloud thermodynamic phase parametrizations in the lmdz gcm by using polder satellite data. Geophys. Res. Lett., 31:6126.

Ducoudré, N. I., Laval, K., and Perrier, A. (1993). Sechiba, a new set of parameterizations of the hydrologic exchanges at the land-atmosphere interface within the lmd atmospheric general circulation model. J. Climate, 6:248–273.

Dufresne, J. L., Foujols, M. A., Denvil, S., Caubel, A., Marti, O., Aumont, O., Balkanski, Y., Bekki, S., Bellenger, H., Benshila, R., Bony, S., Bopp, L., Braconnot, P., Brockmann, P., Cadule, P., Cheruy, F., Codron, F., Cozic, A., Cugnet, D., Noblet, N., Duvel, J. P., Ethé, C., Fairhead, L., Fichefet, T., Flavoni, S., Friedlingstein, P., Grandpeix, J. Y., Guez, L., Guilyardi, E., Hauglustaine, D., Hourdin, F., Idelkadi, A., Ghattas, J., Joussaume, S., Kageyama, M., Krinner, G., Labetoulle, S., Lahellec, A., Lefebvre, M. P., Lefevre, F., Levy, C., Li, Z. X., Lloyd, J., Lott, F., Madec, G., Mancip, M., Marchand, M., Masson, S., Meurdesoif, Y., Mignot, J., Musat, I., Parouty, S., Polcher, J., Rio, C., Schulz, M., Swingedouw, D., Szopa, S., Talandier, C., Terray, P., Viovy, N., and Vuichard, N. (2013). Climate change projections using the ipsl-cm5 earth system model: from cmip3 to cmip5. Clim. Dyn., 40(9-10):2123–2165.

Duynkerke, P. G. and Teixeira, J. (2001). Comparison of the ecmwf reanalysis with fire i observations: Diurnal variation of marine stratocumulus. J. Climate, 14:1466–1478.

Eagle, R., Risi, C., Mitchell, J., Eiler, J., Seibt, U., Neelin, D., Li, G., and Tripati, A. (2013). High regional climate sensitivity over continental China inferred from glacial-recent changes in temperature and the hydrologic cycle. Proc. Natl. Acad. Sci., 110:8813–8818.

Ebert, E. E. and Curry, J. A. (1993). An intermediate one-dimensional thermodynamic sea ice model for investigating ice-atmosphere interactions. J. Geophys. Res., 98C:10,085–10,109.

ECMWF (2002). Part iv: Physical processes. IFS DOCUMENTATION CY25R1 (Operational implementation 9 April 2002), page 168.

Emanuel, K. A. (1991). A scheme for representing cumulus convection in large-scale models. J. Atmos. Sci., 48:2313–2329.

Emanuel, K. A. (1993). A cumulus representation based on the episodic mixing model: the importance of mixing and microphysics in predicting humidity. AMS Meteorol. Monogr., 24:185–192.

Emanuel, K. A. and Živković Rothman, M. (1999). Development and evaluation of a convection scheme for use in climate models. J. Atmos. Sci., 56:1766–1782.

Fouquart, Y. (1987). Radiative transfer in climate modeling. NATO Advanced Study Institute on Physically-Based Modeling and Simulation of Climate and Climate Changes, Erice, Sicily, 11-23 May 1986, M.E. Schlesinger, Ed., pages 223–283.

Fouquart, Y. (1988). Radiative transfer in climate models. In Schlesinger, M., editor, Physically-Based Modelling and Simulation of Climate and Climatic Change, volume 243 of NATO ASI Series, pages 223–283. Springer Netherlands.

Fouquart, Y. and Bonnel, B. (1980). Computations of solar heating of the earth's atmosphere: A new parameterization. Beitr. Phys. Atmos., 53:35–62.

Fu, Q. and Liou, K.-N. (1992). On the correlated k-distribution method for radiative transfer in non-homogeneous atmospheres. J. Atmos. Sci., 49:2139–2156.

Fu, Q., Yang, P., and Sun, W. B. (1998). An accurate parametrization of the infrared radiative properties of cyrrus clouds of climate models. J. Climate, 11:2223–2237.

Geleyn, J. F. (1977). A comprehensive radiation scheme designed for fast computation. Res. Dep. Eur. Cent. for Medium Range Weather Forecasts, Reading, England, Internal Rep. 8.:36.

Grandpeix, J. Y. and Lafore, J. P. (2009). A density current parameterization coupled with emanuels convection scheme. part i: The models. J. Atmos. Sci., 67:881–897.

Grandpeix, J. Y., Lafore, J. P., and Cheruy, F. (2009). A density current parameterization coupled with emanuels convection scheme. part ii: 1d simulations. J. Atmos. Sci., 67:898–922.

Grandpeix, J. Y., Phillips, V., and Tailleux, R. (2004). Improved mixing representation in emanuel's convection scheme. Q. J. R. Meteorol. Soc., 130(604):3207–3222.

Gurevich, M. I. (1965). Theory of Jets in Ideal Fluids. Academic Press (Translated From The Russian Edition).

Held, I. M. and Suarez, M. J. (1994). A proposal for the intercomparison of the dynamical cores of atmospheric general circulation models. Bull. Amer. Meteor. Soc., 75:1825–1830.

Heymsfield, A. J. (1977). Precipitation development in stratiform ice clouds: A microphysical and dynamical study. J. Atmos. Sci., 34:367–381.

Heymsfield, A. J. and Donner, L. J. (1990). A scheme for parameterizing ice-cloud water content in general circulation models. J. Atmos. Sci., 47:1865–1877.

Hines, C. O. (1997a). Doppler-spread parameterization of gravity-wave momentum deposition in the middle atmosphere. part 1: Basic formulation. Journal of Atmospheric and Solar-Terrestrial Physics, 59(4):371 – 386.

Hines, C. O. (1997b). Doppler-spread parameterization of gravity-wave momentum deposition in the middle atmosphere. part 2: Broad and quasi monochromatic spectra, and implementation. Journal of Atmospheric and Solar-Terrestrial Physics, 59(4):387 – 400.

Hourdin, F., Couvreux, F., and Menut, L. (2002). Parameterization of the dry convective boundary layer based on a mass flux representation of thermals. J. Atmos. Sci., 59:1105–1123.

Hourdin, F., Foujols, M. A., Codron, F., Guemas, V., Dufresne, J. L., Bony, S., Denvil, S., Guez, L., Lott, F., Ghattas, J., Braconnot, P., Marti, O., Meurdesoif, Y., and Bopp, L. (2013a). Impact of the lmdz atmospheric grid configuration on the climate and sensitivity of the ipsl-cm5a coupled model. Clim. Dyn., 40(9-10):2167–2192.

Hourdin, F., Grandpeix, J. Y., Rio, C., Bony, S., Jam, A., Cheruy, F., Rochetin, N., Fairhead, L., Idelkadi, A., Musat, I., Dufresne, J. L., Lahellec, A., Lefebvre, M. P., and Roehrig, R. (2013b). Lmdz5b: the atmospheric component of the ipsl climate model with revisited parameterizations for clouds and convection. Clim. Dyn., 40(9-10):2193–2222.

Hourdin, F., Gueye, M., Diallo, B., Dufresne, J.-L., Menut, L., Marticoréna, B., Siour, G., and Guichard, F. (2014). Parametrization of convective transport in the boundary layer and its impact on the representation of diurnal cycle of wind and dust emissions. Atmos. Chem. Phys. Discussions, 14(19):27425–27458.

Hourdin, F., Musat, I., Bony, S., Braconnot, P., Codron, F., Dufresne, J.-L., Fairhead, L., Filiberti, M.-A., Friedlingstein, P., Grandpeix, J.-Y., Krinner, G., LeVan, P., Li, Z.-X., and Lott, F. (2006). The lmdz4 general circulation model: climate performance and sensitivity to parametrized physics with emphasis on tropical convection. Clim. Dyn., 27(7-8):787–813.

Huneeus, N., Boucher, O., and Chevallier, F. (2009). Simplified aerosol modeling for variational data assimilation. Geosci. Model Dev., 2(2):213–229.

Huneeus, N., Chevallier, F., and Boucher, O. (2012). Estimating aerosol emissions by assimilating observed aerosol optical depth in a global aerosol model. Atmos. Chem. Phys., 12(10):4585–4606.

Iacobellis, S. F. and Somerville, R. C. (2000). Implications of microphysics for cloud-radiation parameterizations: Lessons from toga coare. J. Atmos. Sci., 57(2):161–183.

Jam, A. (1998). Thermodynamique de la glace dans le modèle unicolonne du lmd. Master's thesis, Université Pierre et Marie Curie.

Jam, A., Hourdin, F., Rio, C., and Couvreux, F. (2013). Resolved versus parameterized boundary-layer plumes. part iii: a diagnostic boundary-layer cloud parameterization derived from large eddy simulations. Bound.-Lay. Meteorol., 147:421–441.

Jarvis, P. G. (1976). The interpretation of the variations in leaf water potential and stomatal conductance found in canopies in the field. Phil. Trans. R. Soc. Lond. B, 273:593–610.

Kirchoff, G. (1877). Vorlesungen über mathematische physik. Mechanik / von Dr.Gustav Robert Kirchhoff. Leipzig.

Klemp, J. B. and Wilhelmson, R. B. (1978). The simulation of three-dimensional convective storm dynamics. J. Atmos. Sci., 35:1070–1096.

Krinner, G., Viovy, N., de Noblet-Ducoudré, N., Ogée, J., Polcher, J., Friedlingstein, P., Ciais, P., Sitch, S., and Prentice, I. C. (2005). A dynamic global vegetation model for studies of the coupled atmosphere-biosphere system. Global Biogeochem. Cy., 19(1):n/a–n/a.

Lacis, A. A. and Oinas, V. (1991). A description of the correlated k distribution method for modeling nongray gaseous absorption, thermal emission, and multiple scattering in vertically inhomogeneous atmospheres. J. Geophys. Res., 96D:9027–9063.

Landweber, L. (1961). Motion of immersed and floating bodies. McGraw-Hill (1st ed.).

Le Treut, H. and Li, Z. X. (1991). Sensitivity of an atmospheric general circulation model to prescribed sst changes: Feedback effects associated with the simulation of cloud optical properties. Clim. Dyn., 5:175–187.

Lefèvre, F., Brasseur, G. P., Folkins, I., Smith, A. K., and Simon, P. (1994). Chemistry of the 1991-1992 stratospheric winter: Three-dimensional model simulations. Journal of Geophysical Research: Atmospheres, 99(D4):8183–8195.

Li, Z. L. (1998). Description algorithmique d'un ensemble de paramétrisation physique – phylmd. Documentation Technique, LMD (in French).

Lohammar, T., Larsson, S., Linder, S., and Falk, S. O. (1980). Fast: Simulation models of gaseous exchange in scots pine. Ecological Bulletins, 32:505–523.

Lothon, M., Campistron, B., Chong, M., Couvreux, F., Guichard, F., Rio, C., and Williams, E. (2011). Life cycle of a mesoscale circular gust front observed by a c-band doppler radar in west africa. Mon. Wea. Rev., 139:1370–1388.

Lott, F. and Miller, M. J. (1997). A new subgrid-scale orographic drag parametrization: Its formulation and testing. Q. J. R. Meteorolo. Soc., 123(537):101–127.

Matthews, E. (1983a). Global vegetation and land use: New high-resolution data bases for climate studies. J. Climate Appl. Meteor., 22:474–487.

Matthews, E. (1983b). Prescription of land-surface boundary conditions in giss gcm ii: A simple method based on high-resolution vegetation data bases. Tech. Memo. NASA, 86096:20.

Matthews, E. (1984). Vegetation, land-use and seasonal albedo data sets: documentation of archived data tape. Tech. Memo. NASA, 86107:12.

McClatchey, R. A., Fenn, R. W., Selby, J. E. A., Volz, F. E., and Garing, J. S. (1972). Optical Properties of the Atmosphere. Environ. Res. Pap. (3rd Ed.) Air Force Cambridge Research Labs Hanscom Afb MA.

Mellor, G. L. and Yamada, T. (1974). A hierarchy of turbulence closure models for planetary boundary layers. J. Atmos. Sci., 31:1791–1806.

Menut, L., Pérez, C., Haustein, K., Bessagnet, B., Prigent, C., and Alfaro, S. (2013). Impact of surface roughness and soil texture on mineral dust emission fluxes modeling. J. Geophys. Res.: Atmospheres, 118(12):6505–6520.

Mlawer, E. J., Taubman, S. J., Brown, P. D., Iacono, M. J., and Clough, S. A. (1997). Radiative transfer for inhomogeneous atmospheres: Rrtm, a validated correlated-k model for the longwave. J. Geophys. Res., 102D:16663–16682.

Monteith, J. L. (1963). Gas exchange in plant communities. Academic Press, New York, USA.

Morcrette, J. (1990). Impact of changes to the radiation transfer parameterizations plus cloud optical. properties in the ecmwf model. Mon. Wea. Rev., 118:847–873.

Morcrette, J. and Fouquart, Y. (1986). The overlapping of cloud layers in shortwave radiation parameterizations. J. Atmos. Sci., 43:321–328.

Morcrette, J. J. (1991). Radiation and cloud radiative properties in the european centre for medium range weather forecasts forecasting system. J. Geophys. Research: Atmospheres, 96(D5):9121–9132.

Morcrette, J. J. and Fouquart, Y. (1985). On systematic errors in parametrized calculations of longwave radiation transfer. Q. J. of R. Meteorol. Soc., 111(469):691–708.

Morcrette, J. J., Smith, L., and Fouquart, Y. (1986). Pressure and temperature dependence of the absorption in longwave radiation parametrizations. Beiträge zur Physik der Atmosphäre, 59:455–469.

Phillips, D. S. (1984). Analytical surface pressure and drag for linear hydrostatic flow over three-dimensional elliptical mountains. J. Atmos. Sci., 41:1073–1084.

Reddy, M. S., Boucher, O., Bellouin, N., Schulz, M., Balkanski, Y., Dufresne, J.-L., and Pham, M. (2005). Estimates of global multicomponent aerosol optical depth and direct radiative perturbation in the laboratoire de meteórologie dynamique general circulation model. J. Geophys. Res., 110:D10S16.

Rio, C. and Hourdin, F. (2008). A thermal plume model for the convective boundary layer: Representation of cumulus clouds. J. Atmos. Sci., 65:407–425.

Rio, C., Hourdin, F., Couvreux, F., and Jam, A. (2010). Resolved versus parametrized boundary-layer plumes. part ii: Continuous formulations of mixing rates for mass-flux schemes. Boundary-Layer Meteorology, 135(3):469–483.

Risi, C., Bony, S., Vimeux, F., Frankenberg, C., Noone, D., and Worden, J. (2010a). Understanding the Sahelian water budget through the isotopic composition of water vapor and precipitation. J. Geophys. Res., 115:n/a–n/a.

Risi, C., Bony, S., Vimeux, F., and Jouzel, J. (2010b). Water stable isotopes in the LMDZ4 general circulation model: model evaluation for present day and past climates and applications to climatic interpretation of tropical isotopic records. J. Geophys. Res., 115:n/a–n/a.

Risi, C., Landais, A., Winkler, R., and F.Vimeux (2013a). Can we determine what controls the spatio-temporal distribution of d-excess and ^{17}O-excess in precipitation using the LMDZ general circulation model? Clim. Past., 9:2173–2193.

Risi, C., Noone, D., Frankenberg, C., and Worden, J. (2013b). Role of continental recycling in intra-seasonal variations of continental moisture as deduced from model simulations and water vapor isotopic measurements. Water Ressources Res., 49:4136–4156.

Risi, C., Noone, D., Worden, J., Frankenberg, C., Stiller, G., Kiefer, M., Funke, B., Walker, K., Bernath, P., Schneider, M., Bony, S., Lee, J., Brown, D., and Sturm, C. (2012). Process-evaluation of tropospheric humidity simulated by general circulation models using water vapor isotopic observations: 2. Using isotopic diagnostics to understand the mid and upper tropospheric moist bias in the tropics and subtropics. J. Geophys. Res., 117:n/a–n/a.

Sadourny, R. and Laval, K. (1984). January and july performance of the lmd general circulation model. In: Berger A., Nicolis C. (eds) New perspectives in climate modeling. Elsevier, Amsterdam, page 173197.

Sato, N., Sellers, P. J., Randall, D. A., Schneider, E. K., Shukla, J., Kinter, J. L., Hou, Y. T., and Albertazzi, E. (1989). Effects of implementing the simple biosphere model in a general circulation model. J. Atmos. Sci., 46:2757–2782.

Saugier, B. and Katerji, N. (1991). Some plant factors controlling evapotranspiration. Agric. Forest Meteor., 54(2-4):263 – 277.

Savijarvi, H. and Raisanen, P. (1997). Long-wave optical properties of water clouds and rain. Tellus, 50A:1–11.

Scott, N. A. and Chédin, A. (1981). A fast line-by-line method for atmospheric absorption computations - the automatized atmospheric absorption atlas. J. of Appl. Meteor., 20:802–812.

Shuttleworth, W. J. (1988). Evaporation from amazonian rainforest. Proc. R. Soc. Lond. B, 233:321–346.

Sitch, S., Smith, B., Prentice, I. C., Arneth, A., Bondeau, A., Cramer, W., Kaplan, J. O., Levis, S., Lucht, W., Sykes, M. T., Thonicke, K., and Venevsky, S. (2003). Evaluation of ecosystem dynamics, plant geography and terrestrial carbon cycling in the lpj dynamic global vegetation model. Global Change Biol., 9(2):161–185.

Skamarock, W. C., Klemp, J. B., Dudhia, J., Gill, D. O., Baker, D. M., Duda, M. G., Huang, X.-Y., Wang, W., and Powers, J. G. (2008). A description of the advanced research wrf version 3. NCAR Tech. Note NCAR/TN-475+STR, page 125.

Smith, E. A. and Lei, S. (1992). Surface forcing of the infrared cooling profile over the tibetan plateau. part i: Influence of relative longwave radiative heating at high altitude. J. Atmos. Sci., 49:805–822.

Smith, S. D. (1988). Coefficients for sea surface wind stress, heat flux, and wind profiles as a function of wind speed and temperature. J Geophys. Res., 93:15467–15472.

Stephens, G. L. (1978). Radiation profiles in extended water clouds. ii: Parameterization schemes. J. Atmos. Sci., 35:2123–2132.

Stull, R. B. (1988). An introduction to boundary layer meteorology. Kluwer Academic Publishers.

Sundqvist, H. (1978). A parameterization scheme for non-convective condensation including prediction of cloud water content. Q. J. R. Meteorol. Soc., 104(441):677–690.

Sundqvist, H. (1988). Parameterization of condensation and associated clouds in models for weather prediction and general circulation simulation. In Schlesinger, M., editor, Physically-Based Modelling and Simulation of Climate and Climatic Change, volume 243 of NATO ASI Series, pages 433–461. Springer Netherlands.

Tiedtke, M. (1989). A comprehensive mass flux scheme for cumulus parameterization in large-scale models. Mon. Wea. Rev., 117:1779–1800.

Tiedtke, M. (1993). Representation of clouds in large-scale models. Mon. Wea. Rev., 121:3040.

Vigroux, E. (1953). Contribution à l'étude expérimentale de l'absorption de l'ozone. Ann. Phys., 8:709.

Vimeux, F., Tremoy, G., Risi, C., and Gallaire, R. (2011). A strong control of the South American SeeSaw on the intraseasonal variability of the isotopic composition of precipitation in the Bolivian Andes. Earth. Planet. Sci. Lett.

WMO (1984). The intercomparison of radiation codes in climate models (icrccm), longwave, clear-sky calculations. World Climate Programme, Geneva, Switzerland, Rep. WCP-93:37.

Yamada, T. (1983). Simulations of nocturnal drainage flows by a q^2l turbulence closure model. J. Atmos. Sci., 40:91–106.

Zender, C. S. and Kiehl, J. T. (1997). Sensitivity of climate simulations to radiative effects of tropical anvil structure. J. Geophys. Res.: Atmospheres, 102(D20):23793–23803.

Appendix A

physiq.F subroutine

In this appendix detailed information on the principal procedure which deals with the physics is provided.

- Information about initialization of the physics values is given in figure A.1
- Diagram flow of subroutines and internal modules is given in figures A.2 and A.3
- Input/Output variables of the subroutine is provided in table A.1

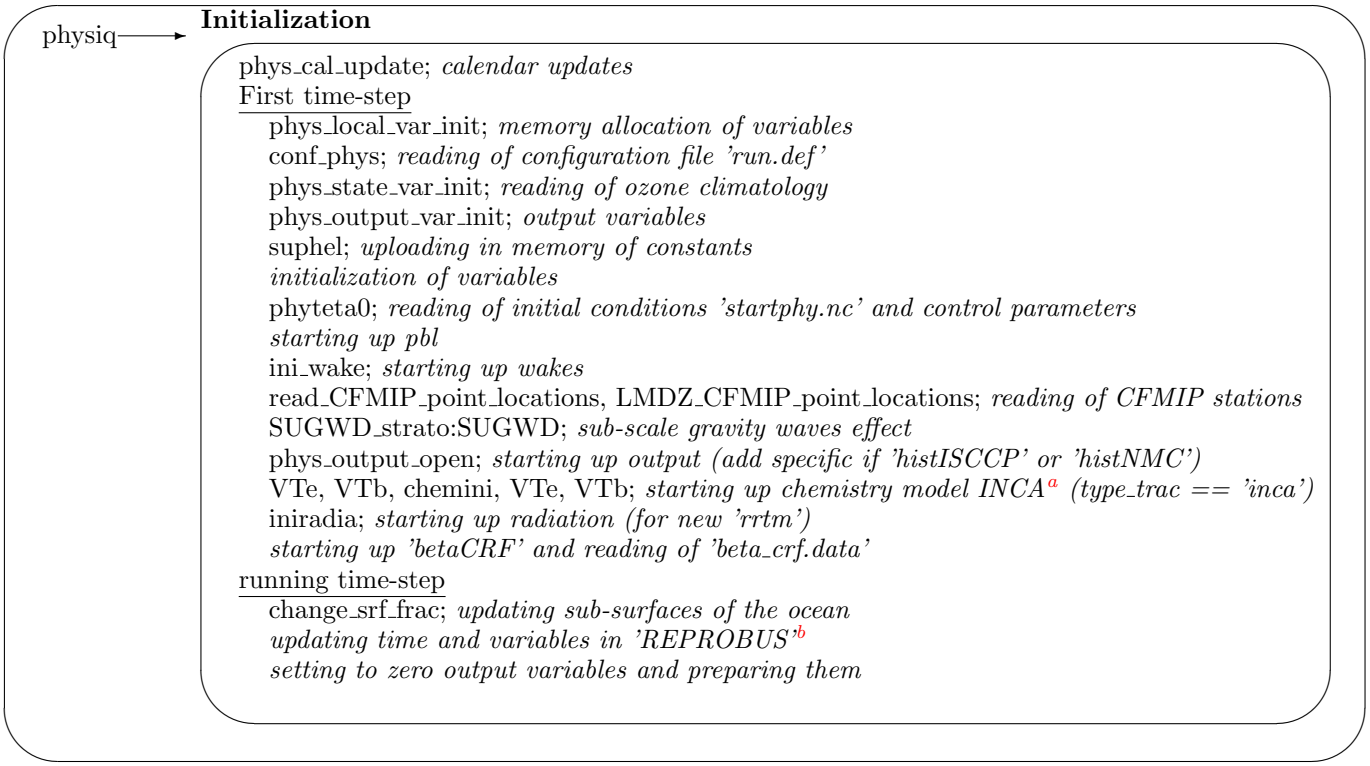

Figure A.1: Schematic representation of the initialization process inside the physics parameterizations

[a] INteraction with Chemistry and Aerosol (see description in (Dufresne et al., 2013))
[b] Reactive Processes Ruling the Ozone Budget in the Stratosphere (Lefèvre et al., 1994)

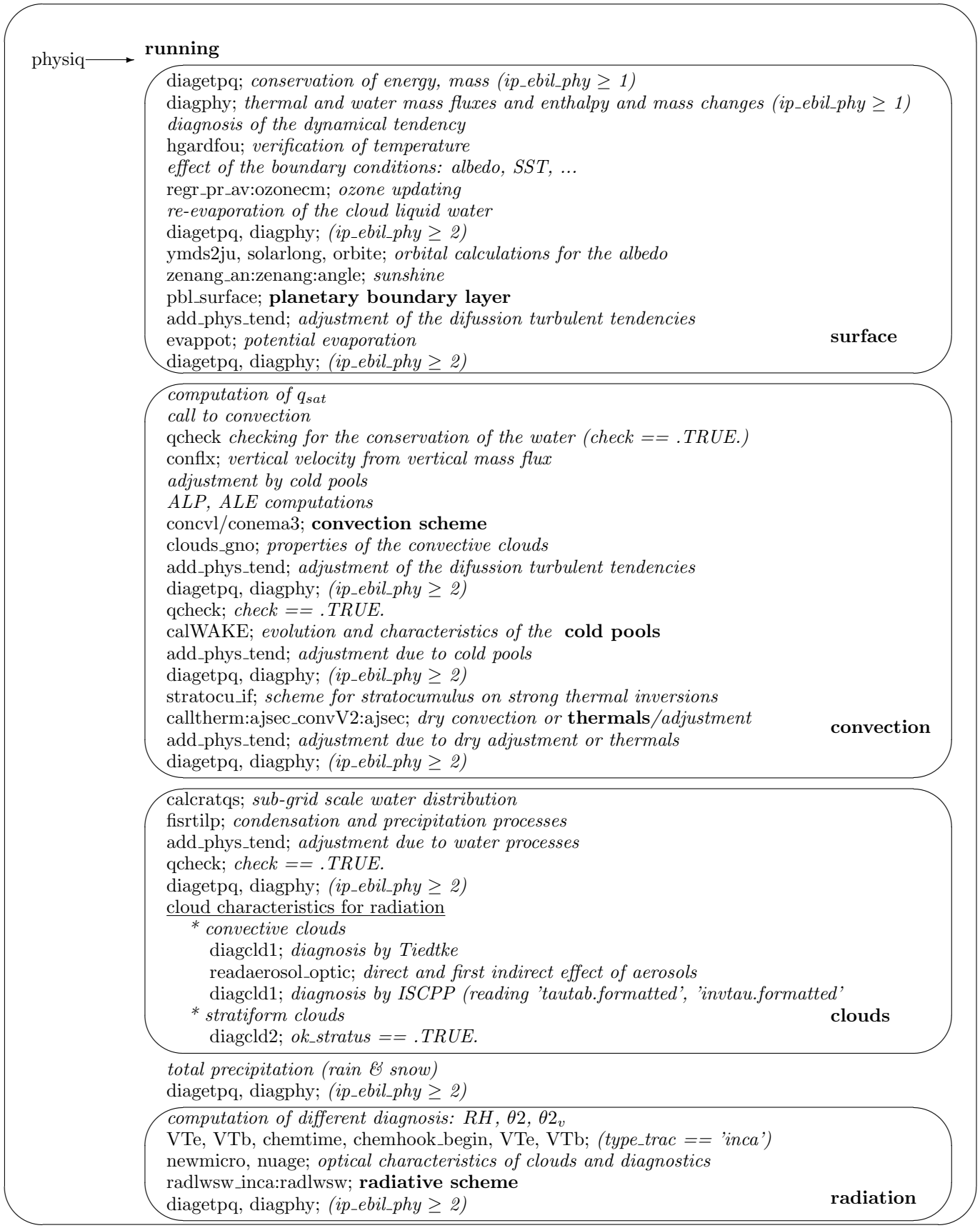

Figure A.2: Schematic representation of the running process inside the physics parameterizations of LMDZ (phylmd version). (1st part)

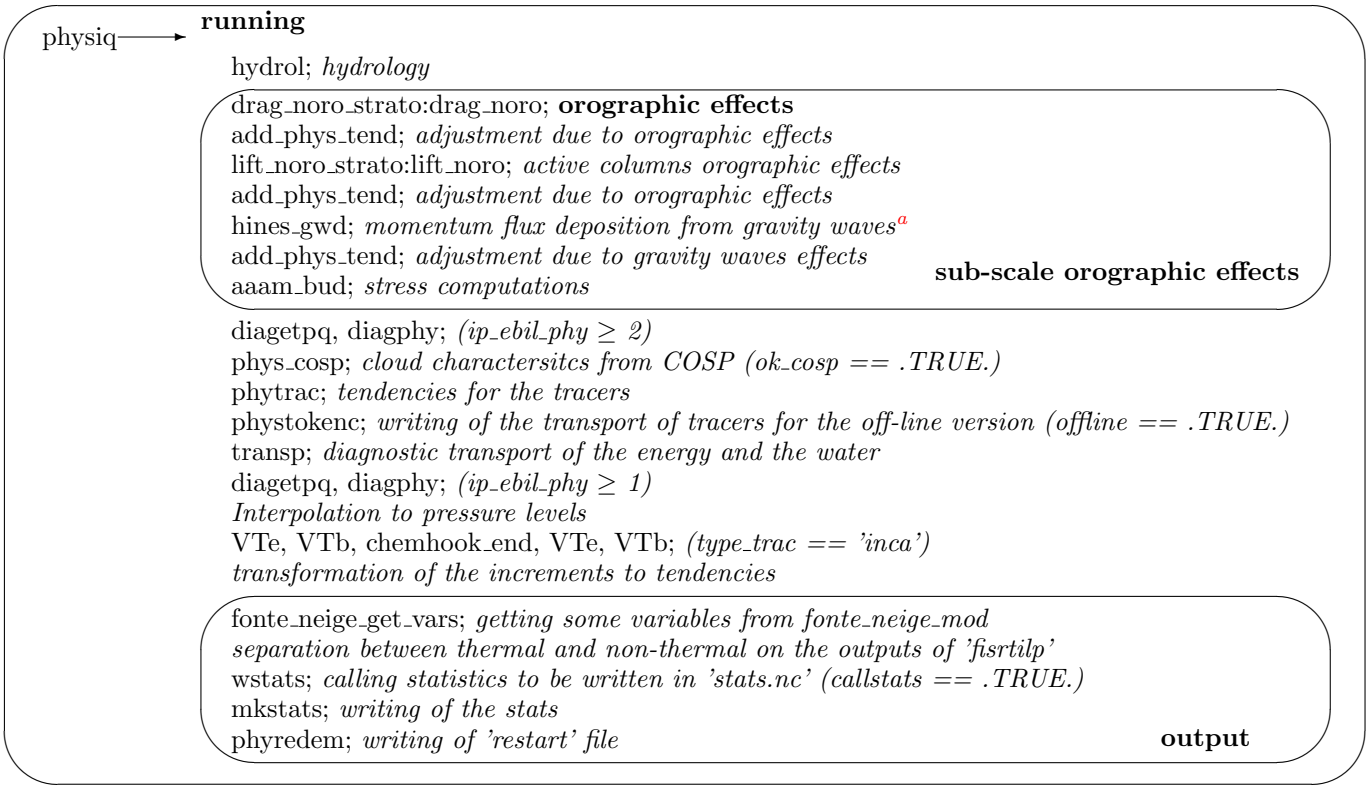

Figure A.3: Schematic representation of the running process inside the physics parameterizations of LMDZ (phylmd version). (2nd part)

[a] following (Hines, 1997a,b)

Table A.1: Variables and modules used by 'physiq' subroutine. (I: integer, R: real, C: complex, L: logical). longcles = 20. `klon`: horizontal size, `klev`: vertical levels, `nqtot`: number of tracers

variable	**type(dimensions)**	**Input/Output**	**meaning**
`nlon`	`I`	I	horizontal number of grid points
`nlev`	`I`	I	number of vertical grid levels, being equal to `'klev'`
`debut`	`L`	I	logical variable indicating first time
`lafin`	`L`	I	logical variable indicating last time
`jD_cur`	`R`	I	current day of calling the physics (in *Julian* days)
`jH_cur`	`R`	I	current hour of calling the physics (in *Julian* days)
`pdtphys`	`R`	I	integrating time-step for the physics (in *seconds*)
`paprs`	`R(klon,klev+1)`	I	pressure at every level (in Pa) - full 'w' levels
`pplay`	`R(klon,klev)`	I	pressure at the center of each level (in Pa) - half 'u,v,t,q' levels
`pphi`	`R(klon,klev)`	I	geopotential of each level (in gz, reference at surface). $phi = pphi + pphis$
`pphis`	`R(klon)`	I	geopotential at the surface
`presnivs`	`R(klev)`	I	output pressures of the levels (in Pa, Vertical levels imposing $P_{sfc} = 1000\ hPa$)
`clesphy0`	`R(longcles)`	I	I/O control checking
`u`	`R(klon,klev)`	I	wind speed on the $\hat{e}_x$ direction (W to E, in m/s)
`v`	`R(klon,klev)`	I	wind speed on the $\hat{e}_y$ direction (S to N, in m/s)
`t`	`R(klon,klev)`	I	temperature (in K)
`qx`	`R(klon,klev,nqtot)`	I	specific humidity and mixing ratios of other tracers (in kg/kg)
`flxmass_w`	`R(klon,klev)`	I	vertical mass flux
`d_u`	`R(klon,klev)`	O	Physical tendency of `'u'` ($m/s/s$)
`d_v`	`R(klon,klev)`	O	Physical tendency of `'v'` ($m/s/s$)
`d_t`	`R(klon,klev)`	O	Physical tendency of `'t'` (K/s)
`d_qx`	`R(klon,klev,nqtot)`	O	Physical tendancy pof `'qx'` ($kg/kg/s$)
`d_ps`	`R(klon)`	O	Physical tendency of the surface pressure (Pa/s)
`dudyn`	`R(iim+1,jjmp1,klev)`	O	
`PVteta`	`R(klon,nbteta)`	O	Potential Vorticity at constant theta

Appendix B

Configuration files: *.def

The choice of variables to be set is simple (e.g. `nday` number of modeled days to run), while the others do not need to be changed for normal use.

The format of the `.def` files is quite straightforward (and flexible): values given to parameters must be given as:

```
parameter = value
```

Any blank line or line beginning with symbol `#` is a comment, and instruction lines may be written in any order. Moreover, not specifying a parameter/value set (e.g. deleting it or commenting it out) means you want the GCM to use a default built-in value. Additionally, one may use a specific keyword `INCLUDEDEF` to specify another (text) file in which to also read values of parameters; e.g.:

```
INCLUDEDEF=physiq.def
```

The `used_*.def` files contain all the values used in the simulation, even the default ones which one has not selected.

B.1 run.def

Configuration ASCII file for the general configuration.
Here are some details about some of the parameters which may be set in `run.def`:

```
## Fichier de configuration general
##
INCLUDEDEF=physiq.def
INCLUDEDEF=gcm.def
INCLUDEDEF=orchidee.def
INCLUDEDEF=output.def
INCLUDEDEF=config.def
```

calendar		
ip_ebil_phy	1	(D: ?) meaning?
ip_ebil_dyn	1	(D: ?) meaning?
calend	earth_360d	Type of calendar to use (D: earth_360d, earth_360: 12 months of 30 days, dearth_365d: no leap years, earth_366d: leap years) does orbital parameters automatically adapt?
dayref	1	day julian with leap years? (units?) of the inital state (D: ?, g.e. 350 if 20 December)
anneeref	1980	year of the initial state (D: ?, in [YYYY] format)
nday	5	number of days of integration (D: ?, fraction?)
raz_date	0	reduction to zero of the inital date (D: ?)
output		

iconser	20	output period (in number of time-steps) of the control variables (D: ?)
iecri	1	writting period (in days) of the history file (D: ?)
ok_dynzon	n	flag of `'dynzon.nc'` output (D: ?, n: no, y: yes)
periodav	30.	storage period (in days) of the `'dynzon.nc'` file (D: ?)
adjust	n	activation of the computation of balancing of the load in the nodes on multiprocessor run (D: ?, n: no, y: yes)
use_filtre_fft	n	activation of the FFT filter. Only works on parallel compilations. If it is not activated there is also a filter in the poles (D: ?, n: no, y: yes)
prt_level	0	level of checking/debugging printing (D: ?)

Table B.1: Configuration parameters of the file `run.def`. 'D' stands for 'default' value. Showed values are from the test simulation LMDZ5 - BENCH48x36x19

B.2 config.def

Configuration ASCII file for the configuration

output						
OK_journe	y					daily (D: ?, n: no, y: yes)
OK_mensuel	y					monthly (D: ?, n: no, y: yes)
ok_hf	y					high frequency (D: ?, n: no, y: yes)
OK_instan	n					instantaneous (D: ?, n: no, y: yes)
ok_LES	n					LES (D: ?, n: no, y: yes)
ok_regdyn	y					computation of the dynamical regimes in the predefined regions (D: ?, n: no, y: yes)
# To transform in the following line when it will be compatible with `'libGCM'`						
phys_out_filekeys	y	y	n	y	n	file keys
phys_out_filenames	histmth	histday	histhf	histins	histLES	file names
phys_out_filetimesteps	5day	1day	1hr	6hr	6hr	file time steps (month, day, hr, mn, sec)
phys_out_filelevels	10	5	0	4	4	number of levels of output (see tables C.1 to C.11 for the values for each variable)
phys_out_filetypes	ave(X)	ave(X)	ave(X)	inst(X)	inst(X)	output types values?
coupling with other modules						
type_ocean	force					option for coupling with the ocean. Without coupling a slab ocean is used (D: force, force: options?)
version_ocean	nemo					version of the ocean (D: ?, nemo: use Nemo model options?)
VEGET	n					coupling with orchidee (D: n, n: no, y: yes)
type_run	CLIM					type of run (D:AMIP, AMIP: ??, ENSP: ??, clim: ??)
soil_model	y					activation of the soil model (D: ?, n: no, y: yes) is it incompatible with VEGET?
radiative transfer						
iflag_radia	1					activation of the radiation (MPL) (D: 1, 0: without, 1: active)
nbapp_rad	12					number of calls per day of the radiation routines (D: ?)
orbital & geological era						
R_ecc	0.016715					eccentricity (D: ?)
R_peri	102.7					equinox (units?) (D: ?)
R_incl	23.441					inclination (degrees) of the rotation of the Earth (D: ?)

solaire	1366.0896	solar constant (Wm^{-2}) (D: ?)
pmagic	0.008	additive factor (1) for the correction of the albedo (D: ?)

ratio of Green House Gases

	CO_2	CH_4	N_2O	$CFC-11$	$CFC-12$
D:	348.	1650.	306.	280.	484.

co2_ppm	0.36886500E+03	CO_2 (ppm)

#RCO2=co2_ppm * 1.0e-06 * 44.011/28.97= 5.286789092164308E-04

CH4_ppb	0.17510225E+04	CH_4 (ppb)

#RCH4=1.65E-06* 16.043/28.97= 9.137366240938903E-07

N2O_ppb	0.31585000E+03	N_2O (ppb)

#RN2O=306.E-09* 44.013/28.97= 4.648939592682085E-07

CFC11_ppt	5.18015181E+01	$CFC-11$ (ppt)

#RCFC11=280.E-12* 137.3686/28.97= 1.327690990680013E-09

CFC12_ppt	0.99862742E+03	$CFC-12$ (ppt)

#RCFC12=484.E-12* 120.9140/28.97= 2.020102726958923E-09

effect of aerosols

ok_ade	n	flag of the direct effect of the aerosol (D: ?, n: no, y: yes)
ok_aie	n	flag of the indirect effect of the aerosol (D: ?, n: no, y: yes)
aer_type	actuel	type of variation of the aerosol (D: ?, `actuel`: current , `prein`: pre-industrial, `scenario`: projection, `annuel`: given annual concentrations (see section 3.15)
flag_aerosol	=0	type of the couple aersol (D: 1, =1: ??, =2: only bc, =3: only pom, =4: only seasalt, =5: only dust, =6: all aerosol)
bl95_b0	1.7	parameter in the CDNC-maer link ($\log_{10}(CDCN) = bl95\_b0 + bl95\_b1 \log(mSO_4)$) (Boucher and Lohmann, 1995) (D: ?)
bl95_b1	0.2	parameter in the CDNC-maer link (Boucher and Lohmann, 1995) (D: ?)
read_climoz	0	ozone file reading (D: ?) 0: do not read an ozone climatology 1: read a single ozone climatology that will be used day and night 2: read two ozone climatologies, the average day and night climatology and the daylight climatology

COSP (CFMIP Observational Simulator Package, http://cfmip.metoffice.com/COSP.html)
Which version?

ok_cosp	n	activation of the COPS simulator (D: ?, n: no, y: yes)
freq_COSP	10800.	frequency (in seconds?) of calling of the COSP simulator (D: ?)
ok_mensuelCOSP	y	outputting of monthly COSP file 'histmthCOSP.nc') (D: ?, n: no, y: yes)
ok_journeCOSP	y	outputting of daily COSP file 'histdayCOSP.nc') (D: ?, n: no, y: yes)
ok_hfCOSP	n	outputting of high frequency COSP file 'histhfCOSP.nc') (D: ?, n: no, y: yes)

ISCPP simulator http://cfmip.metoffice.com/ISCCP.html. REMOVED from LMDZ since version 4.12

Which version?

ok_isccp	n	activation of the ISCCP simulator (D: ?, n: no, y: yes)
top_height	=1	selection of computation of clouds for the simulator when it uses the IR and/or VIS data and the algorithm ISCCP-D1 (D: ?) =1: IR-VIS algorithm =2: same as 1, plus "$p_{top}(ibox) = p_{full}(ilev)$" =3: IR algorithm
overlap	3	Hypothesis of covering (HR) used by the ISCPP simulator (D: ?) 1 Maximum overlap 2 Random overlap 3 Max/Random overlap

Table B.2: Configuration parameters of the file `config.def`. 'D' stands for 'default' value. Showed values are from the test simulation LMDZ5 - BENCH48x36x19

B.3 gcm.def

Configuration ASCII file for the gcm configuration

- **day_step:**, the number of dynamical steps per day to use for the time integration. This needs to be large enough for the model to remain stable (this is related to the CFL stability criterion which essentially depends on the horizontal resolution of the model). Note that `day_step` must also be divisible by `iperiod`.
- **tetagdiv, tetagrot, tetatemp:** control the dissipation intensity. It is better to limit the dissipation intensity (tetagdiv, tetagrot, tetatemp should not be too low). However the model diverges if tetagdiv, tetagrot, tetatemp are too high, especially if there is a lot of dust in the atmosphere. Example used with `nitergdiv=1` and `nitergrot=niterh=2`
- **idissip:** is the time step used for the dissipation: dissipation is computed and added every `idissip` dynamical time step. If `idissip` is too short, the model waste time in these calculations. But if idissip is too long, the dissipation will not be parametrized correctly and the model will be more likely to diverge. A check must be made, so that: `idissip` $<$ `tetagdiv`$\times$`daystep`$/88775$ (same rule for `tetagrot` and `tetatemp`). This is tested automatically during the run.
- **iphysiq:** is the time step used for the physics: physical tendencies are computed every `iphysiq` dynamical time step. In practice, we usually set the physical time step to be of the order of half an hour. We thus generally set `iphysiq`= `day_step`$/48$

day_step	240	number of time-steps per day multiple of 'iperiod' (D: ?)
iperiod	5	period for the Matsuno's time-step (D: ?, in number of time-steps)
dissipation		
idissip	5	dissipasion period (D: ?, in number of time-steps)
lstardis	y	activation of the dissipative operator (D: ?, n: no, y: yes)
nitergdiv	1	number of iterations of the dissipation operator 'gradiv' (D: ?) meaning?
nitergrot	2	number of iterations of the dissipation operator 'nxgradrot' (D: ?) meaning?
niterh	2	number of iterations of the dissipation operator 'divgrad' (D: ?) meaning?
tetagdiv	18000.	dissipation time (in seconds) of the smallest long.d waves for u,v in 'gradiv' (D: ?)
tetagrot	18000.	dissipation time (in seconds) for the smallest waves for u,v in 'nxgradrot' (D: ?)
tetatemp	18000.	dissipation time (in seconds) of the smallest long.d waves for h in 'divgrad' (D: ?)
dissip_period	0	frequency of activation of the dissipation (D: ?, multiple of 'iperiod', 0 if it is done automatically)

coefdis	0.	coefficient (units?) for 'gamdissip' (D: ?) meaning?
purmats	n	selection of the temporal integration scheme (D: ?, y: Matsuno, n: Matsuno-leapfrog)
iflag_phys	1	flag of physics selection (D: ?) 0: without physics (e.g. Shallow Water) 1: with physics (e.g. phylmd physics) 2: with recall to Newtonian inside the dynamics
read_start	y	flag indicating the use of starting files `start.nc` and `startphy.nc` (D: ?, y: yes, n: without. Initialization of fields is done by dynamics using 'iniacademic')
iphysiq	5	period of the physics in dynamical time-steps (D: ?, in combination with iflag_phys=1)
nsplit_phys	1	number of time-steps of the physics (D: ?) Schemes can be run multiple times within the same time-step?
ok_strato	n	flag indicating strato (D: ?, n: no, y: yes)
iflag_top_bound	0	sponge layer of the pressure levels with less than 100 times the pressure of the last level (D: ?)
tau_top_bound	5.e-5	coefficient (units?) for the sponge layer (value at the last level) (D: ?)
zoom		
clon	0.	longitude (in degrees) of the center of the zoom (D: ?)
clat	45.	latitude (in degrees) of the center of the zoom (D: ?)
grossismx	1.0	magnification factor of the zoom according to the longitude (D: ?, value to avoid zoom on x)
grossismy	1.0	magnification factor of the zoom according to the latitude (D: ?, value to avoid zoom on y)
fxyhypb	y	selection of the function 'f(y)' of the zoom (D: ?, .true.: hyperbolic, .false.: sinusoidal)
dzoomx	0.15	extension in longitude (as fraction of the total zone) of the zoom zone (D: ?)
dzoomy	0.15	extension in latitude (as fraction of the total zone) of the zoom zone (D: ?)
taux	3.	rigidity of the zoom in X (D: ?)
tauy	3.	rigidity of the zoom in Y (D: ?)
ysinus	y	kind of latitude dependence of function 'f(y)' (D: ?, n: latitude, y:sin(*latitude*))

Table B.3: Configuration parameters of the file `gcm.def`. 'D' stands for 'default' value. Showed values are from the test simulation LMDZ5 - BENCH48x36x19

B.4 physiq.def

Configuration ASCII file for the physical schemes

```
#*********************************
## Si=.T. , lecture du fichier limit avec la bonne annee          meaning?
```

orographic parametres and cdrags Equivalence with (Lott and Miller, 1997)? Is it called al time-steps?		
ok_limitvrai	n	(D: ?, n: no, y: yes) meaning?
f_cdrag_stable	1.	correcting factor for neutral heat exchange coefficients (1) (D: ?)
f_cdrag_ter	1.	correcting factor for neutral heat exchange (in 1) (D: 1)
f_cdrag_oce	0.8	correcting factor for neutral heat exchange (in 1) (D: 0.8)
cdmmax	2.5E-3	Cdrags (in 1) (D: ?) meaning?
cdhmax	2.0E-3	Cdrags (in 1) (D: ?) meaning?
ok_orodr	y	Orodr for the orography (D: ?, n: no, y: yes) meaning?
ok_orolf	y	Orolf for the orography (D: ?, n: no, y: yes) meaning?

f_rugoro	0.	Rugoro (units?) (D: ?) meaning?
Is it called all time-steps?		
radiation		
iflag_rrtm	0	activation of new radiation scheme RRTM (D: 0, 0: no, 1: yes)
clouds		
cld_lc_lsc	4.16e-4	precipitation threshold (units?) for the stratiform clouds (D: 2.6e-4)
cld_lc_con	4.16e-4	precipitation threshold (units?) for the stratiform clouds (D: 2.6e-4)
cld_tau_lsc	1800.	temporal constant (in seconds?) to remove lsc water (D: 3600.)
cld_tau_con	1800.	temporal constant (in seconds?) to remove convective water (D: 3600.)
ffallv_lsc	0.5	corrective factor for the falling of the ice cristals (D: 1)
ffallv_con	0.5	corrective factor for the falling of the ice cristals (D: 1)
coef_eva	2e-5	re-evaporation coefficient for the rain (D: 2.e-5)
reevap_ice	y	(D: n, n: no, y: yes) meaning?
iflag_cldcon	3	computation of the properties of the convective clouds (D: 1, options?) meaning?
fact_cldcon	1.	computation of the properties (units?) of the convective clouds (D: 0.375) meaning?
facttemps	0.	computation of the properties (units?) of the convective clouds (D: 1.e-4) meaning?
iflag_pdf	1	computation of the condensed water and cloud fraction from the PDF (D=0, 0: version with 'ratqs' , $\neq 0$: new PDFs) meaning?
ok_newmicro	y	computation of the optical thickness and emissivity of the clouds (D: y, n: no, y: yes)
iflag_ratqs	0	computation of the optical (units?) thickness and emissivity of the clouds (D: 1) meaning?
ratqsbas	0.005	computation of the optical (units?) thickness and emissivity of the clouds (D: 0.01) meaning?
ratqshaut	0.33	computation of the optical (units?) thickness and emissivity of the clouds (D: 0.3) meaning?
rad_froid	35	effective radius (units?) for the ice clouds (D:35)
rad_chau1	12	effective radius (units?) for the liquid water clouds (D: 13)
rad_chau2	11	drop size (units?) of cloud water (D: 9)
new_oliq	y	selection of new oliq (D: ?, n: no, y: yes) meaning?
Convection		
iflag_con	30	convection scheme (D: 2, 1: LMD, 2: Tiedtke, 3: KE new physics, 30: KE IPCC)
if_ebil	0	level of output of the diagnostic of the energy conservation (D: ?)
epmax	.999	efficency (units?) of the maximum precipitation (D: .993) (see value ep_{max} in section 3.6)
ok_adj_ema	n	dry convective adjustment at the beginning of the convection (D: n, n: no, y: yes)
iflag_clw	1	dry convective adjustment at the beginning of the convection (D: 0, 0: no, 1: yes)
iflag_clos	1	Closure of the convection (D: 1, 1: AR4, 2: ALE and ALP)
iflag_mix	1	mixing rule at the entrainment (D: 1, 0: plate, 1: AR4: PDF)
qqa1	0.	weigths of the PDFs at the flat (D: 1.)
qqa2	1.	weigths of the PDFs at the bell (D: 0.)
cvl_corr	1.0	multiplicative factor of the convective precipitations in KE (D: ?)
planetary boudary layer		
iflag_thermals	0	CL scheme of the thermals (D: 0, 0: dry adjustment, 1: thermal versions) Is suited with iflag_clos?
nsplit_thermals	1+	TIME-step splitting (units?) for the thermals (D: ?)
tau_thermals	0.+	TIME-step splitting (units?) for the thermals (D: ?)
iflag_thermals_ed	0+	TIME-step splitting (units?) for the thermals (D: ?, 0: no, 1: yes)
iflag_thermals_optflux	0+	TIME-step splitting (units?) for the thermals (D: ?, 0: no, 1: yes)
iflag_pbl	1	surface layer scheme (D: 1, 1: LMD, 8: Mellor-Yamada)
ksta_ter	1.e-7	turbulent diffusion (units?) (D: ?)
ksta	1.e-10	turbulent diffusion (units?) (D: ?)
ok_kzmin	y	computation of Kzmin in the surface CL (D: ?, n: no, y: yes)
iflag_coupl	0	coupling with the convection (D: ?, 0: AR4, 1: new physics)

seuil_inversion	-0.08	(units?) (D: ?) meaning?
wakes		
iflag_wake	0	activation of the wakes (D: 0, 0: no (AR4), 1: new physics)
alp_offset	-0.2	(units?) (D: ?)

Table B.4: Configuration parameters of the file `physiq.def`. 'D' stands for 'default' value. Showed values are from the test simulation LMDZ5 - BENCH48x36x19

Random gravity waves (GW)		
ok_gwd_rando	y	Activitate the stochastic parameterization of convective GWs, should be equal to `ok_strato` (D: ?, n: no, y: yes)
gwd_rando_ruwmax	2.	Scale the momentum fluxes (1) due to convective GWs (D: ?)
gwd_rando_sat	0.2	Scale the saturated momentum flux of convective GWs
cloud characteristics		
rei_min	20.	minimum effective radii (μm) of the cloud particles (D: ?)
rei_max	61.29	maximum effective radii (μm) of the cloud particles (D: ?)
boundary layer		
iflag_fisrtilp_qsat	4	temperature dependency of qsat for iterative procedure temporary flag to switch between the old (CMIP5, D=0) and new versions (=1) versions
iflag_thermals_closure	1	Reactivation du calcul d'un zmax continu pour les thermiques reactivation d'une fermeture humide des thermiques `iflag_thermals_closure=2` (D=1)
Stochastic trigerring		
iflag_trig_bl	2	pbl triggering (0: deterministic, 1: stochastic, D: ?)
s_trig	1.2e7	critical surface at LCL (D: ?)
tau_trig_shallow	1200	de-corrlation time (*seconds*) between cumulus scenes (D: ?)
tau_trig_deep	1200	corrlation time (*seconds*) between cumulunimbus scenes (D: ?)
iflag_clos_bl	1	pbl clousre (0: deterministic, 1: statistic, 2: statistic+convergence large-scale, D: ?)
Micro-physics: thermal modification for the mixed liquid/ice phase in the clouds (see section 3.8)		
t_glace_min	240.	minimum temperature (D: ?)
t_glace_max	273.13	maximum temperature (D: ?)
exposant_glace	1.7	exponential term of the distribution (D: ?)
iflag_t_glace	1	(D=0)
TKE prognostic equation		
iflag_ener_conserv	1	The source terms of the TKE prognostic equation are diagnosed from tendencies (du, dv, dT) associated with subrgrid scaleamotions and treated as an additional heat source. 0: no conservation, -1: old adhoc correction for kinetic E only (used for CMIP5), 1: conservation, 101: conversion from kinetic to heat only, 110: conversion from potential to heat only (D=-1)
ok_conserv_q	y	Conservation of tracers (D=n)

Table B.5: New configuration parameters of the file `physiq.def`. 'D' stands for 'default' value. Showed values are from NPv5.01 version

B.5 traceur.def

Configuration ASCII file for the tracers configuration

Tracers in input (`start.nc` and `startfi.nc`) and output files (`restart.nc` and `restartfi.nc`) are stored using individual tracer names (e.g. `co2` for CO_2 gas, `h2o_vap` for water vapour, `h2o_ice` for water ice, ...).

The first line of the `traceur.def` file (an ASCII file) must contain the number of tracers to load and use (this number should be the same as given to the `-t` option of the `makegcm` script when the GCM was compiled), followed

by the tracer names (one per line). Note that if the corresponding tracers are not found in input files `start.nc` and `startfi.nc`, then the tracer is initialized to zero.

4		(D: ?), total number of tracers (mininum 3)
14	14	H2Ov (D: ?) water vapor
10	10	H2Ol (D: ?) liquid water
10	10	RN (D: ?) Radon
10	10	PB (D: ?) Plomb

Table B.6: Configuration parameters of the file 'traceur.def'. 'D' stands for 'default' value. Showed values are from the test simulation LMDZ5 - BENCH48x36x19

Appendix C

Input/Output files

A detailed description of the content of each input/ouptut file is here given.

C.1 LMDZ output variables

Tables C.1 to C.11 provide a list of variables outputted by LMDZ and the associated numbers for each kind of LMDZ output.

Table C.1: Table of variables included in the file hist LMDZ files. output # stands for (histmth, histday, histhf, histins, values taken from `config.def`, see section B.2). ti86400=t_inst_00086400. Getting the values from 'phylmd/phys_output_ctrlout_mod.F90'. Some variables are only available in NPv3.1 version

ariable name	**Standard name**	**units**	**coordinates**	**output #**
ages_lic	Snow age	*day*	TIME lat lon	3,10,10,10,10,10
ages_oce	Snow age	*day*	TIME lat lon	10,10,10,10,10,10
ages_sic	Snow age	*day*	TIME lat lon	3,10,10,10,10,10
ages_ter	Snow age	*day*	TIME lat lon	10,10,10,10,10,10
Ahyb	model_level_number	*Pa*		1,1,1,1,1,1
aire	Grid area	–	lat lon	1,1,10,10,1,1
aireTER	Grid area CONT	–	TIME lat lon	10,10,1,10,10,10
alb1	Surface VIS albedo	–	TIME lat lon	3,10,10,10,10,10
alb2	Surface Near IR albedo	–	TIME lat lon	3,10,10,10,10,10

Table C.2: Table of variables included in the file hist LMDZ files (cont' 1)

albe_lic	Albedo VIS surf. lic	$m2/s2$	TIME lat lon	3,7,10,7,10,10
albe_oce	Albedo VIS surf. oce	$m2/s2$	TIME lat lon	3,7,10,7,10,10
albe_sic	Albedo VIS surf. sic	$m2/s2$	TIME lat lon	3,7,10,7,10,10
albe_ter	Albedo VIS surf. ter	$m2/s2$	TIME lat lon	3,7,10,7,10,10
a_th	Thermal plume fraction	–	TIME presnivs lat lon	4,10,10,10,10,10
ale	ALE	$m2/s2$	TIME lat lon	1,1,1,10,10,10
ale_bl	ALE BL	$m2/s2$	TIME lat lon	1,1,1,10,10,10
ale_wk	ALE WK	$m2/s2$	TIME lat lon	1,1,1,10,10,10
alp	ALP	$W/m2$	TIME lat lon	1,1,1,10,10,10
alp_bl	ALP BL	$m2/s2$	TIME lat lon	1,1,1,10,10,10
alp_wk	ALP WK	$m2/s2$	TIME lat lon	1,1,1,10,10,10
Alt	model_level_number	Km		1,1,1,1,1,1
beta_prec	LS Conversion rate to prec	$(kg/kg)/s$	TIME presnivs lat lon	4,10,10,10,10,10
Bhyb	model_level_number			1,1,1,1,1,1
bils	Surf. total heat flux	$W/m2$	TIME lat lon	1,2,10,5,10,10
bils_diss	Surf. total heat flux	$W/m2$	TIME lat lon	1,2,10,5,10,10
bils_ec	Surf. total heat flux	$W/m2$	TIME lat lon	1,2,10,5,10,10
bils_enthalp	Surf. total heat flux	$W/m2$	TIME lat lon	1,2,10,5,10,10
bils_kinetic	Surf. total heat flux	$W/m2$	TIME lat lon	1,2,10,5,10,10
bils_latent	Surf. total heat flux	$W/m2$	TIME lat lon	1,2,10,5,10,10
bils_tke	Surf. total heat flux	$W/m2$	TIME lat lon	1,2,10,5,10,10
cape	Conv avlbl pot ener	J/kg	TIME lat lon	1,10,10,10,10,10
cape_max	CAPE max.	J/kg	TIME lat lon	10,1,10,10,10,10
cdrh	Heat drag coef.	–	TIME lat lon	1,10,10,7,10,10
cdrm	Momentum drag coef.	–	TIME lat lon	1,10,10,10,10,10
cldemi	Cloud optical emissivity	1	TIME presnivs lat lon	10,5,10,10,10,10
cldh	High-level cloudiness	–	TIME lat lon	1,1,10,10,10,10
cldl	Low-level cloudiness	–	TIME lat lon	1,1,10,10,10,10
cldm	Mid-level cloudiness	–	TIME lat lon	1,1,10,10,10,10
cldq	Cloud liquid water path	$kg/m2$	TIME lat lon	1,1,10,10,10,10
cldt	Total cloudiness	–	TIME lat lon	1,1,2,10,5,10
cldtau	Cloud optical thickness	1	TIME presnivs lat lon	10,5,10,10,10,10
clwcon	Convective Cloud Liquid water content	kg/kg	TIME presnivs lat lon	4,10,10,10,10,10
contfracATM	% sfce ter+lic	–	lat lon	10,1,1,10,10,10
contfracOR	% sfce terre OR	–	TIME lat lon	10,1,1,10,10,10
cumPB	Cumulated tracer PBVL1	–	TIME lat lon	
cumRN	Cumulated tracer RNVL1	–	TIME lat lon	

Table C.3: Table of variables included in the file hist LMDZ files (cont' 2)

dmc	Deep COnvective Mass Flux	$kg/(m2*s)$	TIME presnivs lat lon	4,10,10,10,10,10
dnwd	saturated downdraft	$kg/m2/s$	TIME presnivs lat lon	4,10,10,10,10,10
dnwd0	unsat. downdraft	$kg/m2/s$	TIME presnivs lat lon	4,10,10,10,10,10
dqajs	Dry adjust. dQ	$(kg/kg)/s$	TIME presnivs lat lon	4,10,10,10,10,10
dqcon	Convection dQ	$(kg/kg)/s$	TIME presnivs lat lon	4,10,10,10,10,10
dqdyn	Dynamics dQ	$(kg/kg)/s$	TIME presnivs lat lon	4,10,10,10,10,10
dqeva	Reevaporation dQ	$(kg/kg)/s$	TIME presnivs lat lon	4,10,10,10,10,10
dqlsc	Condensation dQ	$(kg/kg)/s$	TIME presnivs lat lon	4,10,10,10,10,10
dqlscst	dQ strat.	$(kg/kg)/s$	TIME presnivs lat lon	10,10,10,10,10,10
dqlscth	dQ therm.	$(kg/kg)/s$	TIME presnivs lat lon	10,10,10,10,10,10
dqphy	Physics dQ	$(kg/kg)/s$	TIME presnivs lat lon	2,10,10,10,10,10
dqthe	Thermal dQ	$(kg/kg)/s$	TIME presnivs lat lon	4,10,10,10,10,10
dqvdf	Boundary-layer dQ	$(kg/kg)/s$	TIME presnivs lat lon	4,10,10,10,10,10
dqwak	Wake dQ	$(kg/kg)/s$	TIME presnivs lat lon	4,5,10,10,10,10
dtajs	Dry adjust. dT	K/s	TIME presnivs lat lon	4,10,10,10,10,10
dtcon	Convection dT	K/s	TIME presnivs lat lon	4,10,10,10,10,10
dtdis	TKE dissipation dT	K/s	TIME presnivs lat lon	4,10,10,10,10,10
dtdyn	Dynamics dT	K/s	TIME presnivs lat lon	4,10,10,10,10,10
dtec	Cinetic dissip dT	K/s	TIME presnivs lat lon	4,10,10,10,10,10
dteva	Reevaporation dT	K/s	TIME presnivs lat lon	4,10,10,10,10,10
d_th	Thermal plume detrainment	K/s	TIME presnivs lat lon	4,10,10,10,10,10
dthmin	dTheta mini	K/m	TIME lat lon	10,1,10,10,10,10
dtlif	Orography dT	K/s	TIME presnivs lat lon	4,10,10,10,10,10
dtlsc	Condensation dT	K/s	TIME presnivs lat lon	4,10,10,10,10,10
dtlschr	Large-scale condensational heating rate	K/s	TIME presnivs lat lon	4,10,10,10,10,10
dtlscst	dQ strat.	K/s	TIME presnivs lat lon	10,10,10,10,10,10
dtlscth	dQ therm.	K/s	TIME presnivs lat lon	10,10,10,10,10,10
dtlw0	CS LW radiation dT	K/s	TIME presnivs lat lon	4,10,10,10,10,10
dtlwr	LW radiation dT	K/s	TIME presnivs lat lon	4,10,10,10,10,10
dtoro	Orography dT	K/s	TIME presnivs lat lon	4,10,10,10,10,10
dtphy	Physics dT	K/s	TIME presnivs lat lon	2,10,10,10,10,10
dtsvdfg	Boundary-layer dTs(g)	K/s	TIME lat lon	10,10,10,10,10,10
dtsvdfi	Boundary-layer dTs(g)	K/s	TIME lat lon	10,10,10,10,10,10
dtsvdfo	Boundary-layer dTs(o)	K/s	TIME lat lon	10,10,10,10,10,10
dtsvdft	Boundary-layer dTs(t)	K/s	TIME lat lon	10,10,10,10,10,10
dtsw0	CS SW radiation dT	K/s	TIME presnivs lat lon	4,10,10,10,10,10
dtswr	SW radiation dT	K/s	TIME presnivs lat lon	4,10,10,10,10,10
dtthe	Thermal dT	K/s	TIME presnivs lat lon	4,10,10,10,10,10
dtvdf	Boundary-layer dT	K/s	TIME presnivs lat lon	4,10,10,10,10,10
dtwak	Wake dT	K/s	TIME presnivs lat lon	4,5,10,10,10,10

Table C.4: Table of variables included in the file hist LMDZ files (cont' 3)

ducon	Convection du	$m/s2$	TIME presnivs lat lon	4,10,10,10,10,10
dudyn	Dynamics dU	$m/s2$	TIME presnivs lat lon	4,10,10,10,10,10
dulif	Orography dU	$m/s2$	TIME presnivs lat lon	4,10,10,10,10,10
duoro	Orography dU	$m/s2$	TIME presnivs lat lon	4,10,10,10,10,10
duvdf	Boundary-layer dU	$m/s2$	TIME presnivs lat lon	4,10,10,10,10,10
dvcon	Convection dv	$m/s2$	TIME presnivs lat lon	4,10,10,10,10,10
dvdyn	Dynamics dV	$m/s2$	TIME presnivs lat lon	4,10,10,10,10,10
dvlif	Orography dV	$m/s2$	TIME presnivs lat lon	4,10,10,10,10,10
dvoro	Orography dV	$m/s2$	TIME presnivs lat lon	4,10,10,10,10,10
dvvdf	Boundary-layer dV	$m/s2$	TIME presnivs lat lon	4,10,10,10,10,10
ec550aer	Extinction at 550nm	m^-1	TIME presnivs lat lon	2,6,10,10,10,10
e_th	Thermal plume entrainment	K/s	TIME presnivs lat lon	4,10,10,10,10,10
evap	Evaporat	$kg/(s*m2)$	TIME lat lon	1,1,10,10,10,10
evap_lic	evaporation at surface lic	$kg/(s*m2)$	TIME lat lon	1,6,10,10,10,10
evap_oce	evaporation at surface oce	$kg/(s*m2)$	TIME lat lon	1,6,10,10,10,10
evappot_lic	Temperaturelic	K	TIME lat lon	4,6,10,10,10,10
evappot_oce	Temperatureoce	K	TIME lat lon	4,6,10,10,10,10
evappot_sic	Temperaturesic	K	TIME lat lon	4,6,10,10,10,10
evappot_ter	Temperatureter	K	TIME lat lon	1,6,10,10,10,10
evap_sic	evaporation at surface sic	$kg/(s*m2)$	TIME lat lon	1,6,10,10,10,10
evap_ter	evaporation at surface ter	$kg/(s*m2)$	TIME lat lon	1,6,10,10,10,10
evu	Eddy viscosity coefficient for Momentum Variables	$m2s-1$	TIME presnivs lat lon	4,10,10,10,10,10
fbase	Cld base mass flux	$kg/m2/s$	TIME lat lon	1,10,10,10,10,10
fder	Heat flux derivation	$W/m2$	TIME lat lon	1,2,10,10,10,10
ffonte	Thermal flux for snow melting	$W/m2$	TIME lat lon	1,10,10,10,10,10
fl	Denominator of Cloud droplet effective radius		TIME presnivs lat lon	5,1,10,10,5,10
flat	Latent heat flux	$W/m2$	TIME lat lon	5,1,10,10,5,10
flw_lic	LW lic	$W/m2$	TIME lat lon	1,10,10,10,10,10
flw_oce	LW oce	$W/m2$	TIME lat lon	1,10,10,10,10,10
flw_sic	LW sic	$W/m2$	TIME lat lon	1,10,10,10,10,10
flw_ter	LW ter	$W/m2$	TIME lat lon	1,10,10,10,10,10
fqcalving	Ice Calving	$kg/m2/s$	TIME lat lon	1,10,10,10,10,10
fqfonte	Land ice melt	$kg/m2/s$	TIME lat lon	1,10,10,10,10,10
fract_lic	Fraction lic	1	TIME lat lon	1,6,10,10,10,10
fract_oce	Fraction oce	1	TIME lat lon	1,6,10,10,10,10
fract_sic	Fraction sic	1	TIME lat lon	1,6,10,10,10,10
fract_ter	Fraction ter	1	TIME lat lon	1,6,10,10,10,10
fsnow	Surface snow area fraction	–	TIME lat lon	1,10,10,10,10,10
fsw_lic	SW lic	$W/m2$	TIME lat lon	1,10,10,10,10,10
fsw_oce	SW oce	$W/m2$	TIME lat lon	1,10,10,10,10,10
fsw_sic	SW sic	$W/m2$	TIME lat lon	1,10,10,10,10,10
fsw_ter	SW ter	$W/m2$	TIME lat lon	1,10,10,10,10,10

Table C.5: Table of variables included in the file hist LMDZ files (cont' 4)

ftime_con	Fraction of time convection Occurs		ti86400 lat lon	4,10,10,10,10,10
ftime_th	Fraction of time Shallow convection occurs		TIME lat lon	4,10,10,10,10,10!
geop	Geopotential height	$m2/s2$	TIME presnivs lat lon	2,3,10,10,10,10
h2o	Mass Fraction of Water	1	TIME presnivs lat lon	4,10,10,10,10,10
iwcon	Cloud ice water content	kg/kg	TIME presnivs lat lon	2,5,10,10,10,10
iwp	Cloud ice water path	$kg/m2$	TIME lat lon	1,5,10,10,10,10
kz	Kz melange	$m2/s$	TIME presnivs lat lon	4,10,10,10,10,10
kz_max	Kz melange max	$m2/s$	TIME presnivs lat lon	4,10,10,10,10,10
lambda_th	Thermal plume vertical velocity	m/s	TIME presnivs lat lon	10,10,10,10,10,10
lat	latitude	$degrees\_north$	lat	
lat_lic	Latent heat flux lic	$W/m2$	TIME lat lon	1,6,10,7,10,10
lat_oce	Latent heat flux oce	$W/m2$	TIME lat lon	1,6,10,7,10,10
lat_sic	Latent heat flux sic	$W/m2$	TIME lat lon	1,6,10,7,10,10
lat_ter	Latent heat flux ter	$W/m2$	TIME lat lon	1,6,10,7,10,10
lmaxth	Upper level thermals		TIME lat lon	10,10,10,10,10,10
lon	longitude	$degrees\_east$	lon	
lwcon	Cloud liquid water content	kg/kg	TIME presnivs lat lon	2,5,10,10,10,10
LWdn200	LWdn at 200mb	$W/m2$	TIME lat lon	1,10,10,10,10,10
LWdn200clr	LWdn clear sky at 200mb	$W/m2$	TIME lat lon	1,10,10,10,10,10
LWdnSFC	Down. IR rad. at surface	$W/m2$	TIME lat lon	1,4,10,10,5,10
LWdnSFCclr	Down. CS IR rad. at surface	$W/m2$	TIME lat lon	1,4,10,10,5,10
LWdownOR	Sfce incident LW radiation OR	$W/m2$	TIME lat lon	10,10,2,10,10,10
lwp	Cloud water path	$kg/m2$	TIME lat lon	1,5,10,10,10,10
LWup200	LWup at 200mb	$W/m2$	TIME lat lon	1,10,10,10,10,10
LWup200clr	LWup clear sky at 200mb	$W/m2$	TIME lat lon	1,10,10,10,10,10
LWupSFC	Upwd. IR rad. at surface	$W/m2$	TIME lat lon	1,4,10,10,5,10
LWupSFCclr	CS Upwd. IR rad. at surface	$W/m2$	TIME lat lon	1,4,10,10,5,10
Ma	undilute adiab updraft	$kg/m2/s$	TIME presnivs lat lon	4,10,10,10,10,10
mass	Masse Couches	$kg/m2$	TIME presnivs lat lon	2,3,10,10,10,10
mc	Convective mass flux	$kg/m2/s$	TIME presnivs lat lon	4,5,10,10,10,10
mcd	Downdraft COnvective Mass Flux	$kg/(m2*s)$	TIME presnivs lat lon	4,10,10,10,10,10
msnow	Surface snow amount	$kg/m2$	TIME lat lon	1,10,10,10,10,10
ndayrain	Number of dayrain(liq+sol)	$-$	ti86400 lat lon	1,10,10,10,10,10
nettop	Net dn radiatif flux at TOA	$W/m2$	TIME lat lon	1,4,10,10,10,10
oliq	Condensed water	kg/kg	TIME presnivs lat lon	2,3,4,10,10,10
ovap	Specific humidity	kg/kg	TIME presnivs lat lon	2,3,4,10,10,10
ovapinit	Specific humidity (begin of timestep)	kg/kg	TIME presnivs lat lon	2,10,10,10,10,10
ozone	Ozone mole fraction	$-$	TIME presnivs lat lon	2,10,10,10,10,10
paprs	Air pressure Inter-Couches	Pa	TIME presnivs lat lon	2,3,10,10,10,10
PB	Tracer PBVL1	$-$	TIME presnivs lat lon	
pbase	Cld base pressure	Pa	TIME lat lon	1,5,10,10,10,10
phis	Surface geop.height	$m2/s2$	TIME lat lon	1,1,10,5,1,1

Table C.6: Table of variables included in the file hist LMDZ files (cont' 5)

plcl	Lifting Condensation Level	hPa	TIME lat lon	1,10,10,10,10,10
plfc	Level of Free Convection	hPa	TIME lat lon	1,10,10,10,10,10
pluc	Convective Precip.	$kg/(s*m2)$	TIME lat lon	1,1,1,10,5,10
plul	Large-scale Precip.	$kg/(s*m2)$	TIME lat lon	1,1,1,10,10,10
plulst	Rainfall strat.	K/s	TIME lat lon	10,10,10,10,10,10
plulth	Rainfall therm.	K/s	TIME lat lon	10,10,10,10,10,10
pourc_lic	% lic	%	TIME lat lon	1,7,10,10,10,10
pourc_oce	% oce	%	TIME lat lon	1,7,10,10,10,10
pourc_sic	% sic	%	TIME lat lon	1,7,10,10,10,10
pourc_ter	% ter	%	TIME lat lon	1,7,10,10,10,10
pr_con_i	Convective precipitation ice		TIME presnivs lat lon	2,10,10,10,10,10
pr_con_l	Convective precipitation lic		TIME presnivs lat lon	2,10,10,10,10,10
precip	Precip Totale liq+sol	$kg/(s*m2)$	TIME lat lon	1,1,1,10,5,10
pres	Air pressure	Pa	TIME presnivs lat lon	2,3,10,10,10,10
presnivs	model_level_number	Pa	presnivs	
pr_lsc_i	Large scale precipitation ice		TIME presnivs lat lon	2,10,10,10,10,10
pr_lsc_l	Large scale precipitation lic		TIME presnivs lat lon	2,10,10,10,10,10
prw	Precipitable water	$kg/m2$	TIME lat lon	1,1,10,10,10,10
psol	Surface Pressure	Pa	TIME lat lon	1,1,1,5,10,10
ptconv	POINTS CONVECTIFS		TIME presnivs lat lon	4,10,10,10,10,10
ptop	Cld top pressure	Pa	TIME lat lon	1,5,10,10,10,10
q10	Specific humidity 7hPa	kg/kg	ti86400 lat lon	1,7,7,10,10,10
q100	Specific humidity 5hPa	kg/kg	ti86400 lat lon	1,7,7,10,10,10
q200	Specific humidity 4hPa	kg/kg	ti86400 lat lon	1,7,7,10,10,10
q2m	Specific humidity 2m	kg/kg	TIME lat lon	1,1,1,5,10,10
q50	Specific humidity 6hPa	kg/kg	ti86400 lat lon	1,7,7,10,10,10
q500	Specific humidity 3hPa	kg/kg	ti86400 lat lon	1,7,7,10,10,10
q700	Specific humidity 2hPa	kg/kg	ti86400 lat lon	1,7,7,10,10,10
q850	Specific humidity 1hPa	kg/kg	ti86400 lat lon	1,7,7,10,10,10
qsat2m	Saturant humidity at 2m	%	TIME lat lon	10,5,10,10,10,10
qsol	Soil watter content	mm	TIME lat lon	1,10,10,10,10,10
qsurf	Surface Air humidity	kg/kg	TIME lat lon	1,10,10,10,10,10
q_th	Thermal plume total humidity	kg/kg	TIME presnivs lat lon	4,10,10,10,10,10
radsol	Rayonnement au sol	$W/m2$	TIME lat lon	1,7,10,10,10,10
ratqs	RATQS		TIME presnivs lat lon	4,10,10,10,10,10
re	Cloud droplet effective radius	um	TIME presnivs lat lon	5,10,10,10,10,10
ref_ice	Effective radius of startiform cloud ice particle	m	TIME presnivs lat lon	4,10,10,10,10,10
ref_liq	Effective radius of convective cloud liquid water particle	m	TIME presnivs lat lon	4,10,10,10,10,10
rh2m	Relative humidity at 2m	%	TIME lat lon	5,5,10,10,10,10
rh2m_max	Max Relative humidity at 2m	%	TIME lat lon	10,5,10,10,10,10
rh2m_min	Min Relative humidity at 2m	%	TIME lat lon	10,5,10,10,10,10
rhum	Relative humidity	$-$	TIME presnivs lat lon	2,5,10,10,10,10
rld	LW downward radiation	$Wm-2$	TIME presnivs lat lon	4,10,10,10,10,10
rldcs	LW CS downward radiation	$Wm-2$	TIME presnivs lat lon	4,10,10,10,10,10
rlu	LW upward radiation	$Wm-2$	TIME presnivs lat lon	4,10,10,10,10,10
rlucs	LW CS upward radiation	$Wm-2$	TIME presnivs lat lon	4,10,10,10,10,10
RN	Tracer RNVL1	$-$	TIME presnivs lat lon	

Table C.7: Table of variables included in the file hist LMDZ files (cont' 6)

rneb	Cloud fraction	$-$	TIME presnivs lat lon	2,5,10,10,10,10
rnebcon	Convective Cloud Fraction	$-$	TIME presnivs lat lon	2,5,10,10,10,10
rnebls	LS Cloud fraction	$-$	TIME presnivs lat lon	2,5,10,10,10,10
rsd	SW downward radiation	$Wm-2$	TIME presnivs lat lon	4,10,10,10,10,10
rsdcs	SW CS downward radiation	$Wm-2$	TIME presnivs lat lon	4,10,10,10,10,10
rsu	SW upward radiation	$Wm-2$	TIME presnivs lat lon	4,10,10,10,10,10
rsucs	SW CS upward radiation	$Wm-2$	TIME presnivs lat lon	4,10,10,10,10,10
rugs	rugosity	$-$	TIME lat lon	10,10,10,10,10,10
rugs_lic	Surface roughness lic	m	TIME lat lon	3,6,10,10,10,10
rugs_oce	Surface roughness oce	m	TIME lat lon	3,6,10,10,10,10
rugs_sic	Surface roughness sic	m	TIME lat lon	3,6,10,10,10,10
rugs_ter	Surface roughness ter	m	TIME lat lon	3,6,10,10,10,10
sens	Sensible heat flux	$W/m2$	TIME lat lon	1,1,10,10,5,10
sens_lic	Sensible heat flux lic	$W/m2$	TIME lat lon	1,6,10,7,10,10
sens_oce	Sensible heat flux oce	$W/m2$	TIME lat lon	1,6,10,7,10,10
sens_sic	Sensible heat flux sic	$W/m2$	TIME lat lon	1,6,10,7,10,10
sens_ter	Sensible heat flux ter	$W/m2$	TIME lat lon	1,6,10,7,10,10
sicf	Sea-ice fraction	$-$	TIME lat lon	1,1,10,10,10,10
s_lcl	Condensation level	m	TIME lat lon	1,10,10,10,10,10
slp	Sea Level Pressure	Pa	TIME lat lon	1,1,1,10,10,10
snow	Snow fall	$kg/(s*m2)$	TIME lat lon	1,1,10,10,5,10
snowl	Solid Large-scale Precip.	$kg/(m2*s)$	TIME lat lon	10,1,10,10,10,10
soll	IR rad. at surface	$W/m2$	TIME lat lon	1,1,10,10,10,10
soll0	IR rad. at surface	$W/m2$	TIME lat lon	1,5,10,10,10,10
solldown	Down. IR rad. at surface	$W/m2$	TIME lat lon	10,1,10,10,10,10
sols	Solar rad. at surf.	$W/m2$	TIME lat lon	1,1,10,10,10,10
sols0	Solar rad. at surf.	$W/m2$	TIME lat lon	1,5,10,10,10,10
s_pblh	Boundary Layer Height	m	TIME lat lon	1,10,10,10,10,10
s_pblt	t at Boundary Layer Height	K	TIME lat lon	1,10,10,10,10,10
s_therm	Exces du thermique	K	TIME lat lon	1,10,10,10,10,10
SWdn200	SWdn at 200mb	$W/m2$	TIME lat lon	1,10,10,10,10,10
SWdn200clr	SWdn clear sky at 200mb	$W/m2$	TIME lat lon	10,1,10,10,10,10
SWdnSFC	SWdn at surface	$W/m2$	TIME lat lon	1,1,10,10,5,10
SWdnSFCclr	SWdn clear sky at surface	$W/m2$	TIME lat lon	1,4,10,10,5,10
SWdnTOA	SWdn at TOA	$W/m2$	TIME lat lon	1,4,10,10,10,10
SWdnTOAclr	SWdn clear sky at TOA	$W/m2$	TIME lat lon	1,4,10,10,10,10
SWdownOR	Sfce incident SW radiation OR	$W/m2$	TIME lat lon	10,10,2,10,10,10
SWnetOR	Sfce net SW radiation OR	$W/m2$	TIME lat lon	10,10,2,10,10,10
SWup200	SWup at 200mb	$W/m2$	TIME lat lon	1,10,10,10,10,10
SWup200clr	SWup clear sky at 200mb	$W/m2$	TIME lat lon	10,1,10,10,10,10
SWupSFC	SWup at surface	$W/m2$	TIME lat lon	1,4,10,10,5,10
SWupSFCclr	SWup clear sky at surface	$W/m2$	TIME lat lon	1,4,10,10,5,10
SWupTOA	SWup at TOA	$W/m2$	TIME lat lon	1,4,10,10,10,10
SWupTOAclr	SWup clear sky at TOA	$W/m2$	TIME lat lon	1,4,10,10,10,10

Table C.8: Table of variables included in the file hist LMDZ files (cont' 7)

t10	Temperature 7hPa	K	ti86400 lat lon	1,7,7,10,10,10
t100	Temperature 5hPa	K	ti86400 lat lon	1,7,7,10,10,10
t200	Temperature 4hPa	K	ti86400 lat lon	1,7,7,10,10,10
t2m	Temperature 2m	K	TIME lat lon	1,1,1,5,10,10
t2m_lic	Temp 2m lic	K	TIME lat lon	10,6,10,10,10,10
t2m_max	Temp 2m max	K	TIME lat lon	1,1,10,10,10,10
t2m_min	Temp 2m min	K	TIME lat lon	1,1,10,10,10,10
t2m_oce	Temp 2m oce	K	TIME lat lon	10,6,10,10,10,10
t2m_sic	Temp 2m sic	K	TIME lat lon	10,6,10,10,10,10
t2m_ter	Temp 2m ter	K	TIME lat lon	10,6,10,10,10,10
t50	Temperature 6hPa	K	ti86400 lat lon	1,7,7,10,10,10
t500	Temperature 3hPa	K	ti86400 lat lon	1,7,7,10,10,10
t700	Temperature 2hPa	K	ti86400 lat lon	1,7,7,10,10,10
t850	Temperature 1hPa	K	ti86400 lat lon	1,7,7,10,10,10
taux	Zonal wind stress	Pa	TIME lat lon	1,10,10,10,10,10
taux_lic	Zonal wind stresslic	Pa	TIME lat lon	1,6,10,10,10,10
taux_oce	Zonal wind stressoce	Pa	TIME lat lon	1,6,10,10,10,10
taux_sic	Zonal wind stresssic	Pa	TIME lat lon	1,6,10,10,10,10
taux_ter	Zonal wind stresster	Pa	TIME lat lon	1,6,10,10,10,10
tauy	Meridional wind stress	Pa	TIME lat lon	1,10,10,10,10,10
tauy_lic	Meridional wind stress lic	Pa	TIME lat lon	1,6,10,10,10,10
tauy_oce	Meridional wind stress oce	Pa	TIME lat lon	1,6,10,10,10,10
tauy_sic	Meridional wind stress sic	Pa	TIME lat lon	1,6,10,10,10,10
tauy_ter	Meridional wind stress ter	Pa	TIME lat lon	1,6,10,10,10,10
temp	Air temperature	K	TIME presnivs lat lon	2,3,4,10,10,10
theta	Potential air temperature	K	TIME presnivs lat lon	2,3,4,10,10,10
time+	TIME	*seconds since* $1999-12-31$ $00:00:00$		4,10,10,10,10,10
time_bnds			TIME bnds	
ti86400+	TIME	*seconds since* $1999-12-31$ $00:00:00$		
tke	TKE	$m2/s2$	TIME presnivs lat lon	4,10,10,10,10,10
tke_lic	Max Turb. Kinetic Energy lic	–	TIME lat lon	10,4,10,10,10,10
tke_max	TKE max	$m2/s2$	t_op_00001800 presnivs lat lon	4,10,10,10,10,10
tke_max_lic	Max Turb. Kinetic Energy lic	–	t_op_00001800 lat lon	10,4,10,10,10,10
tke_max_oce	Max Turb. Kinetic Energy oce	–	t_op_00001800 lat lon	10,4,10,10,10,10
tke_max_sic	Max Turb. Kinetic Energy sic	–	t_op_00001800 lat lon	10,4,10,10,10,10
tke_max_ter	Max Turb. Kinetic Energy ter	–	t_op_00001800 lat lon	10,4,10,10,10,10
tke_oce	Max Turb. Kinetic Energy oce	–	TIME lat lon	10,4,10,10,10,10
tke_sic	Max Turb. Kinetic Energy sic	–	TIME lat lon	10,4,10,10,10,10
tke_ter	Max Turb. Kinetic Energy ter	–	TIME lat lon	10,4,10,10,10,10
tnhus	Tendency of specific humidity	$s-1$	TIME presnivs lat lon	4,10,10,10,10,10
tnhusc	Tendency of specific humidity due to convection	$s-1$	TIME presnivs lat lon	4,10,10,10,10,10
tnhusscpbl	Tendency of Specific humidity due to ST cl, precip and BL mixing	$s-1$	TIME presnivs lat lon	4,10,10,10,10,10

Table C.9: Table of variables included in the file hist LMDZ files (cont' 8)

tnt	Tendency of air temperature	$Ks-1$	TIME presnivs lat lon	4,10,10,10,10,10
tntc	Tendency of air temperature due to Moist Convection	$Ks-1$	TIME presnivs lat lon	4,10,10,10,10,10
tntr	Air temperature tendency due to Radiative heating	$Ks-1$	TIME presnivs lat lon	4,10,10,10,10,10
tntscpbl	Air temperature tendency due to St cloud and precipitation and BL mixing	$Ks-1$	TIME presnivs lat lon	4,10,10,10,10,10
t_oce_sic	Temp mixte oce-sic	K	TIME lat lon	1,10,10,10,10,10
t_op_00001800	TIME	*seconds since* $1979-01-01$ $00:00:00$		
t_op_00001800_bnds				
topl	IR rad. at TOA	$W/m2$	TIME lat lon	1,1,10,5,10,10
topl0	IR rad. at TOA	$W/m2$	TIME lat lon	1,5,10,10,10,10
tops	Solar rad. at TOA	$W/m2$	TIME lat lon	1,1,10,10,10,10
tops0	CS Solar rad. at TOA	$W/m2$	TIME lat lon	1,5,10,10,10,10
tpot	Surface air potential temperature	K	TIME lat lon	10,5,10,10,10,10
tpote	Surface air equivalent potential temperature	K	TIME lat lon	10,5,10,10,10,10
tsol	Surface Temperature	K	TIME lat lon	1,1,1,5,10,10
tsol_lic	Temperature lic	K	TIME lat lon	1,6,10,10,10,10
tsol_oce	Temperature oce	K	TIME lat lon	1,6,10,10,10,10
tsol_sic	Temperature sic	K	TIME lat lon	1,6,10,10,10,10
tsol_ter	Temperature ter	K	TIME lat lon	1,6,10,10,10,10
u10	Zonal wind 7hPa	m/s	ti86400 lat lon	1,7,7,10,10,10
u100	Zonal wind 5hPa	m/s	ti86400 lat lon	1,7,7,10,10,10
u10m	Vent zonal 10m	m/s	TIME lat lon	1,1,1,5,10,10
u10m_lic	Vent Zonal 10m lic	m/s	TIME lat lon	10,6,10,10,10,10
u10m_oce	Vent Zonal 10m oce	m/s	TIME lat lon	10,6,10,10,10,10
u10m_sic	Vent Zonal 10m sic	m/s	TIME lat lon	10,6,10,10,10,10
u10m_ter	Vent Zonal 10m ter	m/s	TIME lat lon	10,6,10,10,10,10
u200	Zonal wind 4hPa	m/s	ti86400 lat lon	1,7,7,10,10,10
u50	Zonal wind 6hPa	m/s	ti86400 lat lon	1,7,7,10,10,10
u500	Zonal wind 3hPa	m/s	ti86400 lat lon	1,7,7,10,10,10
u700	Zonal wind 2hPa	m/s	ti86400 lat lon	1,7,7,10,10,10
u850	Zonal wind 1hPa	m/s	ti86400 lat lon	1,7,7,10,10,10
ue	Zonal energy transport	$-$	TIME lat lon	1,10,10,10,10,10
upwd	saturated updraft	$kg/m2/s$	TIME presnivs lat lon	2,10,10,10,10,10
uq	Zonal humidity transport	$-$	TIME lat lon	1,10,10,10,10,10
ustar	Friction velocity	m/s	TIME lat lon	1,1,1,5,10,10
ustar_lic	Friction velocity lic	m/s	TIME lat lon	10,6,10,10,10,10
ustar_oce	Friction velocity oce	m/s	TIME lat lon	10,6,10,10,10,10
ustar_sic	Friction velocity sic	m/s	TIME lat lon	10,6,10,10,10,10
ustar_ter	Friction velocity ter	m/s	TIME lat lon	10,6,10,10,10,10

Table C.10: Table of variables included in the file hist LMDZ files (cont' 9)

v10	Meridional wind 7hPa	m/s	ti86400 lat lon	1,7,7,10,10,10
v100	Meridional wind 5hPa	m/s	ti86400 lat lon	1,7,7,10,10,10
v10m	Vent meridien 10m	m/s	TIME lat lon	1,1,1,5,10,10
v10m_lic	Vent meredien 10m lic	m/s	TIME lat lon	10,6,10,10,10,10
v10m_oce	Vent meredien 10m oce	m/s	TIME lat lon	10,6,10,10,10,10
v10m_sic	Vent meredien 10m sic	m/s	TIME lat lon	10,6,10,10,10,10
v10m_ter	Vent meredien 10m ter	m/s	TIME lat lon	10,6,10,10,10,10
v200	Meridional wind 4hPa	m/s	ti86400 lat lon	1,7,7,10,10,10
v50	Meridional wind 6hPa	m/s	ti86400 lat lon	1,7,7,10,10,10
v500	Meridional wind 3hPa	m/s	ti86400 lat lon	1,7,7,10,10,10
v700	Meridional wind 2hPa	m/s	ti86400 lat lon	1,7,7,10,10,10
v850	Meridional wind 1hPa	m/s	ti86400 lat lon	1,7,7,10,10,10
ve	Merid energy transport	–	TIME lat lon	1,10,10,10,10,10
vitu	Zonal wind	m/s	TIME presnivs lat lon	2,3,4,6,10,10
vitv	Meridional wind	m/s	TIME presnivs lat lon	2,3,4,6,10,10
vitw	Vertical wind	Pa/s	TIME presnivs lat lon	2,3,10,6,10,10
Vprecip	precipitation vertical profile	–	TIME presnivs lat lon	10,10,10,10,10,10
vq	Merid humidity transport	–	TIME lat lon	1,10,10,10,10,10
w10	Vertical wind 7hPa	Pa/s	ti86400 lat lon	1,7,7,10,10,10
w100	Vertical wind 5hPa	Pa/s	ti86400 lat lon	1,7,7,10,10,10
w200	Vertical wind 4hPa	Pa/s	ti86400 lat lon	1,7,7,10,10,10
w50	Vertical wind 6hPa	Pa/s	ti86400 lat lon	1,7,7,10,10,10
w500	Vertical wind 3hPa	Pa/s	ti86400 lat lon	1,7,7,10,10,10
w700	Vertical wind 2hPa	Pa/s	ti86400 lat lon	1,7,7,10,10,10
w850	Vertical wind 1hPa	Pa/s	ti86400 lat lon	1,7,7,10,10,10
wake_deltaq	wake_deltaq		TIME presnivs lat lon	4,5,10,10,10,10
wake_deltat	wake_deltat		TIME presnivs lat lon	4,5,10,10,10,10
wake_h	wake_h	–	TIME lat lon	4,5,10,10,10,10
wake_omg	wake_omg		TIME presnivs lat lon	4,5,10,10,10,10
wake_s	wake_s	–	TIME lat lon	4,5,10,10,10,10
wape			TIME lat lon	1,1,1,10,10,10
wbeff	Conv. updraft velocity at LFC (¡100)	m/s	TIME lat lon	1,10,10,10,10,10
wbilo_lic	Bilan eau lic	$kg/(m2*s)$	TIME lat lon	1,10,10,10,10,10
wbilo_oce	Bilan eau oce	$kg/(m2*s)$	TIME lat lon	1,10,10,10,10,10
wbilo_sic	Bilan eau sic	$kg/(m2*s)$	TIME lat lon	1,10,10,10,10,10
wbilo_ter	Bilan eau ter	$kg/(m2*s)$	TIME lat lon	1,10,10,10,10,10
wbils_lic	Bilan sol lic	$W/m2$	TIME lat lon	1,10,10,10,10,10
wbils_oce	Bilan sol oce	$W/m2$	TIME lat lon	1,10,10,10,10,10
wbils_sic	Bilan sol sic	$W/m2$	TIME lat lon	1,10,10,10,10,10
wbils_ter	Bilan sol ter	$W/m2$	TIME lat lon	1,10,10,10,10,10
wdtrainA	precipitation from AA	–	TIME presnivs lat lon	4,1,10,4,1,10
wdtrainM	precipitation from mixture	–	TIME presnivs lat lon	4,1,10,4,1,10
weakinv	Weak inversion	–	TIME lat lon	10,1,10,10,10,10
wind10m	10-m wind speed	m/s	TIME lat lon	1,1,1,10,10,10
wind10max	10m wind speed max	m/s	TIME lat lon	10,1,10,10,10,10

Table C.11: Table of variables included in the file hist LMDZ files (cont' 10)

z10	Geopotential height 7hPa	m	ti86400 lat lon	1,7,7,10,10,10
z100	Geopotential height 5hPa	m	ti86400 lat lon	1,7,7,10,10,10
z200	Geopotential height 4hPa	m	ti86400 lat lon	1,7,7,10,10,10
z50	Geopotential height 6hPa	m	ti86400 lat lon	1,7,7,10,10,10
z500	Geopotential height 3hPa	m	ti86400 lat lon	1,7,7,10,10,10
z700	Geopotential height 2hPa	m	ti86400 lat lon	1,7,7,10,10,10
z850	Geopotential height 1hPa	m	ti86400 lat lon	1,7,7,10,10,10
zfull	Altitude of full pressure levels	m	TIME presnivs lat lon	2,3,10,10,10,10
zhalf	Altitude of half pressure levels	m	TIME presnivs lat lon	2,3,10,10,10,10
zmax_th	Thermal plume height	K/s	TIME lat lon	4,4,4,5,10,10

Table C.12: Varible name, dimensions and definition of the variables in 'startphy.nc/restartphy.nc' initial conditions LMDZ file

name of the variable	dimensions	description
controle	index	control parametres (see next the equivalencies)
longitude	points_physiques	Longitudes
latitude	points_physiques	Latitudes
masque	points_physiques	land/sea mask
FTER	points_physiques	FTER sub-grid fraction of land
FLIC	points_physiques	FLIC sub-grid fraction land covered by ice
FOCE	points_physiques	FOCE sub-grid fraction ocean
FSIC	points_physiques	FSIC sub-grid fraction ocean covered by ice
TS01	points_physiques	Surface temperature num.01 (ter)
TS02	points_physiques	Surface temperature num.02 (lic)
TS03	points_physiques	Surface temperature num.03 (oce)
TS04	points_physiques	Surface temperature num.04 (sic)
Tsoil01srf01	points_physiques	Soil temperature num.01 for surface 1 (ter)
Tsoil02srf01	points_physiques	Soil temperature num.02 for surface 1 (ter)
Tsoil03srf01	points_physiques	Soil temperature num.03 for surface 1 (ter)
Tsoil04srf01	points_physiques	Soil temperature num.04 for surface 1 (ter)
Tsoil05srf01	points_physiques	Soil temperature num.05 for surface 1 (ter)
Tsoil06srf01	points_physiques	Soil temperature num.06 for surface 1 (ter)
Tsoil07srf01	points_physiques	Soil temperature num.07 for surface 1 (ter)
Tsoil08srf01	points_physiques	Soil temperature num.08 for surface 1 (ter)
Tsoil09srf01	points_physiques	Soil temperature num.09 for surface 1 (ter)
Tsoil10srf01	points_physiques	Soil temperature num.10 for surface 1 (ter)
Tsoil11srf01	points_physiques	Soil temperature num.11 for surface 1 (ter)
Tsoil01srf02	points_physiques	Soil temperature num.01 for surface 2 (lic)
Tsoil02srf02	points_physiques	Soil temperature num.02 for surface 2 (lic)
Tsoil03srf02	points_physiques	Soil temperature num.03 for surface 2 (lic)
Tsoil04srf02	points_physiques	Soil temperature num.04 for surface 2 (lic)
Tsoil05srf02	points_physiques	Soil temperature num.05 for surface 2 (lic)
Tsoil06srf02	points_physiques	Soil temperature num.06 for surface 2 (lic)
Tsoil07srf02	points_physiques	Soil temperature num.07 for surface 2 (lic)
Tsoil08srf02	points_physiques	Soil temperature num.08 for surface 2 (lic)
Tsoil09srf02	points_physiques	Soil temperature num.09 for surface 2 (lic)
Tsoil10srf02	points_physiques	Soil temperature num.10 for surface 2 (lic)
Tsoil11srf02	points_physiques	Soil temperature num.11 for surface 2 (lic)

C.2 startphy.nc

See `startphy.nc` or `restartphy.nc` content in tables from C.12 to C.14.

Table C.13: Varible name, dimensions and definition of the variables in 'startphy.nc' initial conditions LMDZ file (con't 1)

Tsoil01srf03	points_physiques	Soil temperature num.01 for surface 3 (oce)
Tsoil02srf03	points_physiques	Soil temperature num.02 for surface 3 (oce)
Tsoil03srf03	points_physiques	Soil temperature num.03 for surface 3 (oce)
Tsoil04srf03	points_physiques	Soil temperature num.04 for surface 3 (oce)
Tsoil05srf03	points_physiques	Soil temperature num.05 for surface 3 (oce)
Tsoil06srf03	points_physiques	Soil temperature num.06 for surface 3 (oce)
Tsoil07srf03	points_physiques	Soil temperature num.07 for surface 3 (oce)
Tsoil08srf03	points_physiques	Soil temperature num.08 for surface 3 (oce)
Tsoil09srf03	points_physiques	Soil temperature num.09 for surface 3 (oce)
Tsoil10srf03	points_physiques	Soil temperature num.10 for surface 3 (oce)
Tsoil11srf03	points_physiques	Soil temperature num.11 for surface 3 (oce)
Tsoil01srf04	points_physiques	Soil temperature num.01 for surface 4 (sic)
Tsoil02srf04	points_physiques	Soil temperature num.02 for surface 4 (sic)
Tsoil03srf04	points_physiques	Soil temperature num.03 for surface 4 (sic)
Tsoil04srf04	points_physiques	Soil temperature num.04 for surface 4 (sic)
Tsoil05srf04	points_physiques	Soil temperature num.05 for surface 4 (sic)
Tsoil06srf04	points_physiques	Soil temperature num.06 for surface 4 (sic)
Tsoil07srf04	points_physiques	Soil temperature num.07 for surface 4 (sic)
Tsoil08srf04	points_physiques	Soil temperature num.08 for surface 4 (sic)
Tsoil09srf04	points_physiques	Soil temperature num.09 for surface 4 (sic)
Tsoil10srf04	points_physiques	Soil temperature num.10 for surface 4 (sic)
Tsoil11srf04	points_physiques	Soil temperature num.11 for surface 4 (sic)
QS01	points_physiques	Surface humidity num. 01
QS02	points_physiques	Surface humidity num. 02
QS03	points_physiques	Surface humidity num. 03
QS04	points_physiques	Surface humidity num. 04
QSOL	points_physiques	soil water (mm)
ALBE01	points_physiques	Albedo for surface num. 01
ALBE02	points_physiques	Albedo for surface num. 02
ALBE03	points_physiques	Albedo for surface num. 03
ALBE04	points_physiques	Albedo for surface num. 04
ALBLW01	points_physiques	LW albedo for surface num. 01
ALBLW02	points_physiques	LW albedo for surface num. 02
ALBLW03	points_physiques	LW albedo for surface num. 03
ALBLW04	points_physiques	LW albedo for surface num. 04
EVAP01	points_physiques	evaporation for surface num. 01
EVAP02	points_physiques	evaporation for surface num. 02
EVAP03	points_physiques	evaporation for surface num. 03
EVAP04	points_physiques	evaporation for surface num. 04
SNOW01	points_physiques	snow for surface num. 01
SNOW02	points_physiques	snow for surface num. 02
SNOW03	points_physiques	snow for surface num. 03
SNOW04	points_physiques	snow for surface num. 04
RADS	points_physiques	net radiatio at the surface
solsw	points_physiques	Sun radiation at the surface
sollw	points_physiques	Infra-red radiation at the surface
fder	points_physiques	drift of the flux
rain_f	points_physiques	liquid precipitation
snow_f	points_physiques	solid precipitation

Table C.14: Varible name, dimensions and definition of the variables in 'startphy.nc' initial conditions LMDZ file (con't 2)

RUG01	points_physiques	roughness length for surface num. 01
RUG02	points_physiques	roughness length for surface num. 02
RUG03	points_physiques	roughness length for surface num. 03
RUG04	points_physiques	roughness length for surface num. 04
AGESNO01	points_physiques	snow age for surface num. 01
AGESNO02	points_physiques	snow age for surface num. 02
AGESNO03	points_physiques	snow age for surface num. 03
AGESNO04	points_physiques	snow age for surface num. 04
ZMEA	points_physiques	mean of the sub-scale topography at the grid point
ZSTD	points_physiques	standard deviation of the sub-scale topography at the grid point
ZSIG	points_physiques	ZSIG mean of the sub-scale topography at the grid point
ZGAM	points_physiques	gamma of the sub-scale topography at the grid point
ZTHE	points_physiques	angle of the sub-scale topography at the grid point
ZPIC	points_physiques	ZPIC of the sub-scale topography at the grid point
ZVAL	points_physiques	ZVAL of the sub-scale topography at the grid point
RUGSREL	points_physiques	RUGSREL
TANCIEN	horizon_vertical	previous temperature
QANCIEN	horizon_vertical	previous mixing ratio
UANCIEN	horizon_vertical	previous WE-wind speed
VANCIEN	horizon_vertical	previous NS-wind speed
RUGMER	points_physiques	roughness length on the sea
CLWCON	horizon_vertical	convective liquid water
RNEBCON	horizon_vertical	convective cloud
RATQS	horizon_vertical	liquid water proportion
RUNOFFLIC0	points_physiques	run-off from the melting of lic
ZMAX0	points_physiques	ZMAX0
F0	points_physiques	F0
EMA_WORK1	horizon_vertical	EMA_WORK1
EMA_WORK2	horizon_vertical	EMA_WORK2
WAKE_DELTAT	horizon_vertical	thermal tendency from the wakes
WAKE_DELTAQ	horizon_vertical	humidity tendency from the wakes
WAKE_S	points_physiques	wake area fraction
WAKE_CSTAR	points_physiques	WAKE_CSTAR
WAKE_PE	points_physiques	WAKE_PE
WAKE_FIP	points_physiques	WAKE_FIP
FM_THERM	horizon_klevp1	thermals mass flux
ENTR_THERM	horizon_vertical	thermals entrainment
DETR_THERM	horizon_vertical	thermals detrainment

The `control` array

Both physical and dynamical headers of the GCM NetCDF files start with a `controle` variable. This variable is an array of 100 reals (the vector called `tab_cntrl` in the program), which contains the program control parameters.

Parameters differ between the `startphy.nc` and `restartphy.nc` files, and examples of both are listed below. The contents of table `tab_cntrl`. These values will significantly change for no-Earth planets simualtions.

- The `controle` array in the header of a dynamical NetCDF file for Mars: `start`

```
tab_cntrl(1)  = FLOAT(iim) ! number of nodes along longitude
tab_cntrl(2)  = FLOAT(jjm) ! number of nodes along latitude
tab_cntrl(3)  = FLOAT(llm) ! number of atmospheric layers
tab_cntrl(4)  = FLOAT(idayref) ! initial day
tab_cntrl(5)  = rad   ! radius of the planet
tab_cntrl(6)  = omeg  ! rotation of the planet (rad/s)
tab_cntrl(7)  = g     ! gravity (m/s2) ~3.72 for Mars
tab_cntrl(8)  = cpp
tab_cntrl(9) = kappa   ! = r/cp
tab_cntrl(10) = daysec ! lenght of a sol (s) ~88775
tab_cntrl(11) = dtvr   ! dynamical time step (s)
tab_cntrl(12) = etot0  ! total energy
tab_cntrl(13) = ptot0  ! total pressure
tab_cntrl(14) = ztot0  ! total enstrophy
tab_cntrl(15) = stot0  ! total enthalpy
tab_cntrl(16) = ang0   ! total angular momentum
tab_cntrl(17) = pa
tab_cntrl(18) = preff  ! reference pressure (Pa)
tab_cntrl(19)  = clon  ! longitude of center of zoom
tab_cntrl(20)  = clat  ! latitude of center of zoom
tab_cntrl(21)  = grossismx ! zooming factor, along longitude
tab_cntrl(22)  = grossismy ! zooming factor, along latitude

tab_cntrl(24) = dzoomx ! extention (in longitude) of zoom
tab_cntrl(25) = dzoomy ! extention (in latitude) of zoom

tab_cntrl(27) = taux ! stiffness factor of zoom in longitude
tab_cntrl(28) = tauy ! stiffness factor of zoom in latitude
```

- The `controle` array in the header of a physical NetCDF file for Mars: `startfi.nc`

```
c Informations on the physics grid
      tab_cntrl(1) = float(ngridmx)  ! number of nodes on physics grid
      tab_cntrl(2) = float(nlayermx) ! number of atmospheric layers
      tab_cntrl(3) = day_ini + int(time)         ! initial day
      tab_cntrl(4) = time -int(time)            ! initiale time of day

c Informations about Mars, used by dynamics and physics
      tab_cntrl(5) = rad      ! radius of Mars (m) ~3397200
      tab_cntrl(6) = omeg     ! rotation rate (rad.s-1)
      tab_cntrl(7) = g        ! gravity (m.s-2) ~3.72
      tab_cntrl(8) = mugaz    ! Molar mass of the atmosphere (g.mol-1) ~43.49
      tab_cntrl(9) = rcp      !  = r/cp  ~0.256793 (=kappa dans dynamique)
      tab_cntrl(10) = daysec  ! length of a sol (s)  ~88775

      tab_cntrl(11) = phystep  ! time step in the physics
      tab_cntrl(12) = 0.
      tab_cntrl(13) = 0.

c Informations about Mars, only for physics
      tab_cntrl(14) = year_day  ! length of year (sols) ~668.6
      tab_cntrl(15) = periheli  ! min. Sun-Mars distance (Mkm) ~206.66
      tab_cntrl(16) = aphelie   ! max. SUn-Mars distance (Mkm) ~249.22
      tab_cntrl(17) = peri_day  ! date of perihelion (sols since N. spring)
      tab_cntrl(18) = obliquit  ! Obliquity of the planet (deg) ~23.98

c Boundary layer and turbulence
      tab_cntrl(19) = z0        ! surface roughness (m) ~0.01
```

```
      tab_cntrl(20) = lmixmin   ! mixing length ~100
      tab_cntrl(21) = emin_turb ! minimal energy ~1.e-8

c Optical properties of polar caps and ground emissivity
      tab_cntrl(22) = albedice(1)  ! Albedo of northern cap ~0.5
      tab_cntrl(23) = albedice(2)  ! Albedo of southern cap ~0.5
      tab_cntrl(24) = emisice(1)   ! Emissivity of northern cap ~0.95
      tab_cntrl(25) = emisice(2)   ! Emissivity of southern cap ~0.95
      tab_cntrl(26) = emissiv      ! Emissivity of martian soil ~.95
      tab_cntrl(31) = iceradius(1) ! mean scat radius of CO2 snow (north)
      tab_cntrl(32) = iceradius(2) ! mean scat radius of CO2 snow (south)
      tab_cntrl(33) = dtemisice(1) ! time scale for snow metamorphism (north)
      tab_cntrl(34) = dtemisice(2) ! time scale for snow metamorphism (south)

c dust aerosol properties
      tab_cntrl(27) = tauvis      ! mean visible optical depth

      tab_cntrl(28) = 0.
      tab_cntrl(29) = 0.
      tab_cntrl(30) = 0.

! Soil properties:
      tab_cntrl(35) = volcapa ! soil volumetric heat capacity
```

Table C.15: Varible name, dimensions and definition of the variables in `limit.nc` boundary conditions LMDZ file

name of the varibale	dimensions	description
TEMPS	TIME	day within the year
NAT	TIME, points_physiques	Type of soil (0,1,2,3)
SST	TIME, points_physiques	Sea surface temperature
BILS	TIME, points_physiques	heat flux refernce at the surface
ALB	TIME, points_physiques	Albedo at the surface (from `Albedo.nc`)
RUG	TIME, points_physiques	Roughness length (from `Rugos.nc`)
FTER	TIME, points_physiques	Fraction of ter
FOCE	TIME, points_physiques	Fraction of lic
FSIC	TIME, points_physiques	Fraction of oce
FLIC	TIME, points_physiques	Fraction of sic

C.3 limit.nc: LMDZ variables

See `limit.nc` content in table C.15

C.4 paramLMDZ_phy.nc

See `paramLMDZ_phy` content in table C.16.

C.5 Ozone files

C.6 Aerosol files

See an example of content of an aerosols file in table C.17.

Table C.16: Varible name, dimensions and definition of the variables in `paramLMDZ_phy.nc` LMDZ file

name of the varibale	**dimensions**	**description**	**units**
`bils`	time_counter, lat, lon	Surface total heat flux	Wm^{-2}
`CFC11_ppt`	time_counter, lat, lon	Concentration of CFC-11	*ppt*
`CFC12_ppt`	time_counter, lat, lon	Concentration of CFC-12	*ppt*
`CH4_ppb`	time_counter, lat, lon	Concentration of CH_4	*ppb*
`co2_ppm`	time_counter, lat, lon	Concentration of CO_2	*ppm*
`evap_land`	time_counter, lat, lon	Land evaporation	$kgm^{-2}s^{-1}$
`evap`	time_counter, lat, lon	Evaporation	$kgm^{-2}s^{-1}$
`flat`	time_counter, lat, lon	Latent heat flux	Wm^{-2}
`lat`	lat	latitude	*degrees North*
`lon`	lon	longitude	*degrees East*
`N2O_ppb`	time_counter, lat, lon	Concentration of N_2O	*ppb*
`nettop0`	time_counter, lat, lon	Clear sky net downward radiatif flux at TOA	Wm^{-2}
`nettop`	time_counter, lat, lon	Net downward radiatif flux at TOA	Wm^{-2}
`precip`	time_counter, lat, lon	Total precipitation (liq+sol)	$kgm^{-2}s^{-1}$
`prw`	time_counter, lat, lon	Precipitable water	kgm^{-2}
`R_ecc`	time_counter, lat, lon	Excentricity	–
`R_incl`	time_counter, lat, lon	Inclination	*deg*
`R_peri`	time_counter, lat, lon	Equinoxe	–
`solaire`	time_counter, lat, lon	Solar constant	Wm^{-2}
`t2m`	time_counter, lat, lon	Temperature at 2m	K
`time_counter_bnds`	time_counter	time-bounds	*seconds* since 1979-12-01 00:00:00
`time_counter`	time_counter	time	*seconds* since 1979-12-01 00:00:00
`tsol`	time_counter, lat, lon	Surface temperature	K

Table C.17: Content of aerosols file `aerosols1980.nc`

Variable name	dimensions	description
AIBCM	TIME, lev, lat, lon	concentration of accumulation mode insoluble black carbon aerosol
AIPOMM	TIME, lev, lat, lon	concentration of accumulation mode insoluble particle organic matter aerosol
ASBCM	TIME, lev, lat, lon	concentration of accumulation mode soluble black carbon aerosol
ASPOMM	TIME, lev, lat, lon	concentration of accumulation mode soluble particle organic matter aerosol
ASSSM	TIME, lev, lat, lon	concentration of accumulation mode soluble sea salt aerosol
CIDUSTM	TIME, lev, lat, lon	concentration of coarse mode insoluble dust aerosol
CSSO4M	TIME, lev, lat, lon	contration of coarse mode soluble sulphate aerosol
CSSSM	TIME, lev, lat, lon	concentration of coarse mode soluble sea salt aerosol
load_AIBCM	TIME, lat, lon	burden of accumulation mode insoluble black carbon aerosol
load_AIPOMM	TIME, lat, lon	burden of accumulation mode insoluble particle organic matter aerosol
load_ASBCM	TIME, lat, lon	burden of accumulation mode soluble black carbon aerosol
load_ASPOMM	TIME, lat, lon	burden of accumulation mode soluble particle organic matter aerosol
load_ASSSM	TIME, lat, lon	burden of accumulation mode soluble sea salt aerosol
load_CIDUSTM	TIME, lat, lon	burden of coarse mode insoluble dust aerosol
load_CSSO4M	TIME, lat, lon	burden of coarse mode soluble sulphate aerosol
load_CSSSM	TIME, lat, lon	burden of coarse mode soluble sea salt aerosol
load_SO4	TIME, lat, lon	burden of accumulation mode soluble sulphate aerosol
load_SSSSM	TIME, lat, lon	burden of super coarse mode soluble sea salt aerosol
O3	TIME, lev, lat, lon	ozone
p0		
PMID	TIME, lev, lat, lon	pressure at mid-levels
ps	TIME, lat, lon	surface pressure
SO4	TIME, lev, lat, lon	concentration of accumulation mode sulphate aerosol
SSSSM	TIME, lev, lat, lon	concentation of super coarse mode soluble sea salt aerosol
TEMP	TIME, lev, lat, lon	atmospheric temperature
ZRHO	TIME, lev, lat, lon	atmopheric density

Appendix D

LMDZ versions: .def files

Table D.1: Changes on the `.def` files introduced from `AR4.0` to `NPv3.1` LMDZ version. This is an accumulative table. The `.def` files of a given version, take the files from the previous version as reference. Starting point is the `AR4.0` version from which the files are taken as examples in this document. Some of them might be automatically generated, but they are shown for complementariness (this would be the case of new variables in the `run.def`, which are generated when new schemes are activated (like from `AR4.0` to `NPv3.1` where *'thermals'* and *'wakes'* are activated)

config	gcm	output	physiq		run		orchidee
AR4.0							
			iflag_pbl	1			
			iflag_con	30			
			iflag_thermalsl	0			
			iflag_wake	0			
NPv3.1							
			iflag_con	3	iapp_tracvl	1	
			epmax	0.997	solarlong0	0.0000000	
			iflag_clw	0	freq_calNMC__00001	150.00000	
			cld_lc_lsc	6.0E-04	freq_calNMC__00002	150.00000	
			cld_lc_con	6.0E-04	freq_calNMC__00003	150.00000	
			ffallv_lsc	1.35	flag_tke_ter__0000[1-6][a]	10,4,10,10,10,10	
			ffallv_con	1.35	name_tke_ter	tke_ter	
			coef_eva	1E-04	flag_tke_max_ter__0000[1-6]	10,4,10,10,10,10	
			iflag_ratqs	2	name_tke_max_ter	tke_max_ter	
			iflag_cldcon	6	flag_tke_lic__0000[1-6]	10,4,10,10,10,10	
			ratqsbas	0.002	name_tke_lic	tke_lic	
			ratqshaut	0.25	flag_tke_max_lic__0000[1-6]	10,4,10,10,10,10	
			t_glace_min	258.	name_tke_max_lic	tke_max_lic	
			t_glace_max	273.13	flag_tke_oce__0000[1-6]	10,4,10,10,10,10	
			rei_min	20.	name_tke_oce	tke_oce	
			rei_max	61.29	flag_tke_max_oce__00001	10,4,10,10,10,10	
			iflag_pbl	11	flag_tke_sic__0000[1-6]	10,4,10,10,10,10	
			iflag_thermals	17	name_tke_sic	tke_sic	
			iflag_thermals_ed	10	flag_tke_max_sic__0000[1-6]	10,4,10,10,10,10	
			alp_bl_k	0.5	name_tke_max_sic	tke_max_sic	
			iflag_trig_bl	0	flag_plcl__0000[1-6]	1,10,10,10,10,10	
			s_trig	1.2E7	name_plcl	plcl	
			tau_trig_shallow	600	flag_plfc__0000[1-6]	1,10,10,10,10,10	
			tau_trig_deep	1800	name_plfc	plfc	
			iflag_clos_bl	0	flag_wbeff__0000[1-6]	1,10,10,10,10,10	
			iflag_coupl	5	name_wbeff	wbeff	
			iflag_clos	2	flag_ale_bl__0000[1-6]	1,1,1,10,10,10	
			iflag_wake	1	name_ale_bl	ale_bl	
			alp_offset	0.	flag_alp_bl__0000[1-6]	1,1,1,10,10,10	
			f_cdrag_oce	0.7	name_alp_bl	alp_bl	
			qqa1	1.	flag_tke__0000[1-6]	4,10,10,10,10,10	
			qqa2	0.	name_tke	tke	
			Fmax	0.65	flag_tke_max__0000[1-6]	4,10,10,10,10,10	

[a] [1-6] all the 6 values

Table D.2: Changes on the `.def` files introduced from `AR4.0` to `NPv3.1` (con't 1), but only for the `run.def` file

name_tke_max	tke_max	flag_ale_wk__0000[1-6]	1,1,1,10,10,10
name_ale_wk	ale_wk	flag_alp_wk__0000[1-6]	1,1,1,10,10,10
name_alp_wk	alp_wk	flag_ale__0000[1-6]	1,1,1,10,10,10
name_ale	ale	flag_alp__0000[1-6]	1,1,1,10,10,10
name_alp	alp	flag_cin__0000[1-6]	1,1,1,10,10,10
name_cin	cin	flag_wape__0000[1-6]	1,1,1,10,10,10
name_wape	wape	flag_wake_h__0000[1-6]	4,5,10,10,10,10
name_wake_h	wake_h	flag_wake_s__0000[1-6]	4,5,10,10,10,10
name_wake_s	wake_s	flag_dtwak__0000[1-6]	4,5,10,10,10,10
name_dtwak	dtwak	flag_dqwak__0000[1-6]	4,5,10,10,10,10
name_dqwak	dqwak	flag_wake_deltat__0000[1-6]	4,5,10,10,10,10
name_wake_deltat	wake_deltat	flag_wake_deltaq__0000[1-6]	4,5,10,10,10,10
name_wake_deltaq	wake_deltaq	flag_wake_omg__0000[1-6]	4,5,10,10,10,10
name_wake_omg	wake_omg	flag_ftd__0000[1-6]	4,5,10,10,10,10
name_ftd	ftd	flag_fqd__0000[1-6]	4,5,10,10,10,10
name_fqd	fqd	flag_dqlscth__0000[1-6]	10,10,10,10,10,10
name_dqlscth	dqlscth	flag_dqlscst__0000[1-6]	10,10,10,10,10,10
name_dqlscst	dqlscst	flag_d1lscth__0000[1-6]	10,10,10,10,10,10
name_dtlscth	dtlscth	flag_dtlscst__0000[1-6]	10,10,10,10,10,10
name_dtlscst	dtlscst	flag_pluth__0000[1-6]	10,10,10,10,10,10
name_pluth	pluth	flag_plulst__0000[1-6]	10,10,10,10,10,10
name_plulst	plulst	flag_tmaxth__0000[1-6]	10,10,10,10,10,10
name_lmaxth	lmaxth	flag_ptconvth__0000[1-6]	10,10,10,10,10,10
name_ptconvth	ptconvth	flag_f_th__0000[1-6]	4,10,10,10,10,10
name_f_th	f_th	flag_e_th__0000[1-6]	4,10,10,10,10,10
name_e_th	e_th	flag_w_th__0000[1-6]	4,10,10,10,10,10
name_w_th	w_th	flag_lambda_th__0000[1-6]	10,10,10,10,10,10
name_lambda_th	lambda_th	flag_ftime_th__0000[1-6]	4,10,10,10,10,10
name_ftime_th	ftime_th	flag_q_th__0000[1-6]	4,10,10,10,10,10
name_q_th	q_th	flag_a_th__0000[1-6]	4,10,10,10,10,10
name_a_th	a_th	flag_d_th__0000[1-6]	4,10,10,10,10,10
name_d_th	d_th	flag_f0_th__0000[1-6]	4,10,10,10,10,10
name_f0_th	f0_th	flag_zmax_th__0000[1-6]	4,4,4,5,10,10
name_zmax_th	zmax_th	flag_dqthe__0000[1-6]	4,10,10,10,10,10
name_dqthe	f0_th		

Table D.3: Changes on the `.def` files introduced from `NPv3.1` to `NPv4.12` each LMDZ version

config	gcm		output	physiq		run		orchidee
NPv4.12								
	day_step	960		ok_limitvrai	n	iconser	240	
	iperiod	5		f_cdrag_stable	1.			
	tetagdiv	3600.		f_cdrag_ter	1.			
	tetagrot	5400.		f_cdrag_oce	0.7			
	tetatemp	5400.		cdmmax	2.5E-3			
	physic	y		cdhmax	2.0E-3			
	ok_strato	y		ok_orodr	y			
	iflag_top_bound	2		ok_orolf	y			
	clat	0.		f_rugoro	0.			

Table D.4: Changes on the `.def` files introduced from `NPv3.1` to `NPv4.12` (con't 1), but only for the `run.def` file

`iflag_rrtm`	0	`cld_lc_lsc`	0.000192
`cld_lc_con`	0.000192	`cld_tau_lsc`	1800.
`cld_tau_con`	1800.	`ffallv_lsc`	0.9504
`ffallv_con`	0.9504	`coef_eva`	1e-5
`reevap_ice`	y	`iflag_cldcon`	6
`fact_cldcon`	1.	`facttemps`	0.
`iflag_pdf`	1	`ok_newmicro`	y
`iflag_ratqs`	4	`ratqsbas`	0.002
`ratqshaut`	0.24	`rad_froid`	35
`rad_chau1`	12	`rad_chau2`	11
`new_oliq`	y	`rei_min`	20.
`rei_max`	61.29	`t_glace_min`	258.
`t_glace_max`	273.13	`iflag_con`	3
`if_ebil`	0	`epmax`	0.97
`ok_adj_ema`	n	`iflag_clw`	0
`iflag_clos`	2	`iflag_mix`	1
`qqa1`	1.	`qqa2`	0.
`cvl_corr`	1.0	`Fmax`	0.65
`iflag_thermals`	18	`nsplit_thermals`	1
`tau_thermals`	0.	`iflag_thermals_ed`	8
`iflag_thermals_optflux`	0	`iflag_pbl`	11
`ksta_ter`	1.e-7	`ksta`	1.e-10
`ok_kzmin`	y	`iflag_coupl`	5+
`seuil_inversion`	-0.08	`alp_bl_k`	0.5
`iflag_fisrt_qsat`	3	`iflag_thermals_closure`	1
`iflag_wake`	1	`alp_offset`	0.
`iflag_trig_bl`	2	`s_trig`	1.2e7
`tau_trig_shallow`	1200	`tau_trig_deep`	1200
`iflag_clos_bl`	1	`dsigmin`	0.125
`t_glace_min`	240.	`t_glace_max`	273.13
`exposant_glace`	1.7	`iflag_t_glace`	1

Table D.5: Changes on the `.def` files introduced from `NPv4.12` to `NPv4.12bis` each LMDZ version (COSP simulator 4.9.5 is activated)

config	gcm	output	physiq	run	orchidee
NPv4.12bis					
flag_u850	1			ok_dynzon	y
flag_v850	1			cosp_outfilenames__00001	histmthCOSP
flag_t850	1			cosp_outfilenames__00002	histdayCOSP
flag_u300	1			cosp_outfilenames__00003	histhfCOSP
flag_v300	1			cosp_outfilekeys__0000[1-3]	TRUE, TRUE, TRUE
flag_t300	1			cosp_outfiletimesteps__00001	2592000.
flag_u500	1			cosp_outfiletimesteps__00002	86400.
flag_v500	1			cosp_outfiletimesteps__00003	10800.
flag_t500	1			cosp_outfiletypes__0000[1-3]	ave(X), ave(X), ave(X)
flag_u200	1			cles_cllcalipso__0000[1-3]	TRUE, TRUE, TRUE
flag_v200	1			name_cllcalipso	cllcalipso
flag_t200	1			cles_clhcalipso__0000[1-3]	TRUE, TRUE, TRUE
ok_cosp	y			name_clhcalipso	clhcalipso
				cles_clmcalipso__0000[1-3]	TRUE, TRUE, TRUE
				name_clmcalipso	clmcalipso
				cles_cltcalipso__0000[1-3]	TRUE, TRUE, TRUE
				name_cltcalipso	cltcalipso
				cles_clcalipso__0000[1-3]	TRUE, TRUE, TRUE
				name_clcalipso	clcalipso
				cles_cfad_lidarsr532__0000[1-3]	FALSE, FALSE, FALSE
				name_cfad_lidarsr532	cfad_lidarsr532
				cles_parasol_refl__0000[1-3]	TRUE, TRUE, TRUE
				name_parasol_refl	parasol_refl
				cles_parasol_crefl__0000[1-3]	TRUE, TRUE, TRUE
				name_parasol_crefl	parasol_crefl
				cles_atb532__0000[1-3]	FALSE, FALSE, FALSE
				name_atb532	atb532
				cles_beta_mol532__0000[1-3]	FALSE, FALSE, FALSE
				name_beta_mol532	beta_mol532
				cles_sunlit__0000[1-3]	TRUE, TRUE, TRUE
				name_sunlit	sunlit
				cles_clisccp2__0000[1-3]	TRUE, TRUE, TRUE
				name_clisccp2	clisccp2
				cles_boxtauisccp__0000[1-3]	FALSE, FALSE, FALSE
				name_boxtauisccp	boxtauisccp
				cles_boxptopisccp__0000[1-3]	FALSE, FALSE, FALSE
				name_boxptopisccp	boxptopisccp
				cles_tclisccp__0000[1-3]	TRUE, TRUE, TRUE
				name_tclisccp	tclisccp
				cles_ctpisccp__0000[1-3]	TRUE, TRUE, TRUE
				name_ctpisccp	ctpisccp
				cles_tauisccp__0000[1-3]	TRUE, TRUE, TRUE
				name_tauisccp	tauisccp
				cles_albisccp__0000[1-3]	TRUE, TRUE, TRUE
				name_albisccp	albisccp
				cles_meantbisccp__0000[1-3]	FALSE, FALSE, FALSE
				name_meantbisccp	meantbisccp
				cles_meantbclrisccp__0000[1-3]	FALSE, FALSE, FALSE
				name_meantbclrisccp	meantbclrisccp

Table D.6: Changes on the `.def` files introduced from `NPv4.12bis` to `NPv4.12OR11` each LMDZ version (ORCHIDDEE model 4.9.1 is activated)

config	gcm	output	physiq	run	orchidee	
NPv4.12OR11						
					HYDROL_SOIL_DEPTH	2.
					HYDROL_HUMCSTE	0.8
					HYDROL_CWRR	y

Table D.7: Changes on the `.def` files introduced from `NPv4.12OR11` to `NPv4.12qsat` each LMDZ version

config	gcm	output	physiq		run	orchidee	
NPv4.12qsat							
			iflag_fisrtilp_qsat	3		HYDROL_SOIL_DEPTH	4.
						HYDROL_HUMCSTE	5.
						HYDROL_CWRR	n

Table D.8: Changes on the `.def` files introduced from `NPv4.12qsat` to `NPv4.12tglaceoff` LMDZ version

config	gcm	output	physiq		run	orchidee
NPv4.12tglaceoff						
ok_cosp	n		t_glace_min	258.	ok_dynzon	n
			t_glace_max	273.13	iflag_fisrtilp_qsat	0
			iflag_fisrt_qsat	3	flag_u850__0000[1-10]	1,7,7,10,10,10,11,11,11
			iflag_t_glace	0	flag_v850__0000[1-10]	1,7,7,10,10,10,11,11,11
					flag_t850__0000[1-10]	1,7,7,10,10,10,11,11,11
					flag_u500__0000[1-10]	1,7,7,10,10,10,11,11,11
					flag_v500__0000[1-10]	1,7,7,10,10,10,11,11,11
					flag_t500__0000[1-10]	1,7,7,10,10,10,11,11,11
					flag_u200__0000[1-10]	1,7,7,10,10,10,11,11,11
					flag_v200__0000[1-10]	1,7,7,10,10,10,11,11,11
					flag_t200__0000[1-10]	1,7,7,10,10,10,11,11,11

Table D.9: Changes on the `.def` files introduced from `NPv4.12tglaceoff` to `NPv4.16` LMDZ version (COSP activated, with same values as in D.5)

config	gcm	output	physiq		run	orchidee
NPv4.16						
flag_u850	1		ok_conserv_q	y	resetvarc	FALSE
flag_v850	1		iflag_fisrtilp_qsat	3	ok_dynzon	y
flag_t850	1		t_glace_min	240.	t_coupl	86400.0000000000
flag_u300	1		t_glace_max	273.13	gwd_rando_ruwmax	1.0E-002
flag_v300	1		iflag_t_glace	1	gwd_rando_sat	0.250000000000000
flag_t300	1					
flag_u500	1					
flag_v500	1					
flag_t500	1					
flag_u200	1					
flag_v200	1					
flag_t200	1					
ok_cosp	y					

Table D.10: Changes on the `.def` files introduced from `NPv4.16` to `NPv4.17` LMDZ version

config	gcm	output	physiq		run	orchidee
NPv4.17						
			iflag_mix	0		

Table D.11: Changes on the `.def` files introduced from `NPv4.17` to `NPv4.18` LMDZ version

config	gcm	output	physiq		run	orchidee
NPv4.18						
			iflag_ice_thermo	1		
			iflag_fisrtilp_qsat	4		

Table D.12: Changes on the `.def` files introduced from `NPv4.18` to `NPv5.01` LMDZ version (zoom parameters not included)

config		gcm		output	physiq		run		orchidee
NPv5.01									
phys_out_regfkey	n	day_step	720		ok_gwd_rando	y	omp_chunk	10	
phys_out_filekeys	y	idissip	5		gwd_rando_ruwmax	2.	dsigmin	1.0	
nbapp_rad	48	tetagdiv	1800.		gwd_rando_sat	0.2	ok_all_xml	FALSE	
ok_cdnc	n	#tetagrot	5400.		iflag_mix	1	NSW	2	
ok_ade	n	tetagrot	7200.		iflag_fisrtilp_qsat	4	tau_ratqs	1800.0	
ok_aie	n	iflag_phys	1		iflag_ener_conserv	1	solarlong0	-999.999	
flag_aerosol	0	read_start	y		ok_conserv_q	y	qsol0	-1.0	
read_climoz	0	iphysiq	5				evap0	-1.0000	
ok_cosp	n	vert_sampling	strato_custom				albsno0	-1.0	
		vert_scale	7.				inertie_ice	2000.0	
		vert_dzmin	0.017				inertie_sno	2000.0	
		vert_dzlow	1.				inertie_sol	2000.0	
		vert_z0low	8.7				iflag_ice_thermo	0	
		vert_dzmid	2.				f_ri_cd_min	0.1	
		vert_z0mid	70.				fmagic	1.0	
		vert_h_mid	20.				ok_lic_melt	FALSE	
		vert_dzhig	11.				fact_thermals_ed_dz	0.1	
		vert_z0hig	75.				iflag_cvl_sigd	0	
		vert_h_hig	20.				lev_histhf	1	
		vert_prof_dissip	1				lev_histday	1	
		dissip_zref	50				lev_histmth	2	
		ok_strato	y				lev_histins	1	
		ok_hines	y				lev_histLES	1	
		tau_top_bound	5.e-4				levout_histNMC__0000[1-3]	5, 5, 5	

Table D.13: As in D.12, added/changed values from `NPv4.18` to `NPv5.01`, but only for `run.def` file

freq_outNMC__0000[1-3]	30., 1., 0.25
lonmin_ins	100.0
latmin_ins	-20.0
ecrit_hf	0.125
ecrit_day	1.0
ecrit_tra	0.0
supcrit1	0.54
scut	0.95
alphas	-5.0
callstats	FALSE
carbon_cycle_tr	FALSE
tau_calv	3600.0
phys_out_lonmin__0000[1-9]	-180. (for all)
phys_out_latmin__0000[1-9]	-90. (for all)
phys_out_levmin__0000[1-9]	1 (for all)
phys_out_filestations__0000[1-9]	FALSE (for all)
SOILTYPE_CLASSIF	zobler
CHECK_WATERBAL	FALSE
DIFFUCO_OK_INCA	FALSE
CANOPY_EXTINCTION	FALSE
NOx_RAIN_PULSE	FALSE
NOx_FERTILIZERS_USE	FALSE
NVM	13
PFT_TO_MTC__0000[1-13]	1, 2, 3, 4, 5, 6, 7, 8, 9, 10, 11, 12, 13
PFT_NAME__00002	tropical
PFT_NAME__00004	temperate
PFT_NAME__00006	temperate
PFT_NAME__00008	boreal
PFT_NAME__00010	C3
PFT_NAME__00012	C3
SPINUP_ANALYTIC	FALSE
LEAF_TAB__0000[1-13]	4, 1, 1, 3, 1, 1, 2, 1, 2, 3, 3, 3, 3
PHENO_MODEL__00002	none
PHENO_MODEL__00004	none
PHENO_MODEL__00006	ncdgdd
PHENO_MODEL__00008	ncdgdd
PHENO_MODEL__00010	moigdd
PHENO_MODEL__00012	moigdd
LLAIMIN__0000[1-13]	0., 8., 0., 4., 4.5, 0.0, 4.0, 0.0, 0.0, 0.0, 0.0, 0.0, 0.0
NATURAL__0000[1-13]	TRUE, TRUE, TRUE, TRUE, TRUE, TRUE, TRUE, TRUE, TRUE, TRUE, TRUE, FALSE, FALSE
freq_calNMC__0000[1-3]	600., 600., 600.
lonmax_ins	130.0
latmax_ins	20.0
ecrit_ins	0.02083333333333333
ecrit_mth	30.0
ecrit_reg	0.25
supcrit2	0.6
gammas	0.05
OK_LES	FALSE
ecrit_LES	0.12500
carbon_cycle_cpl	FALSE
ok_sync	FALSE
phys_out_lonmin__0000[1-9]	180. (for all)
phys_out_latmin__0000[1-9]	90. (for all(
phys_out_levmax__0000[1-9]	79, 79, 79, 79, 79, 79, 17, 17, 17
CHECKTIME	FALSE
ORCHIDEE_WATCHOUT	FALSE
OK_EXPLICITSNOW	FALSE
LEAFAGE_OK_INCA	FALSE
CANOPY_MULTILAYER	FALSE
NOx_BBG_FERTIL	FALSE
STOMATE_WATCHOUT	FALSE
IMPOSE_PARAM	TRUE
PFT_NAME__00001	bare
PFT_NAME__00003	tropical
PFT_NAME__00005	temperate
PFT_NAME__00007	boreal
PFT_NAME__00009	boreal
PFT_NAME__00011	C4
PFT_NAME__00013	C4
LAI_MAP	FALSE
PHENO_MODEL__00001	none
PHENO_MODEL__00003	moi
PHENO_MODEL__00005	none
PHENO_MODEL__00007	none
PHENO_MODEL__00009	ngd
PHENO_MODEL__00011	moigdd
PHENO_MODEL__00013	moigdd
TYPE_OF_LAI__0000[1-13]	inter (for all)
IS_C4__0000[1-13]	FALSE, FALSE, FALSE, FALSE, FALSE, FALSE, FALSE, FALSE, FALSE, FALSE, TRUE, FALSE, FALSE

Table D.14: As in D.12, added/changed values from `NPv4.18` to `NPv5.01`, but only for `run.def` file (con't 1)

VCMAX_FIX__0000[1-13]	0.0, 40.0, 50.0, 30.0, 35.0, 40.0, 30.0, 40.0, 35.0, 60.0, 60.0, 70.0, 70.0
DOWNREGULATION_CO2_COEFF__0000[1-13]	0.0, 0.38, 0.38., 0.28, 0.28, 0.28, 0.22, 0.22, 0.22, 0.26, 0.26, 0.26, 0.26
E_KMO__0000[1-13]	-9999.0, 36380.0, 36380.0, 36380.0, 36380.0, 36380.0, 36380.0, 36380.0, 36380.0, 36380.0, 36380.0, 36380.0
E_VCMAX__0000[1-13]	-9999.0, 71513.0, 71513.0, 71513.0, 71513.0, 71513.0, 71513.0, 71513.0, 71513.0, 71513.0, 67300.0, 71513.0, 67300.0
ASV__0000[1-13]	-9999.0, 668.39, 668.39, 668.39, 668.39, 668.39, 668.39, 668.39, 668.39, 668.39, 641.64, 668.39, 641.64
TPHOTO_MIN__0000[1-13]	-9999.0, -4.0, -4.0, -4.0, -4.0, -4.0, -4.0, -4.0, -4.0, -4.0, -4.0, -4.0, -4.0
ASJ__0000[1-13]	-9999.0, 659.7, 659.7, 659.7, 659.7, 659.7, 659.7, 659.7, 659.7, 659.7, 659.7, 630.0, 659.7, 630.0
D_VCMAX__0000[1-13]	-9999.0, 200000.0, 200000.0, 200000.0, 200000.0, 200000.0, 200000.0, 200000.0, 200000.0, 200000.0, 192000.0, 200000.0, 192000.0
E_RD__0000[1-13]	-9999.0, 46390.0, 46390.0, 46390.0, 46390.0, 46390.0, 46390.0, 46390.0, 46390.0, 46390.0, 46390.0, 46390.0, 46390.0
ARJV__0000[1-13]	-9999.0, 2.59, 2.59, 2.59, 2.59, 2.59, 2.59, 2.59, 2.59, 1.715, 2.59, 1.715
KMC25__0000[1-13]	-9999.0, 404.9, 404.9, 404.9, 404.9, 404.9, 404.9, 404.9, 404.9, 404.9, 650.0, 404.9, 650.0
gamma_star25__0000[1-13]	-9999.0, 42.75, 42.75, 42.75, 42.75, 42.75, 42.75, 42.75, 42.75, 42.75, 42.75, 42.75, 42.75
B1__0000[1-13]	-9999.0, 0.14, 0.14, 0.14, 0.14, 0.14, 0.14, 0.14, 0.14, 0.20, 0.14, 0.20
H_PROTONS__0000[1-13]	-9999.0, 4.0, 4.0, 4.0, 4.0, 4.0, 4.0, 4.0, 4.0, 4.0, 4.0, 4.0, 4.0
FQ__0000[1-13]	-9999.0, -9999.0, -9999.0, -9999.0, -9999.0, -9999.0, -9999.0, -9999.0, -9999.0, -9999.0, 1.0, -9999.0, 1.0
KP__0000[1-13]	-9999.0, -9999.0, -9999.0, -9999.0, -9999.0, -9999.0, -9999.0, -9999.0, -9999.0, -9999.0, 0.7, -9999.0, 0.7
GBS__00001	-9999.0, -9999.0, -9999.0, -9999.0, -9999.0, -9999.0, -9999.0, -9999.0, -9999.0, -9999.0, , 0.003, -9999.0, 0.003
ALPHA_LL__00001	-9999.0, 0.3, 0.3, 0.3, 0.3, 0.3, 0.3, 0.3, 0.3, 0.3, 0.3, 0.3, 0.3
PREF_SOIL_VEG__0000[1-13]	1, 2, 2, 2, 2, 2, 2, 2, 2, 3, 3, 3, 3
SNOWCRI	1.5000
MAX_SNOW_AGE	50.000
ZO_OVER_HEIGHT	0.00625
ZO_BARE	0.01
TCST_SNOWA	5.0000
VIS_DRY__0000[1-9]	0.24, 0.22, 0.2, 0.18, 0.16, 0.14, 0.12, 0.1, 0.27
VIS_WET__0000[1-9]	0.12, 0.11, 0.1, 09, 0.08, 0.07, 0.06, 0.05, 0.15
ALBSOIL_VIS__0000[1-9]	0.18, 0.16, 0.16, 0.15, 0.12, 0.105, 0.09, 0.075, 0.25
ALB_DEADLEAF__0000[1-2]	0.12, 0.35
XANSMAX	0.85
XANSDRY	0.008
XRHOSMAX	750.00
XWSNOWHOLDMAX2	0.10000
ZSNOWTHRMCOND1	0.02
ZSNOWTHRMCOND_AVAP	-0.06023
ZSNOWTHRMCOND_CVAP	-289.99
ZSNOWCMPCT_ACM	2.8E-006
ZSNOWCMPCT_CCM	460.00
ZSNOWCMPCT_VT	8.1E-002
E_KMC__0000[1-13]	-9999.0, 79430.0, 79430.0, 79430.0, 79430.0, 79430.0, 79430.0, 79430.0, 79430.0, 79430.0, 79430.0, 79430.0
E_GAMMA_STAR__0000[1-13]	-9999.0, 37830.0, 37830.0, 37830.0, 37830.0, 37830.0, 37830.0, 37830.0, 37830.0, 37830.0, 37830.0, 37830.0
E_JMAX__0000[1-13]	-9999.0, 49884.0, 49884.0, 49884.0, 49884.0, 49884.0, 49884.0, 49884.0, 49884.0, 49884.0, 77900.0, 49884.0, 77900.
BSV__0000[1-13]	-9999.0, -1.07, -1.07, -1.07, -1.07, -1.07, -1.07, -1.07, -1.07, -1.07, 0.0, -1.07, 0.0
TPHOTO_MAX__0000[1-13]	-9999.0, 55.0, 55.0, 55.0, 55.0, 55.0, 55.0, 55.0, 55.0, 55.0, 55.0, 55.0, 55.0
BSJ__0000[1-13]	-9999.0, -0.75, -0.75, -0.75, -0.75, -0.75, -0.75, -0.75, -0.75, -0.75, 0.0, -0.75, 0.0
D_JMAX__0000[1-13]	-9999.0, 200000.0, 200000.0, 200000.0, 200000.0, 200000.0, 200000.0, 200000.0, 200000.0, 200000.0, 192000.0, 200000.0, 192000.0
VCMAX25__0000[1-13]	-9999.0, 65.0, 65.0, 45.0, 45.0, 55.0, 45.0, 45.0, 35.0, 70.0, 70.0, 70.0, 70.0
BRJV__0000[1-13]	-9999.0, -0.035, -0.035, -0.035, -0.035, -0.035, -0.035, -0.035, -0.035, -0.035, 0.0, -0.035, 0.0
KMO25__0000[1-13]	-9999.0, 278400.0, 278400.0, 278400.0, 278400.0, 278400.0, 278400.0, 278400.0, 278400.0, 278400.0, 450000.0, 278400.0, 450000.0
A1__0000[1-13]	-9999.0, 0.85, 0.85, 0.85, 0.85, 0.85, 0.85, 0.85, 0.85, 0.85, 0.85, 0.85, 0.85
GO__0000[1-13]	-9999.0, 0.00625, 0.00625, 0.00625, 0.00625, 0.00625, 0.00625, 0.00625, 0.00625, 0.01875, 0.00625, 0.01875
FPSIR__0000[1-13]	-9999.0, -9999.0, -9999.0, -9999.0, -9999.0, -9999.0, -9999.0, -9999.0, -9999.0, -9999.0, -9999.0, 0.4, -9999.0, 0.4
FPSEUDO__0000[1-113]	-9999.0, -9999.0, -9999.0, -9999.0, -9999.0, -9999.0, -9999.0, -9999.0, -9999.0, -9999.0, -9999.0, 0.1, -9999.0, 0.1
ALPHA__0000[1-13]	-9999.0, -9999.0, -9999.0, -9999.0, -9999.0, -9999.0, -9999.0, -9999.0, -9999.0, -9999.0, -9999.0, 0.1, -9999.0, 0.1
THETA__0000[1-13]	-9999.0, 0.7, 0.7, 0.7, 0.7, 0.7, 0.7, 0.7, 0.7, 0.7, 0.7, 0.7, 0.7
EXT_COEFF__0000[1-13]	0.5 (for all)
MAXMASS_SNOW	3000.0
MIN_WIND	0.10000
SNOW_TRANS	0.30000
HEIGHT_DISPLACEMENT	0.75000
ZO_ICE	0.001
SNOWCRI_ALB	10.000
NIR_DRY__0000[1-9]	0.48, 0.44, 0.4, 0.36, 0.32, 0.28, 0.24, 0.2, 0.55
NIR_WET__0000[1-9]	0.24, 0.22, 0.20, 0.18, 0.16, 0.14, 0.12, 0.10, 0.31
ALBSOIL_NIR__0000[1-9]	0.36, 0.34, 0.34, 0.33, 0.3, 0.25, 0.20, 0.15, 0.45
ALB_ICE__0000[1-2]	0.6, 0.2
XANSMIN	0.5
XANS_T	0.24000
XWSNOWHOLDMAX1	0.03
XSNOWRHOHOLD	200.00
ZSNOWTHRMCOND2	2.5E-006
ZSNOWTHRMCOND_BVAP	-2.5425
ZSNOWCMPCT_RHOD	150.00
ZSNOWCMPCT_BCM	0.04
ZSNOWCMPCT_V0	37000000.0
ZSNOWCMPCT_VR	1.8E-002

Table D.15: As in D.12, added/changed values from `NPv4.18` to `NPv5.01`, but only for `run.def` file (con't 2)

CB	5.0
CD	5.0
DEFC_PLUS	0.023
NLAI	20
DEW_VEG_POLY_COEFF__0000[1-6]	0.887773, 0.205673, 0.110112, 1.4843E-2, 8.24E-4, 1.7E-5
DOWNREGULATION_CO2_BASELEVEL	280.00
MIN_VEGFRAC	1.0E-003
RSTRUCT_CONST__0000[1-13]	0.0, 25.0, 25.0, 25.0, 25.0, 25.0, 25.0, 25.0, 25.0, 2.5, 2.0, 2.0, 2.0
WMAX_VEG__0000[1-13]	150.0 (for all)
SNOWA_DEC__0000[1-13]	0.45, 0.0, 0.0, 0.06, 0.06, 0.11, 0.06, 0.11, 0.11, 0.52, 0.52, 0.52, 0.52
ALB_LEAF_NIR__0000[1-13]	0.0, 0.2, 0.22, 0.22, 0.22, 0.22, 0.22, 0.22, 0.3, 0.3, 0.3, 0.3
DRY_SOIL_HEAT_CAPACITY	1800000.0
WET_SOIL_HEAT_CAPACITY	3030000.0
SNOW_HEAT_COND	0.30000
NOBIO_WATER_CAPAC_VOLUMETRI	150.00
CHOISNEL_DIFF_MAX	0.1
CHOISNEL_RSOL_CSTE	33000.
OK_FREEZE	FALSE
READ_PERMAFROST_MAP	FALSE
OK_FREEZE_THERMIX	FALSE
FR_DT	2.0000
OK_FREEZE_CWRR	FALSE
Oi	210000.0
TAU_FIRE	30.000
FIRE_RESIST_STRUCT	0.50000
BCFRAC_COEFF__0000[1-3]	0.3, 1.3, 88.2
AVAILABILITY_FACT	0.10000
OK_MINRES	TRUE
RESERVE_TIME_TREE	30.000
R0	0.30000
ALLOC_SAP_ABOVE_GRASS	1.0000
MAX_LTOLSR	0.50000
LAI_MAX_TO_HAPPY	0.50000
PIPE_TUNE1	100.00
PIPE_TUNE3	0.50000
PIPE_DENSITY	200000.0
PIPE_TUNE_EXP_COEFF	1.6000
GDD_CRIT_ESTAB	150.00
ALPHA_GRASS	0.50000
MASS_RATIO_HEART_SAP	3.0000
TAU_HUM_MONTH	20.000
TAU_T2M_MONTH	20.000
TAU_TSOIL_MONTH	20.000
TAU_GPP_WEEK	7.0000
TAU_NGD	50.000
BM_SAPL_CARBRES	5.0000
BM_SAPL_HEARTABOVE	2.0000
INIT_SAPL_MASS_LEAF_NAT	0.10000
INIT_SAPL_MASS_CARBRES	5.0000
INIT_SAPL_MASS_FRUIT	0.30000
MIGRATE_TREE	10000.
LAI_INITMIN_TREE	0.30000
DIA_COEFF__00001	4.0000
MAXDIA_COEFF__00001	100.00
BM_SAPL_LEAF__0000[1-4]	4.0, 4.0, 0.8, 5.0
Z_DECOMP	0.20000
LC__0000[1-8]	0.22, 0.35, 0.35, 0.35, 0.35, 0.22, 0.22, 0.22
FRAC_SOIL_STRUCT_AB	0.45000
FRAC_SOIL_STRUCT_SB	0.70000
FRAC_SOIL_METAB_AB	0.45000
TAU_METABOLIC	6.6E-002
SOIL_Q10	0.69000
LITTER_STRUCT_COEF	3.0000
FRAC_TURNOVER_DAILY	0.55000
ALWAYS_INIT	FALSE
MOIAVAIL_ALWAYS_TREE	1.0000
T_ALWAYS_ADD	10.000
GDDNCD_CURVE	9.1E-003
CC	5.0
RAYT_CSTE	125.0
DEFC_MULT	1.5
LAIMAX	12.000
DOWNREGULATION_CO2	FALSE
CLAYFRACTION_DEFAULT	0.20000
STEMPDIAG_BID	280.00
KZERO__0000[1-13]	0.0, 1.2E-4, 1.2E-4, 1.2E-4, 1.2E-4, 2.5E-4, 1.2E-4, 2.5E-4, 2.5E-4, 3.0E-4, 1.2E-4, 1.2E-4, 1.2E-4
SNOWA_AGED__0000[1-13]	0.35, 0.0, 0.0, 0.14, 0.14, 0.14, 0.14, 0.14, 0.14, 0.18, 0.18, 0.18, 0.18
ALB_LEAF_VIS__0000[1-13]	0.0, 0.04, 0.06, 0.06, 0.06, 0.06, 0.06, 0.06, 0.06, 0.1, 0.1, 0.1, 0.1
THERMOSOIL_NBLEV	7
DRY_SOIL_HEAT_COND	0.4
WET_SOIL_HEAT_COND	1.89
SNOW_DENSITY	330.00
CHOISNEL_DIFF_MIN	1.0E-003
CHOISNEL_DIFF_EXP	1.5
HCRIT_LITTER	8.0E-002
OK_ECORR	FALSE
READ_REFTEMP	FALSE
POROS	0.41000
OK_SNOWFACT	FALSE
LAI_LEVEL_DEPTH	0.15000
TOO_LONG	5.0000
LITTER_CRIT	200.00
CO2FRAC__0000[1-8]	0.95, 0.95, 0.0, 0.3, 0.0, 0.0, 0.95, 0.95
FIREFRAC_COEFF__0000[1-4]	0.45, 0.8, 0.6, 0.13
REF_GREFF	0.035
TAU_LEAFINIT	10.000
RESERVE_TIME_GRASS	20.000
F_FRUIT	0.10000
MIN_LTOLSR	0.20000
Z_NITROGEN	0.20000
NLIM_TREF	25.000
PIPE_TUNE2	40.000
PIPE_TUNE4	0.30000
PIPE_K1	8000.0
PRECIP_CRIT	100.00
FPC_CRIT	0.95000
ALPHA_TREE	1.0000
FRAC_GROWTHRESP	0.28000
TAU_HUM_WEEK	7.0000
TAU_T2M_WEEK	7.0000
TAU_SOILHUM_MONTH	20.000
TAU_GDD	40.000
COEFF_TAU_LONGTERM	3.0000
BM_SAPL_SAPABOVE	0.50000
BM_SAPL_HEARTBELOW	2.0000
INIT_SAPL_MASS_LEAF_AGRI	1.0000
INIT_SAPL_MASS_ROOT	0.10000
CN_SAPL_INIT	0.50000
MIGRATE_GRASS	10000.
LAI_INITMIN_GRASS	0.10000
DIA_COEFF__00002	0.50000
MAXDIA_COEFF__00002	1.0E-002
METABOLIC_REF_FRAC	0.85000
CN__0000[1-9]	40.0 (fdor all)
FRAC_SOIL_STRUCT_AA	0.55000
FRAC_SOIL_STRUCT_SA	0.70000
FRAC_SOIL_METAB_AA	0.45000
METABOLIC_LN_RATIO	1.8E-002
TAU_STRUCT	0.24500
TSOIL_REF	30.000
MOIST_COEFF__0000[1-3]	1.1, 2.4, 0.29
TAX_MAX	0.80000
MIN_GROWTHINIT_TIME	300.00
MOIAVAIL_ALWAYS_GRASS	0.60000
GDDNCD_REF	603.00
GDDNCD_OFFSET	64.000

Table D.16: As in D.12, added/changed values from `NPv4.18` to `NPv5.01`, but only for `run.def` file (con't 3)

BM_SAPL_RESCALE	40.000
MAINT_RESP_COEFF	1.4000
FRAC_CARB_SA	0.42000
FRAC_CARB_PA	0.45000
ACTIVE_TO_PASS_CLAY_FRAC	0.68000
CARBON_TAU_ISLOW	5.4800
FLUX_TOT_COEFF__0000[1-3]	1.2, 1.4, 0.75000
DT_TURNOVER_TIME	10.000
LEAF_AGE_CRIT_COEFF__0000[1-3]	1.5, 0.75, 10.0
LEAFAGE_FIRSTMAX	3.0E-002
LEAFAGE_OLD	1.0000
TAU_CLIMATOLOGY	20.000
HVC2	1.3800
TLONG_REF_MAX	303.10
NCD_MAX_YEAR	3.0000
GREEN_AGE_EVER	2.0000
SLA__0000[1-13]	1.5E-2, 1.53E-002, 2.6E-002, 9.26E-003, 2.0E-002, 2.6E-002, 9.26E-003, 2.6E-002, 1.9E-002, 2.6E-002, 2.6E-002, 2.6E-002, 2.6E-002, 2.6E-002
MAINT_RESP_SLOPE_C__0000[1-13	-9999.0, 0.20, 0.20, 0.16, 0.16, 0.16, 0.16, 0.16, 0.16, 0.16, 0.12, 0.16, 0.12
MAINT_RESP_SLOPE_A__0000[1-9]	-9999.0, 0.0, 0.0, 0.0, 0.0, 0.0, 0.0, 0.0, 0.0 0.0, 0.0, 0.0, 0.0
CM_ZERO_SAPABOVE__0000[1-13]	-9999.0, 1.19E-004, 1.19E-004, 1.19E-004, 1.19E-004, 1.19E-004, 1.19E-004, 1.19E-004, 1.19E-004, 1.19E-004, 1.19E-004, 1.19E-004
CM_ZERO_HEARTABOVE__0000[1-13]	-9999.0, 0.0, 0.0, 0.0, 0.0, 0.0, 0.0, 0.0, 0.0, 0.0, 0.0, 0.0, 0.0
CM_ZERO_ROOT__0000[1-13]	-9999.0, 1.67E-003, 1.67E-003, 1.67E-003, 1.67E-003, 1.67E-003, 1.67E-003, 1.67E-003, 1.67E-003, 1.67E-003, 1.67E-003, 1.67E-003, 1.67E-003
CM_ZERO_CARBRES__0000[1-13]	-9999.0, 1.19E-004, 1.19E-004, 1.19E-004, 1.19E-004, 1.19E-004, 1.19E-004, 1.19E-004, 1.19E-004, 1.19E-004, 1.19E-004, 1.19E-004
RESIST__0000[1-13]	-9999.0, 0.95, 0.9, 0.12, 0.5, 0.12, 0.12, 0.12, 0.12, 0.0, 0.0, 0.0, 0.0
COEFF_LCCHANGE_10__0000[1-13]	-9999.0, 0.103, 0.103, 0.299, 0.299, 0.299, 0.299, 0.299, 0.299, 0.299, 0.403, 0.299, 0.403
LAI_MAX__0000[1-13]	-9999.0, 7.0, 7.0, 5.0, 5.0, 5.0, 4.5, 4.5, 3.0, 2.5, 2.5, 5.0, 5.0
PHENO_GDD_CRIT_C__0000[1-13]	-9999.0, -9999.0, -9999.0, -9999.0, -9999.0, -9999.0, -9999.0, -9999.0, -9999.0, -9999.0, 320.0, 400.0, 320.0, 700.0
PHENO_GDD_CRIT_A__0000[1-13]	-9999.0, -9999.0, -9999.0, -9999.0, -9999.0, -9999.0, -9999.0, -9999.0, -9999.0, -9999.0, 0.03125, 0.0, 0.0315, 0.0
NCDGDD_TEMP__0000[1-13]	-9999.0, -9999.0, -9999.0, -9999.0, -9999.0, 5.0, -9999.0, 0.0, -9999.0, -9999.0, -9999.0, -9999.0, -9999.0
HUM_MIN_TIME__0000[1-13]	-9999.0, -9999.0, 50.0, -9999.0, -9999.0, -9999.0, -9999.0, -9999.0, -9999.0, -9999.0, 35.0, 35.0, 75.0, 75.0
TAU_FRUIT__0000[1-13]	-9999.0, 90.0, 90.0, 90.0, 90.0, 90.0, 90.0, 90.0, 90.0, -9999.0, -9999.0, -9999.0, -9999.0
ALLOC_MIN__0000[1-13]	-9999.0, 0.2, 0.2, 0.2, 0.2, 0.2, 0.2, 0.2, 0.2, -9999.0, -9999.0, -9999.0, -9999.0
MAINT_RESP_MIN_VMAX	0.30000
FRAC_CARB_AP	4.0E-003
FRAC_CARB_SP	3.0E-002
FRAC_CARB_PS	0.0
CARBON_TAU_IACTIVE	0.14900
CARBON_TAU_IPASSIVE	241.00
NEW_TURNOVER_TIME_REF	20.000
LEAF_AGE_CRIT_TREF	20.000
VMAX_OFFSET	0.30000
LEAFAGE_LASTMAX	0.50000
GPPFRAC_DORMANCE	0.20000
HVC1	1.9E-002
LEAF_FRAC_HVC	0.33000
TLONG_REF_MIN	253.10
GDD_THRESHOLD	5.0000
GREEN_AGE_DEC	0.50000
SO__0000[1-13]	-9999.0, 0.25, 0.25, 0.30, 0.30, 0.30, 0.30, 0.30, 0.30, 0.30, 0.30, 0.30, 0.30
MAINT_RESP_SLOPE_B__0000[1-13]	-9999.0, 0.0, 0.0, 0.0, 0.0, 0.0, 0.0, 0.0, 0.0, -1.33E-003, 0.0, -1.33E-003, 0.0
CM_ZERO_LEAF__0000[1-13]	-9999.0, 2.35E-003, 2.62E-003, 1.01E-003, 2.35E-003, 2.62E-003, 1.01E-003, 2.62E-003, 2.05E-003, 2.62E-003, 2.62E-003, 2.62E-003, 2.62E-003
CM_ZERO_SAPBELOW__0000[1-13]	-9999.0, 1.19E-004, 1.19E-004, 1.19E-004, 1.19E-004, 1.19E-004, 1.19E-004, 1.19E-004, 1.19E-004, 1.19E-004, 1.19E-004, 1.19E-004
CM_ZERO_HEARTBELOW__0000[1-13]	-9999.0, 0.0, 0.0, 0.0, 0.0, 0.0, 0.0, 0.0, 0.0, 0.0, 0.0, 0.0, 0.0
CM_ZERO_FRUIT__0000[1-13]	-9999.0, 1.19E-004, 1.19E-004, 1.19E-004, 1.19E-004, 1.19E-004, 1.19E-004, 1.19E-004, 1.19E-004, 1.19E-004, 1.19E-004, 1.19E-004
FLAM__0000[1-13]	-9999.0, 0.15, 0.25, 0.25, 0.25, 0.25, 0.25, 0.25, 0.25, 0.25, 0.25, 0.35, 0.35
COEFF_LCCHANGE_1__0000[1-13]	-9999.0, 0.897, 0.897, 0.597, 0.597, 0.597, 0.597, 0.597, 0.597, 0.597, 0.597, 0.597, 0.597
COEFF_LCCHANGE_100__0000[1-13]	-9999.0, 0.0, 0.0, 0.104, 0.104, 0.104, 0.104, 0.104, 0.104, 0.104, 0.0, 0.104, 0.0
PHENO_TYPE__0000[1-13]	0, 1, 3, 1, 1, 2, 1, 2, 2, 4, 4, 2, 3
PHENO_GDD_CRIT_B__0000[1-13]	-9999.0, -9999.0, -9999.0, -9999.0, -9999.0, -9999.0, -9999.0, -9999.0, -9999.0, -9999.0, 6.25, 0.0, 6.25, 0.0
NGD_CRIT__0000[1-13]	-9999.0, -9999.0, -9999.0, -9999.0, -9999.0, -9999.0, -9999.0, -9999.0, -9999.0, 17.0, -9999.0, -9999.0, -9999.0, -9999.0
HUM_FRAC__0000[1-13]	-9999.0, -9999.0, 0.5, -9999.0, -9999.0, -9999.0, -9999.0, -9999.0, -9999.0, 0.5, 0.5, 0.5, 0.5
TAU_SAP__0000[1-13]	-9999.0, 730.0, 730.0, 730.0, 730.0, 730.0, 730.0, 730.0, 730.0, -9999.0, -9999.0, -9999.0, -9999.0
ECUREUIL__0000[1-13]	-9999.0, 0.0, 1.0, 0.0, 0.0, 1.0, 0.0, 1.0, 1.0, 1.0, 1.0, 1.0, 1.0
ALLOC_MAX__0000[1-13]	-9999.0, 0.8, 0.8, 0.8, 0.8, 0.8, 0.8, 0.8, 0.8, -9999.0, -9999.0, -9999.0, -9999.0

Table D.17: As in D.12, added/changed values from `NPv4.18` to `NPv5.01`, but only for `run.def` file (con't 4)

DEMI_ALLOC__0000[1-13	-9999.0, 5.0, 5.0, 5.0, 5.0, 5.0, 5.0, 5.0, 5.0, -9999.0, -9999.0, -9999.0, -9999.0
LEAFFALL__0000[1-13]	-9999.0, -9999.0, 10.0, -9999.0, -9999.0, 10.0, -9999.0, 10.0, 10.0, 10.0, 10.0, 10.0, 10.0
SENESCENCE_TYPE__0000[1-13]	none, none, dry, none, none, cold, none, cold, cold, mixed, mixed, mixed, mixed
NOSENESCENCE_HUM__0000[1-13]	-9999.0, -9999.0, 0.8, 9999.0, 9999.0, 9999.0, 9999.0, 9999.0, 9999.0, 0.3, 0.3, 0.3, 0.3
MIN_TURNOVER_TIME__0000[1-13]	-9999.0, -9999.0, -9999.0, -9999.0, -9999.0, -9999.0, -9999.0, -9999.0, -9999.0, 10.0, 10.0, 10.0, 10.0
SENESCENCE_TEMP_C__0000[1-13]	-9999.0, -9999.0, -9999.0, -9999.0, -9999.0, 12.0, -9999.0, 7.0, 2.0, -1.375, 5.0, 5.0, 10.0
SENESCENCE_TEMP_A__0000[1-13]	-9999.0, -9999.0, -9999.0, -9999.0, -9999.0, 0.0, -9999.0, 0.0, 0.0, 3.75, 0.0, 0.0, 0.0
RESIDENCE_TIME__0000[1-13]	-9999.0, 30.0, 30.0, 40.0, 40.0, 40.0, 80.0, 80.0, 80.0, 0.0, 0.0, 0.0, 0.0
TMIN_CRIT__0000[1-13]	-9999.0, 0.0, 0.0, -30.0, -14.0, -30.0, -45.0, -45.0, -9999.0, -9999.0, -9999.0, -9999.0, -9999.0
XIOS_ORCHIDEE_OK	FALSE
soilcap	FALSE
shumdiag	FALSE
EPS_CARBON	0.01
STOMATE_DIAGPT	1
STOMATE_CFORCING_NAME	NONE
runoff	FALSE
cgrnd	FALSE
z1	FALSE
pcapa_en	FALSE
zdz1	FALSE
temp_sol_beg	FALSE
thermals_betalpha	0.90000
thermals_fact_shell	0.60000
thermals_entr_min	1.0E-004
thermals_detr_q_power	0.50000
flag_t2m_min__00001	20
flag_t2m_max_mon__0000[1-9]	1, 20, 20, 20, 20, 20, 20, 20, 20
flag_t2m_min_mon__0000[1-9]	1, 20, 20, 20, 20, 20, 20, 20, 20
flag_bils_ech__0000[1-9]	1, 2, 10, 5, 10, 10, 11, 11, 11
flag_duhin__0000[1-9]	4, 10, 10, 10, 10, 10, 11, 11, 11
flag_dvhin__0000[1-9]	4, 10, 10, 10, 10, 10, 11, 11, 11
flag_dthin__0000[1-9]	4, 10, 10, 10, 10, 10, 11, 11, 11
flag_du_gwd_rando__0000[1-9]	4, 10, 10, 10, 10, 10, 11, 11, 11
flag_dv_gwd_rando__0000[1-9]	4, 10, 10, 10, 10, 10, 11, 11, 11
flag_vstr_gwd_rando__0000[1-9]	4, 10, 10, 10, 10, 10, 11, 11, 11
flag_dRN_vdf__00001	4
ECCENTRICITY	0.016724
OBLIQUITY	23.446
LEAFLIFE_TAB__0000[1-13]	-9999.0, 0.5, 2.0, 0.33, 1.0, 2.0, 0.33, 2.0, 2.0, 2.0, 2.0, 2.0, 2.0
LEAFAGECRIT__0000[1-13]	-9999.0, 730.0, 180.0, 910.0, 730.0, 180.0, 910.0, 180.0, 180.0, 120.0, 120.0, 90.0, 90.0
SENESCENCE_HUM__0000[1-13]	-9999.0, -9999.0, 0.3, -9999.0, -9999.0, -9999.0, -9999.0, -9999.0, -9999.0, 0.2, 0.2, 0.3, 0.2
MAX_TURNOVER_TIME__0000[1-13]	-9999.0, -9999.0, -9999.0, -9999.0, -9999.0, -9999.0, -9999.0, -9999.0, -9999.0, 80.0, 80.0, 80.0, 80.0
MIN_LEAF_AGE_FOR_SENESCENCE__0000[1-13	-9999.0, -9999.0, 90.0, -9999.0, -9999.0, 90.0, -9999.0, 60.0, 60.0, 30.0, 30.0, 30.0, 30.0
SENESCENCE_TEMP_B__0000[1-13	-9999.0, -9999.0, -9999.0, -9999.0, -9999.0, 0.0, -9999.0, 0.0, 0.0, 0.1, 0.0, 0.0, 0.0
GDD_SENESCENCE__0000[1-13]	-9999.0, -9999.0, -9999.0, -9999.0, -9999.0, -9999.0, -9999.0, -9999.0, -9999.0, -9999.0, -9999.0, -9999.0, 950.0, 4000.0
TCM_CRIT__0000[1-13]	-9999.0, -9999.0, -9999.0, 5.0, 15.5, 15.5, -8.0, -8.0, -8.0, -9999.0, -9999.0, -9999.0, -9999.0
ALMA_OUTPUT	FALSE
soilflx	FALSE
GET_SLOPE	FALSE
SPINUP_PERIOD	-1
STOMATE_FORCING_NAME	NONE
CDRAG_from_GCM	TRUE
drainage	FALSE
dgrnd	FALSE
pcapa	FALSE
pkappa	FALSE
zdz2	FALSE
thermals_fact_epsilon	2.0E-003
thermals_afact	0.666666666666667
thermals_detr_min	1.0E-004
thermals_detr_q_coef	0.012
thermals_mix0	0.0
flag_t2m_max__00001	20
name_t2m_max_mon	t2m_max_mon
name_t2m_min_mon	t2m_min_mon
name_bils_ech	bils_ech
name_duhin	duhin
name_dvhin	dvhin
name_dthin	dthin
name_du_gwd_rando	du_gwd_rando
name_dv_gwd_rando	dv_gwd_rando
name_vstr_gwd_rando	vstr_gwd_rando
flag_dPB_vdf__00001	4
PERIHELIE	102.04

Appendix E

LMDZ parallel grids slices

Some code parameters linked to parallelism and how grid size is distributed according to shared (OpenMP)/distributed (MPI) parallel paradigms.

In the dynamics, MPI is used to discretize the horizontal grid and the OpenMP the vertical. In the physics, space is discretized only horizontally.

- **Global grid:** module `mod_grid_phy_lmdz`
  - `klon_glo`: number of horizontal nodes of the global domain (1D grid)
  - `nbp_lon`: number of longitude nodes (2D grid) = `iim`
  - `nbp_lat`: number of latitude nodes (2D grid) = `jjm+1`
  - `nbp_lev`: number of vertical levels = `klev` or `llm`
- **MPI grid:** module `mod_phys_lmdz_mpi_data`
  - `klon_mpi`: number of nodes in the MPI local domain.
  - `klon_mpi_begin`: start index of the domain on the 1D global grid.
  - `klon_mpi_end`: end index of the end of the domain on the 1D global grid.
  - `ii_begin`: longitude index of the beginning of the domain (2D global grid).
  - `ii_end`: longitude index of the end of the domain (2D global grid).
  - `jj_begin`: latitude index of the beginning of the domain (2D global grid).
  - `jj_end`: latitude index of the end of the domain (2D global grid).
  - `jj_nb`: number of latitude bands = `jj_end-jj_begin+1`
  - `is_north_pole`: `.true.` If the process includes the North pole.
  - `is_south_pole`: `.true.` If the process includes the south pole.
  - `is_mpi_root`: `.true.` If the process is the MPI master.
  - `mpi_rank`: rank of the MPI process.
  - `mpi_size`: total number of MPI processes.
- **OpenMP grid:** module `mod_phys_lmdz_mpi_data`
  - `klon_omp`: number of nodes in the local OpenMP domain.
  - `klon_omp_begin`: beginning index of the OpenMP domain within the MPI domain.
  - `klon_omp_end`: end index of the OpenMP domain.
  - `is_omp_root`: `.true.` If the task is the OpenMP master thread.
  - `omp_size`: number of OpenMP threads in thhe MPI process.
  - `omp_rank`: rank of the OpenMP thread.